Sublacustrine landslides and associated hazards along the Western Slope of Lake Ohrid (Macedonia/Albania)

Master Thesis

by
Matthias Grün
November 2010

First Advisor: **Prof. Dr. S. Krastel-Gudegast**
Second Advisor: **Dr. W. Weinrebe**

Abstract

Submarine mass failures are very complex features and studying their processes is of great importance as they imply mayor geohazards. Their effects range from erosion of submarine slope areas over destruction of offshore infrastructure to the generation of tremendous tsunamis. In general submarine mass failures occur along continental margins or ocean island flanks but are also observed in fjords or lakes.

Lake Ohrid (Macedonia/Albania) is situated in a tectonic active region surrounded by high and steep mountain chains. Numerous mass wasting deposits have been detected inside the lake through different geophysical surveys including side-scan and seismic and sediment echo sounder measurements. The BLOSSOM campaign of September/October 2009 additionally provided high resolution bathymetry of Lake Ohrid.

Relatively young sub aquatic landslides were found at the steep western slope at the lake at the transition to the plain Central Basin in nearly 250 m depth. The largest mass movement that occurred in the lake is the so called Udenisht Slide at the south western margin of the lake. High resolution bathymetric data allows close analysis of slide specific features. Indicated by sidewalls of 20 m in height, more than $100 \cdot 10^6$ m^3 of material was removed during this event together with numerous large blocks that have been activated and were transported. Seismic and sediment echo sounder data reveals that this event must have happened not more than 800 years ago and that it had large impact on the whole south western margin as well as the southern part of the Central Basin. Significant erosion took place during the mass movement indicating a high energetic landslide. Analysis of the available data let assume that the large mass movement deposition body probably is the result of two successive slides while the second event was overriding the first deposition and destroying the interface by erosion.

Buried mass wasting deposits have been discovered below the Udenisht unit pointing out the unstable condition of the south western part of Lake Ohrid. They also show that mass failure events occur rather irregular. Since earthquakes are the most probable trigger mechanisms for landslides in this seismic active region additional pre-conditioning factors have been found like the occurrence of gas seepages at the base of the slope, fault zones and undercutting by retrogressive failure slides.

While sub aquatic landslides not only affect the lake floor topography but are also able to generate tsunami waves, special interest was given to the question if Udenisht Slide might have released a tsunami. Therefore key parameters of the landslide have been analyzed that influence tsunamigenic potential of sub aquatic landslides. Volume-to-wave-height relations and comparisons with other case studies have been evaluated showing that Udenisht Slide indeed must be considered as a potential tsunami source. This is not only important for the hazard estimation of this particular slide but also shows that for future mass movements in this tectonic active region tsunamis must be taken into account as an additional threat.

Zusammenfassung

Der Ohrid See befindet sich in einer tektonisch aktiven Region, umgeben von relativ hohen und steilen Bergrücken. Mit Hilfe von geophysikalischen Messungen (Mehrkanal-Seismik, Sediment Echolot und Side-Scan-Sonar) wurden einige Ablagerungen im See gefunden die durch unterseeische Hangrutschungen entstanden sind. Im Herbst 2009 wurde der See im Rahmen der BLOSSOM Kampagne zusätzlich hochauflösend mit einem Fächerecholot vermessen.

Am Westhang des Sees wurden relativ junge Hangrutschungen gefunden die sich am Übergang zum Zentralen Seebecken in fast 250 m Tiefe stattfanden. Die größte Rutschung die sich im Ohrid See ereignet hat ist die sogenannte Udenisht Rutschung am südwestlichen Bereich des Sees. Begrenzt von ca. 20 m hohen seitlichen Abbruchkanten hat sich ein Sedimentpacket von mehr als $100*10^6$ m^3 aus dem Hang gelöst und wurde in Richtung des Zentralen Beckens abwärts transportiert. Selbst große Blöcke konnten durch diesen Prozess mobilisiert werden. Während dem Rutschungsprozesses wurden zusätzlich enorme Mengen an ungestörten Sedimenten des Zentralen Beckens erodiert und umgelagert was dafür spricht dass es sich um ein sehr Energie reiches Ereignis gehandelt haben muss. Seismische Daten sowie Sediment Echolot Daten zeigen dass die Rutschung nicht mehr als 800 Jahre zurückgelegen haben kann und dass sie große Bereiche des Südwestlichen Teils des Sees sowie des südlichen Zentralen Beckens beeinflusst hat. Anhand von den vorhandenen Daten lässt sich vermuten dass die Rutschung aus zwei aufeinander folgenden Ereignissen bestand, wobei die zweite Rutschung die erste überlagerte und dabei die Grenzschicht der beiden Ablagerungen durch Erosion zerstörte.

Desweiteren finden sich ältere Ablagerungen aus Massenumlagerungen die mittlerweile von mächtigen Sediment Schichten überlagert sind und die instabile Situation des südwestlichen Teils des Sees aufzeigen. Diese älteren Rutschungen ereigneten sich sehr unregelmäßig. Erdbeben stellen den wahrscheinlichsten Auslösemechanismus für Hangrutschungen dar, besonders in seismisch aktiven Regionen wie des Ohrid Sees. Daneben fanden sich noch weitere Faktoren die sich destabilisierend auf den Hang auswirkten wie z.B. das Austreten von Gas an der Basis der Hänge, Verwerfungszonen und das Untergraben der Hänge durch regressive Hangversagen.

Submarine Hangrutschungen beeinflussen nicht nur die Struktur des Seebodens sondern bewirken auch Bewegungen in der darüber liegenden Wassersäule und können sogar Tsunamis auslösen. Um die Frage zu klären ob auch durch die Udenisht Rutschung ein Tsunami ausgelöst werden konnte wurden Rutschungsparamter analysiert die die Entstehung einer Welle beeinflussen um das Tsunamipotential dieser Rutschung einschätzen zu können. Relationen zwischen Rutschungsvolumen und Wellenhöhe wurden angewendet und das Udenisht Ereignis mit anderen Fallstudien verglichen. Dabei zeigt sich dass die Udenisht Rutschung durchaus das Potential besaß um eine Tsunamiwelle ausgelöst zu haben. Diese Erkenntnis ist nicht nur für diesen speziellen Fall wichtig sondern zeigt dass diese zusätzliche Gefahr durch unterseeische Hangrutschungen auch bei zukünftigen Rutschungen berücksichtigt werden muss.

Table of contents

1. Introduction

1.1. Submarine mass wasting

Submarine mass wasting events are a common process on continental slope areas or ocean island flanks. Together with significant impacts on geological developments of these areas, like erosion, rearrangement and deposition of sediments, they also contain a high risk for offshore infrastructure for example on communication cables, oil platforms or pipelines. Mosher el al., (2010) note that damages on offshore pipelines due to submarine mass movements cost about $400 million every year. But they can even have direct impacts on onshore infrastructure. Slope failure in proximity to the coast can affect the shore as it occurred in 1979 in the French Riviera where a submarine mass movement removed parts of the Nice harbor that was constructed near the Nice Airport (Dan et al., 2007). The most dangerous effect of submarine landslides is that they have the possibility to generate tsunamis able to destroy large parts of coastal settlements and causing the death of many lives. With nearly 3 billion people living in vicinity to oceans or marginal seas (Mosher et al., 2010) tsunamis reveal a severe risk for coastal settlements. Submarine landslides can have large variety of consequences and therefore studying submarine mass wasting events helps to understand related processes such as slope destabilization, flow dynamics and generation of tsunamis and so to estimate the risk they contain.

During submarine mass wasting events large amounts of material are transported downward into greater depths of the sea. Volume of submarine slides can be much larger than slides that occur on land. The material consists especially of unlithified sediments but can also involve volcanic rocks and great blocks. In contrast to landslides occurring onshore with implications that can be seen directly on the surface, submarine mass wasting processes are not that easy to investigate. But in the last decades several geophysical methods have been developed that allow detailed investigation of the deposition and erosion areas of such events even in water depths of more than 1000 m. Surface structures of mass wasting events can be studied using multibeam bathymetry systems or side scan sonars while seismic measurements allow investigating internal structures of deposited material. Additionally information derived from sediment cores provides a good basis for analyzing transported and rearranged material and to understand the processes behind those transportation events.

In general submarine landslides occur in regions with rather steep slopes. Fjords or river deltas present a potential location for sliding (Syvitski et al., 1987, Mulder and Syvitski 1995). However, sliding processes on nearly flat surfaces of less than 1° gradient have been observed as well (Hampton et al., 1996). Slope failure will take place if the shear stress of the slope exceeds its shear strength. A lot of different processes can be mentioned that have the capability either to increase the shear stress or to decrease the strength. For example high sediment accumulation rates can favor the destabilization of the slope. Elevated pore pressures within slope sediments reduce the frictional resistance and alleviate sliding (Masson et al., 2006). Also gas charging or gas hydrate disassociation at the base of slopes can play an important role for destabilizing slope sediments (Locat and Lee, 2002). Seismic loading and the occurrence of earthquakes is a major mechanism for stress release and is very often related to mass failure events. The initial composition of the slope sediments plays an important role. Specific geological horizons can act as weak layers and provide potential gliding planes for sliding slope sediments (Masson et al., 2006). Waves or low tides affect the deposited material with pressure

changes through the water column. Affecting the slope in a similar way also sea level changes can be mentioned. Growth of volcanic islands, evolution of salt diapirs and glacial loading are also major features that can be related to mass wasting processes. Last but not least human activity can affect significantly stability of slopes especially in coastal areas (Masson et al., 2006).

Most submarine mass wasting events have similar characteristics which enables their detection in geophysical data. Typical features of those gravity driven processes are a main scarp or headwall which usually indicates the upper margin of the slide, a glide plane or rupture surface along which the material was transported, sidewalls determining the width of the slide and the deposited material, usually with a toe at the maximum run-out distance (Hampton et al., 1996), (Figure 1).

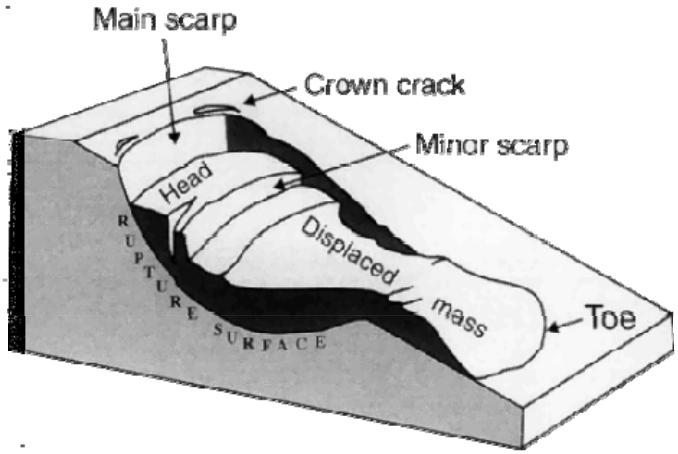

Figure 1: Main features of submarine landslides. From Hampton et al., 2006.

Mass movement processes can be classified into several basic types whereby slides represent only one type. According to their kinematics, the composition and shape of the deposited material and its deformation Coleman and Prior (1988) illustrate three classes of sub-aquatic mass wasting processes:

Falls: Falls occur along extremely steep, nearly vertical slopes and represent a relatively free fall of rock, mud or sand particles. They are the fastest moving mass movements and are not guided by slip surfaces.

Slides: Slides are sediment transportation processes along basal shear planes. They can either be translational or rotational (**slumps**) or multiple retrogressive. These groups are mainly divided by the geometry of their basal shear plane and the relation between thickness and length of the sliding body.

Flows: Flows can be subdivided into four main types: debris flows, liquefaction flows, grain flows and turbidity currents. **Debris flows** are rapid down slope moving flows of debris containing larger clasts that are held together by a cohesive sediment matrix. In **liquefaction flows** grains lose contact with each other and the particle weight is transferred to the pore fluid. **Grain flows** by contrast transport rather loose individual sediment grains. **Turbiditiy currents** are gravity-driven sediment flows where the grains are suspended by turbulence.

Mass movement processes are not limited to one single type but can comprise multiple material transporting mechanisms. For example slides can evolve into turbidity currents (Locat

and Lee, 2002). Breaking and falling of blocks may occur at steep headwalls generated by a slide or flow (Coleman and Prior, 1988). Figure 2 shows a compilation of several mass movement processes that are common on continental slope and how they can be associated with each other (Mienert et al., 2002).

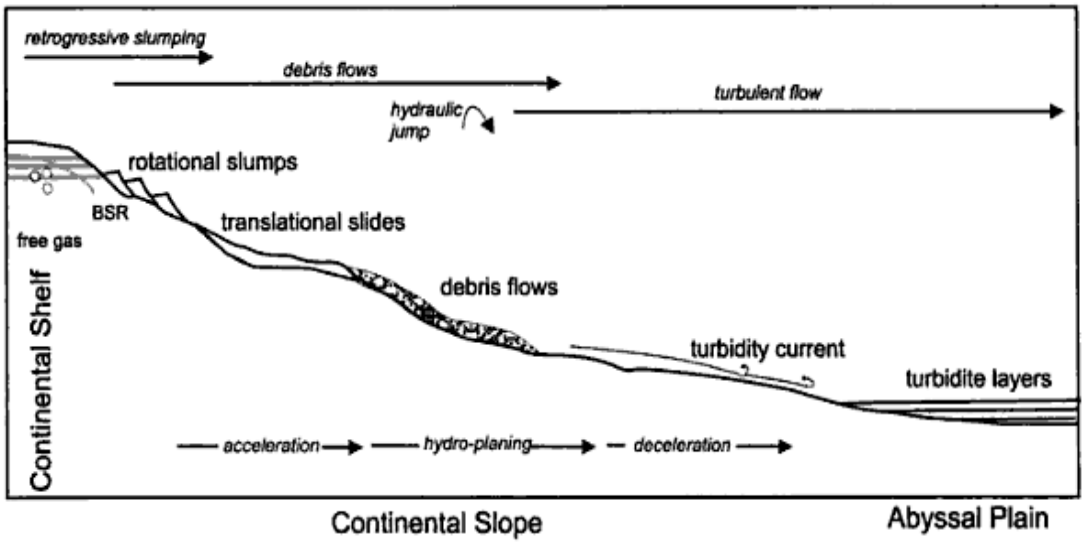

Figure 2: Schematic diagram for down-slope mass movements on continental margins. From Mienert et al., 2002.

Each slope failure usually occurs in different stages (Locat, 2001):

- **Pre-failure stage:** whole slope sediments are unbroken and in equilibrium
- **Failure stage:** activation of the slope mass by formation of shear bands. The mechanism for the onset of the failure can be of various reasons
- **Post failure stage:** involving the behavior of the sliding mass until the movement stops
- **Re-activation stage:** relates to movements on pre-existing failure planes

While pre-conditioning factors like undercutting, sediment load or steep slopes provide an instable position for the slope, most cases need an additional trigger mechanism that finally starts the failure and activates the sliding process. The most important trigger mechanisms for landslides are earthquakes which can cause slope failure in sub-aerial regions but also in sub-aquatic regions (Moernaut et al, 2005). Even smaller earthquakes like magnitude 4 are known to trigger landslides. In tectonic active regions it is therefore more likely that mass wasting events can occur along slope areas. Other potential triggers include oversteepening of the slope and excess pore pressure.

Several case studies proofed that submarine landslides also have the possibility to trigger tsunami waves like for example in Papua New Guinea 1998 (Synolakis et al, 2002) or the great Storegga landslide in the northern Atlantic (Bondevik et al., 2005). Tsunamis have great impact on the surrounding coastal areas. The tsunami happened in 2004 in south eastern Asia is one of the major catastrophic events that caused over 200.000 deaths and tremendous damage on coastal areas. Although this tsunami was not caused by landslide but by earthquake, also landslide triggered tsunamis can have enormous and disastrous impacts. The above mentioned

Papua New Guinea landslide tsunami in 1998 was triggered by a relatively small slump of 5 – 10 km^3 but caused significant damage on land including over 2000 casualties (Satake and Tanioka, 2003; Matsumoto and Tappin, 2003). For the population of these areas, tsunamis always contain a major hazard and also might cause enormous damage for onshore infrastructure.

Submarine landslides do not occur exclusively in the open ocean. Studies about mass wasting events in lakes show that they are also a common feature especially on steep flanks of lakes located in rather mountainous regions. Schnellmann et al. (2005) reported several historic mass movement structures that occurred in Lake Lucerne (Switzerland) and were investigated mainly with seismic measurements. Strasser et al. (2007) found out that stability conditions of slope areas can change relatively fast due variations in postglacial sedimentation rates. Moernaut et al. (2007) used mass wasting deposits in Lake Puyehue (Chile) for paleoseismic analysis. Historically reported strong earthquakes could be related to individual mass wasting events and allow also estimation about recurrence rates of these enormous events. Also Lake Tahoe is situated in a tectonic very active region in the Sierra Nevada-Great Basin boundary zone. Large earthquakes (M>7) occurred here and triggered landslides. Several field measurements took place to study submarine mass wasting events in order to better understand the tectonic environment and evolution (Gardner et al., 2000). Ichinose et al. (2000) concentrated on tsunami hazards that are related to mass movement events within Lake Tahoe. Tsunami waves triggered by typical sliding events were modeled and might reach wave heights of up to 10m.

1.2. Lake Ohrid

Another interesting location for studying submarine mass wasting processes is Lake Ohrid, a transboundary lake on the Balkan Peninsula between Macedonia and Albania (Figure 3). It is surrounded by high and steep mountain chains. But also flanks of the nearly 300 m deep lake are relatively steep and provide the potential for submarine landslides. Several widespread mass wasting deposits have been found within Lake Ohrid of different ages and various dimensions.

Figure 3: Map of the south western part of the Balkan Peninsula and the study area of Lake Ohrid, marked by the white rectangle.

Lake Ohrid is one of the oldest lakes in Europe (3-5 Mio years). An ICDP (International Continental Drilling Program) is planning to core into the deep sediments of Lake Ohrids Central Basin where undisturbed sediments shall reveal essential information about precise age of the lake as well as regional climate changes and shall help to understand the unique richness in endemic species that evolved in Lake Ohrid. Wagner et al. (2009) showed that tephra layers located in a sediment core could be identified which contain information about eruptions from Italian volcanoes. In order to encounter undisturbed sediments within the lake knowledge of mass wasting deposits is fundamental to exclude these zones from potential drilling positions.

The southern Balkan Peninsula is an active tectonic region characterized by the occurrence of abundant earthquakes. While submarine mass wasting processes are strongly related to a high seismicity detection and analysis of these events can be used for the study of paleo-seismicity of the region of Lake Ohrid. Recurrence rate of submarine landslides can be estimated by studying older mass depositions and can give information about typical dimension of these events in Lake Ohrid. Compared to submarine mass wasting events in open oceans, landslides in lakes are usually smaller. Slide deposits in Lake Ohrid can be studied very detailed and therefore allow close characterization and analysis of these events. This will also be used to estimate the risk that submarine mass wasting processes keep in this particular region.

In September/October 2009 a field campaign took place in Lake Ohrid for high resolution bathymetric mapping. Multibeam bathymetric data and sediment echo sounder data were collected with special interest in studying large mass movement processes in Lake Ohrid. Processing and interpretation of these data is one of the primary targets of this master thesis.

1.3. Motivation

This thesis is divided in three main parts:

- Processing and visualization of bathymetric data collected from the field campaign 2009
- Evaluation of the landslides on the western slope area of Lake Ohrid with main interest in a major sliding event in the south western part of Lake Ohrid (Udenisht Slide)
- Discussion of the tsunamigenic potential of Udenisht Slide

The first part deals with processing of the obtained high resolution bathymetric data. The new map will allow a more precise description of recent mass movement deposits that have already been identified in previous bathymetric maps of the lake. These old bathymetric maps were based on single beam echo sounders and thus do not have a sufficient resolution.

The second part will focus on the western slope area of Lake Ohrid as it seems to be a rather unstable part of the lake where several mass movement deposits have been found. Near the Albanian coast one of the largest landslides of Lake Ohrid occurred, the so called Slide. Its dimension and relatively young age provide the possibility for a detailed investigation which will be the main target of this study. In addition to bathymetric data backscatter data was derived from the multibeam echo sounder as well as high resolution sediment echo sounder profiles that are used to describe structures of the uppermost subsurface of the Udenisht Slide. From seismic data of previous field campaigns deeper mass deposits can be detected and allows insight of the development of the western slope area.

Besides the implications of the slope area and the sediments that are eroded and redeposited, submarine landslides also keep the possibility of triggering tsunami waves. It is reported that tsunamis in lakes were generated through large mass wasting events (Strasser et al., 2007). Therefore the last part will focus on the question if Udenisht Slide might have triggered a tsunami. Classifications over landslide aspect ratios and basic volume-to-wave-height calculations will be applied. Comparison to similar case studies shall help to classify the tsunamigenic potential of the Udenisht Slide and to understand if tsunamis must be considered as a risk within Lake Ohrid.

The specific objectives of this thesis are:

- Investigation of mass movement deposits on the western slope area

  How often do mass wasting events take place and what dimensions do they have? Are the landslides of this area bounded to specific geological features? What does this mean in terms of slope stability of the western slope area? What do older sliding events reveal about paleo-seismicity of this area?

- Budget of Udenisht Slide

  What amount of sediments was removed from the slope and how much material was deposited? Did erosion play a significant role during the sliding process?

- Kinematics of the Udenisht Slide

  Can the event be divided into several successive events or was it one large, single process? How far was the material transported? Do backscatter data reveal any obvious material changes? And do they provide information about the progress of the slide?

- Age and origin of the Udenisht Slide

  Where did the movement start? Was it a submarine event or did it start onshore and subsequently propagated into the lake?

- Tsunamigenic potential of the Udenisht Slide

  Was it possible that this landslide triggered a tsunami wave? Based on the available data, what wave height must be expected?

2. Study Area

2.1. Lake Ohrid

Lake Ohrid is located between Macedonia and Albania and is most likely the oldest or at least one of the oldest lakes in Europe (3-5 Mio years). It was declared as UNESCO World Heritage in 1979 due to its extraordinary ecological relevance. Lake Ohrid is surrounded by high mountains of the Galičica National Park (> 2200 m) to the east and the Mokra Mountain chain (> 1500 m) to the west while the lake itself is at 693 m above sea level (a.s.l., Figure 4). With 30 km north-south and ca. 15 km east-west extension the lake covers an area of about 360 km². Being one of the most voluminous lakes in Europe (55 km³), Lake Ohrid is also a comparatively deep lake with a maximum water depth of 289 m. North of the lake two relatively flat plains are situated (Ohrid and Struga plain) as well as a minor one south of the lake (Pogradec plain) (Vogel et al., 2010). Three larger cities are located on the relatively straight coastline around the lake: Ohrid and Struga on its northern part in Macedonia and Pogradec on the south western coast in Albania (Figure 4). The only out flowing river, the Crni Drim (Black Drin) is draining Lake Ohrid near Struga. Water influx is coming from small rivers (~23%), surface springs and several sub-aquatic inflows especially at the southern margin near the town Sveti Naum (~53%) and direct precipitation (~23%) (Matzinger et al., 2006). South-east of Lake Ohrid the mountain chain of Galicica National Park separates Lake Ohrid from the higher located sister Lake Prespa (840 m a.s.l.). Via underground connections through karstified carbonates water is draining Lake Prespa and entering into Lake Ohrid through subsurface and sub-aquatic springs.

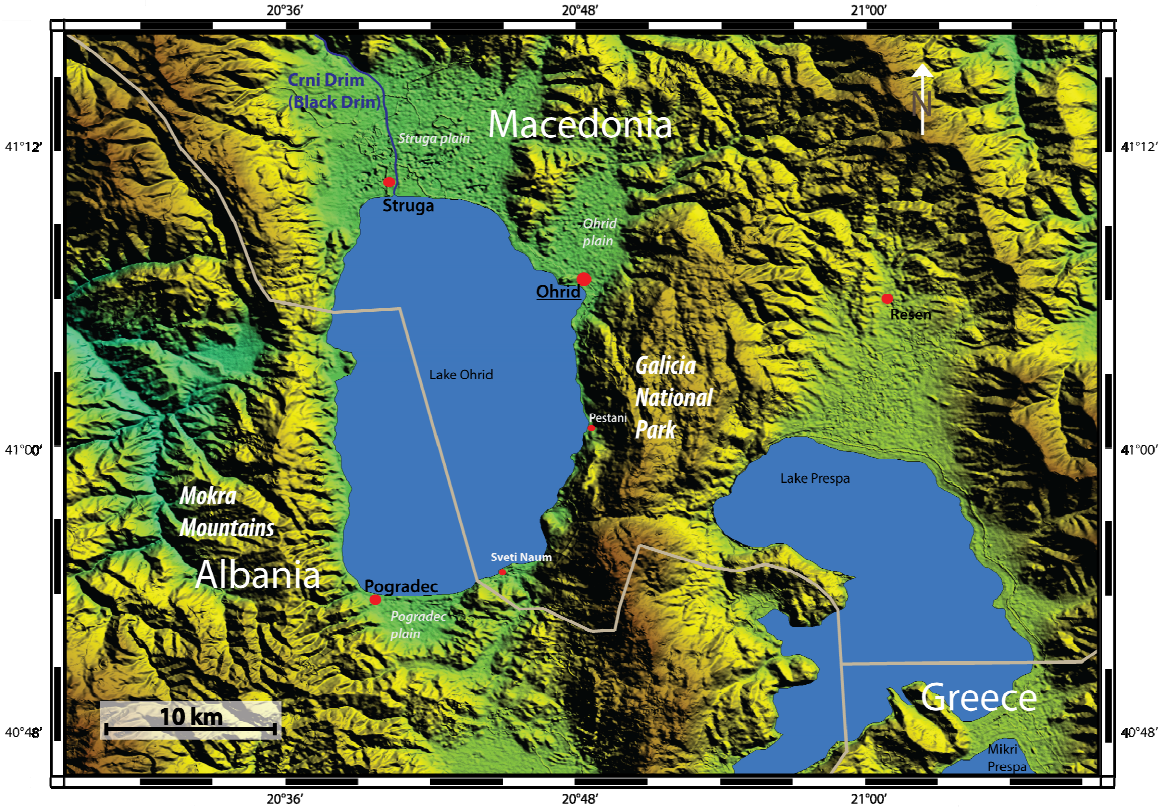

Figure 4: Topographical map of Lake Ohrid and the surrounding area showing enclosure of Lake Ohrid by Mokra Mountains and Galičica Mountains and the neighboring Lake Prespa.

Lake Ohrid is classified as an oligotrophic lake (low amount of nutrients) with a high transparency up to 20 m (Popovska and Bonacci, 2007). It hosts more than 200 endemic species mostly benthic and planktonic groups but also special kind of fish that can only be found in this separated environment. Taking surface area into account Lake Ohrid has the highest degree of biodiversity worldwide (Albrecht and Wilke, 2008).

2.2. Overview of geological and tectonic evolution within the Tethyan realm

The geological evolution of the entire Balkan Peninsula (BP) is characterized by the interplay between two continents - Eurasia and Gondwana and the Tethyan Ocean. The overall evolution of the Balkan Peninsula is still highly debated and many models exist explaining the existence of continental fragments (Ionian, Pelagonian, and Serbo-Macedonian Zone, Figure 5) and zones that exhibit ophiolites indicating that they represent oceanic basins that experienced seafloor spreading at least over some period of time (Pindos, Vardar zone, Figure 5, Robertson, 2007). Robertson et al. (1996) describe a model with a single Tehtyan ocean from Late Palaeozoic on situated between the active southern margin of Eurasia (in the north) represented by the Serbo-Macedonian Zone (Figure 5) and a passive northern margin of Gondwana in the south.

During the Permian and into the Triassic, microcontinents such as Adria (also called Apulia being the largest fragment that is seen as a promontory of Gondwana represented by the Ionian Zone in Figure 5) rifted from Gondwana and drifted northward into the Tethyan Ocean (Robertson et al., 1996). During Early-Middle Triassic, Pelagonia (an additional microcontinent) rifted away from Apulia with a final continental break up in Late Triassic to later form a small basin (the Pindos Ocean) in between these two microcontinents (Robertson et al., 1991). Triassic was characterized by subduction of oceanic lithosphere of the Vardar Ocean (a remnant of the Tethys between Gondwana and Pelagonia) beneath the Serbo-Macedonian continent now evident by the Vardar Zone (Figure 5).

Two types of ophiolites can be found within the NW-trending Pindos Zone: Mid Ocean Ridge Basalt (MORB) and Suprasubduction Zone (SSZ, Robertson et al., 1991) indicating that after Triassic rifting, seafloor spreading took place followed by a westward dipping intra oceanic subduction (Robertson et al., 1991, Dilek et al., 2005). A volcanosedimentary unit overlain by deep water sediments further indicates that the basin progressively deepened after rifting (Dilek et al., 2005). In Late Jurassic the northern part of the Pindos Ocean collided with the western passive margin of the Pelagonian microcontinent that subsequently led to the obduction of ophiolites that are now present on the western side of Lake Ohrid (Figure 5).

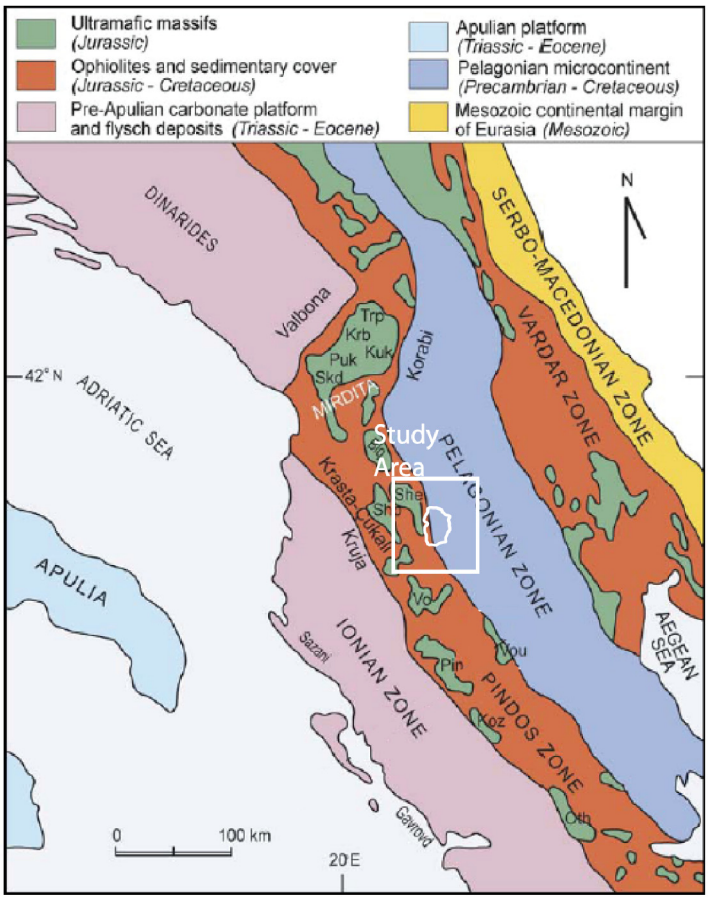

Figure 5: Simplified geological map of the west-central Balkan Peninsula and Adriatic Sea region. Study area of Lake Ohrid is highlighted by the white rectangle. Modified after Ghikas et al., 2010

2.3. Neotectonic evolution

Macedonia and Albania are part of the South Balkan Extensional Regime (SBER) that is affecting also Serbia, Montenegro, Bulgaria and northern Greece (Dumurdzanov et al., 2005; Burchfiel et al., 2008; Figure 6). This region experienced three phases of extension: (1) a Paleogene extension that is most likely connected to the final closure of the Vardar Ocean, (2) Early to Late Miocene extension related to processes at the Hellenic subduction zone, and (3) Late Miocene to Recent extension still connected to subduction at the Hellenic trench but additionally influenced by the onset of the North Anatolian Fault zone.

The oldest extension period started in late Eocene creating a NW-trending half graben system in eastern Macedonia and a large basin in central Macedonia. It was followed by a short period of compression in eastern Macedonia. In Early Miocene the Strymon graben formed as a major sedimentary basin over a Master Detachment fault that was active until Pliocene time (Burchfiel et al., 2008). North trending extensional basins most likely related to the Strymon Valley Detachment fault (SVD, Figure 6) became active progressively farther west into western Macedonia and eastern Albania. Although the Strymon Valley Detachment fault was still active, an additional N-S extension caused by the subduction at the south Hellenic trough became more important in early Pliocene time. Since late Pleistocene time these two systems act more or less independently: (1) an E-W extension in western Macedonia and shortening in western Albania caused by convergence of the north Hellenic trough , and (2) a westward migrating N-S extension related to geodynamic processes at the south Hellenic trough (Burchfiel et al., 2008).

Some of the graben structures being formed during extensional periods were partially filled with water and became lakes such as the Butrinti or Shkodra graben lakes in Albania (Aliaj et al., 2001) and Lake Ohrid between Albania and Macedonia (Figure 7). The Korca plain in east Albania (bordered by Pliocene or Quaternary normal faults) developed through intense subsidence and is now covered by more than 200 m of Quaternary alluvial sediments and lagoonal deposits on its northern margin (Aliaj et al., 2001). Uplift of the surrounding areas and subsidence of the Korca and Pogradec plains caused the formation of a deep graben restricted by normal faults along its northern and southern margin. This graben structure became the origin for Lake Ohrid.

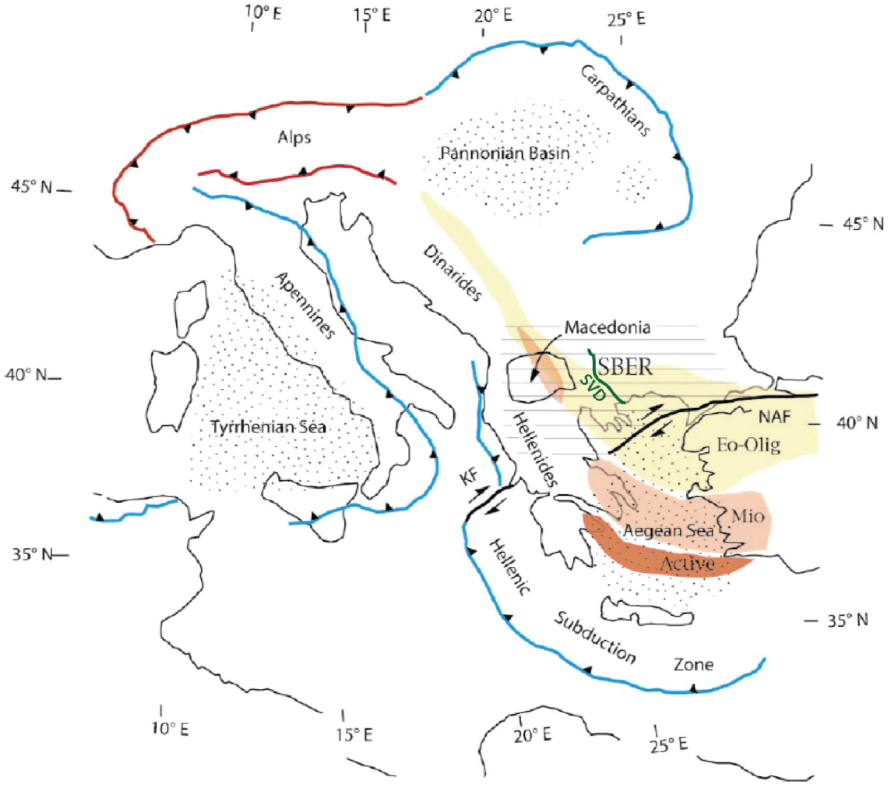

Figure 6: Simplified tectonic map of Eastern Mediterranean region showing Southern Balkan Extensional Regime (SBER). NAF=North Anatolian Fault, SVD=Strymon Valley Detachement fault. Modified after Dumurdzanov et al., 2005

2.4. Geology at Lake Ohrid

Paleozoic metamorphic and magmatic rocks that can be found along the entire western Macedonian Zone form the country rock around Lake Ohrid (Wagner et al., 2008, Reicherter et al., submitted). Being located in an active tectonic graben system, large amounts of deposited sediments are exposed in the Ohrid basin such as karstified Triassic carbonates and clastics on the southwestern and northwestern side of the lake. Quaternary sediments are located in the plains around Struga and Ohrid in the north as well as at the south-western area near Pogradec (Figure 4). Mirdita ophiolites from the Pindos Zone are exposed on the Albanian side, west of Lake Ohrid in a northwest trending zone (Ghikas et al., 2010).

2.5. Active Tectonics

Today the area around Lake Ohrid is characterized by high seismicity reflecting in the occurrence of numerous micro-earthquakes as well as medium-sized earthquakes. In addition some large and devastating historic earthquakes are documented such as the 518 AD event that nearly destroyed the entire city of Ohrid and Skopje (Hoffmann et al., 2010), the 1911 event at Lake Ohrid with a Magnitude of M_s=6.7 (Muco et al., 2002; Ambraseys and Jackson, 1990) or the most destructive earthquake in the younger history of Macedonia in 1963 close to Skopje (M=6.1) (Suhadolc et al., 2004). More recent events are recorded for example on 23rd of November 2004 (M_w=5.4) or on 6th of September 2009 (M_w=5.6) proofing the status of the Ohrid-Korca zone as one of the highest seismic hazard regions in Albania and Macedonia (Wagner et al., 2008). Seismicity is mainly concentrated along N-S trending normal faults on the eastern and western side of the Ohrid basin (Hoffmann et al., 2010) usually in depths of about 10 km (Aliaj et al., 2004). Most of the earthquakes occur along three distinct seismic belts (Figure 7): 1) North Hellenic Trench (falling together with the boundary between European plate and Adrian microplate), 2) Ohrid-Korca belt (north-south elongated in the eastern part of Albania) and 3) Elbasani-Dibra-Tetova transverse belt (extending southwest-northeast) (Aliaj et al., 2004; Burchfiel et al., 2008).

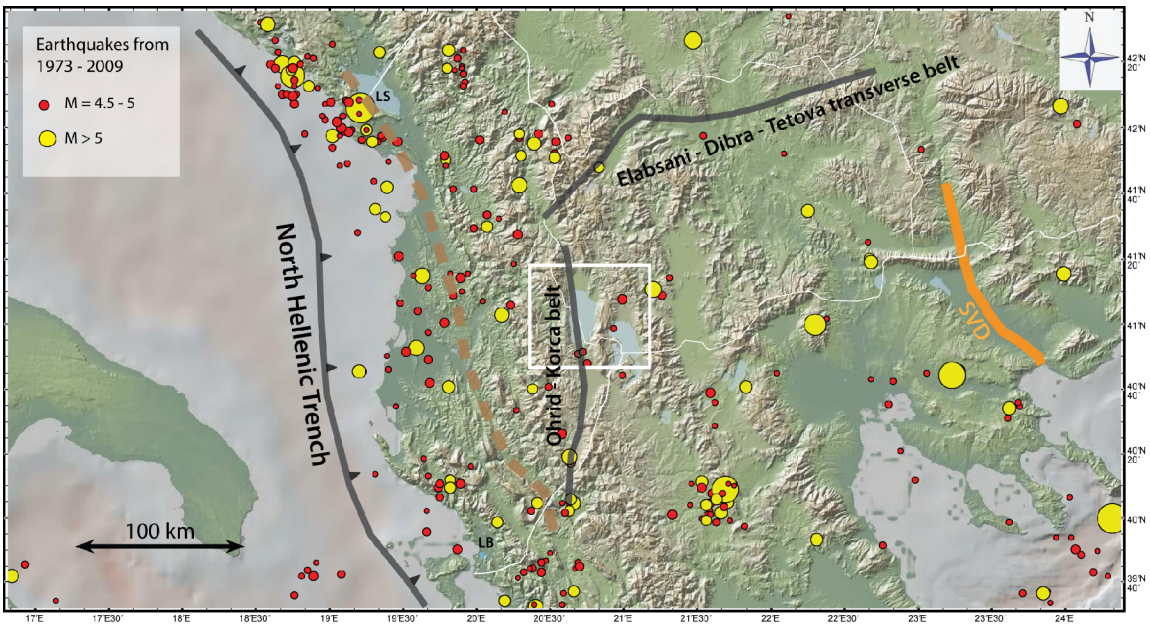

Figure 7: Tectonic map of Macedonia and Albania showing locations of earthquakes (M>4.5: red, M>5: yellow) occurring between 1973 and 2009 (Source: USGS-NEIC). Main seismic belts are marked by black lines. Dashed brown line indicate boundary between extension and shortening in Albania (Burchfiel et al., 2008). Strymon Valley Detachment fault (SVD) shown in orange. Graben lakes in Albania such as Shkodra (LS, northern Albania) and Butrinti (LB, southern Albania) are marked as well as the study area of Lake Ohrid highlighted by white rectangle.

3. Methods and Data

3.1. The field campaign BLOSSOM September/October 2009

Most of the data used in this study were collected during the BLOSSOM (Bathymetry at Lake Ohrid for Sub-aquatic Slide Overview Mapping) campaign that took place between September 17th and October 12th 2009. The primary goal of this project was high resolution bathymetric mapping of Lake Ohrid. This is of great importance for analyzing numerous geological processes, such as mass wasting and tectonics. The Hydrobiological Institute of Ohrid provided a vessel on which the instruments could be installed. Special construction had to be built for attaching the multibeam echo sounder to the bow of the vessel (Figure 8). The bathymetric mapping campaign lasted for twelve days. Additionally to bathymetric measurements, sediment echo sounder data was recorded during the entire cruise.

Figure 8: Research vessel of the Hydrobiological Institute of Ohrid used during the BLOSSOM campaign showing constructions for multibeam and sediment echo sounder system. Inlet: Multibeam holder construction at the bow of the vessel.

3.2. Description of instruments

For bathymetric mapping ELAC Seabeam 1180 multibeam sonar was used during the campaign. A CTD48M memory probe from Sea & Sun Technologies was deployed to measure sound velocity profiles at different locations of the lake. Sediment echo sounder profiles were taken with an INNOMAR SES 2000 "Compact" echo sounder system.

3.2.1. Multibeam

The multibeam system on the vessel consisted of two transducer arrays (LSE 307), the control unit SEE 30-1180 and a motion sensor (IXSEA Octans IV).

General

Multibeam sonar systems are active sonar system which means that they are transmitting and receiving acoustic pulses. In contrast to single beam sonar systems, multibeam systems

produce several acoustic pulses at the same time. Energy is transmitted with large opening angles in a swath perpendicular to the course of the vessel. The sum of all signals transmitted at the same time is called a ping. Beams travel through the water column with water sound velocity until they are reflected and scattered at the seafloor. From there they return to the transducer. After all beams from one ping were recorded, another ping transmits the next series of beams. The recorded travel time of every single beam allows calculating the length of signal path from the reflection point to the vessel. This is done for all signals of one ping and therefore provides a large area to be covered with one profile. The dimension of the ensonified area depends on the water depth. Greater depths allow a greater coverage of the sea floor. However, this implies that reflecting points of two adjacent beams are further apart than in shallow water. This leads to a lower lateral resolution. In general the most accurate depth measurement will be given from beams directly below the survey vessel.

Energy loss

Detection of incoming signals is done by hydrophones measuring pressure oscillations of traveling sound waves. Amplitude of the wave is related to its energy. Energy loss for travelling sound waves can be described by the sonar equation expressing different factors involved in transmitting and receiving sonar signals:

$$SE=SL-2TL+BS-NL+TA$$

SE (Signal Excess) is the measured signal at the hydrophone and SL (Source Level) the transmitted energy. Traveling through the water column causes a loss of energy, described by transmission loss (TL). Compared to light or radio waves, sound waves only loose a small amount of their energy while travelling through water. Subtraction of noise level (NL) leaves the backscattering strength (BS) of the target and the signal of the target area (TA), (SeaBeam, 2000). The percentage of reflected and scattered energy from the seafloor depends on the impedance of the surface material as well as its roughness. Part of the sound pulse will be absorbed by the sea floor material while the rest is being reflected and scattered. Also the angle of incidence and the distance the beam is travelling influence the amount of energy arriving at the transducer.

While bathymetric instruments aim in receiving accurate information from the seafloor they transmit acoustic pulses with rather high frequency (12-120 kHz for deep water systems and > 100 kHz for shallow waters) causing mainly reflection and scattering of the signal at the seafloor instead of penetration into the underlying sediments.

Projectors and hydrophones

For transmitting acoustic pulses bathymetric sonars are using piezo-electric ceramic constructions called projectors that are triggered when a voltage is applied. A vibrating membrane allows transmitting specific frequencies (SeaBeam, 2000).

Hydrophones measure continuous strength and phase of incoming signals. Over an analog-to-digital converter this is converted to discrete digital measurements. While measuring continuous signals and thus not only signals returning from the sea floor also background noise is recorded by the hydrophones. Usually amplitudes coming from background noise are smaller than those from transmitted acoustic pulses. True signals can be separated from noise by "noise discrimination" which means computing a detection threshold for amplitude data. Signals with

lower amplitude than the threshold are ignored. Calculating the threshold level is dynamic and the system will calculate the threshold individual for every ping.

Projector Arrays and Beam Forming

The aim of transmitting acoustic pulses for multibeam measurements is to generate beams that have wide opening angles perpendicular to the vessel but are narrow in profile direction. Single pulses are expanding spherically in water and would spread their energy in all directions. Projector arrays are used to transmit directed pulses in a way that a large (in across track direction) but narrow (in along track direction) strip of the seafloor is ensonified. To achieve these kinds of non-isotropic waves an array of several neighboring projectors is applied. Every single projector is emitting a signal that will interfere with the signal from other projectors. Distance between adjacent projectors and wavelength of the signal determine when constructive or destructive interference will take place and thus allow transmitting high amplitude signals under certain angles (constructive interference) while energy spreading in other directions is reduced (destructive interference). The pressure front of the transmitted pulse is called the "main lobe" and depends on the dimension of the projector array. The larger the projector arrays the narrower are the main lobes. Together with the main lobe also "side lobes" are generated through partial constructive interference at both sides of the main lobe. Side lobes also lead to reflected and scattered energy that can affect precise detection of returning signal of the main lobe. So called shading algorithms try to minimize unwanted side lobe effects. Therefore multibeam systems are designed in a way that the strength of transmitted signals is higher for projector elements from the array center than for the array edges.

Hydrophone Arrays and Beam Steering

Usually hydrophones are arranged equidistant in an array to receive acoustic impulses. While each single hydrophone is measuring arrival time of the signal as well as phase and amplitude, combination of all hydrophones allows allocating amplitude and timing measurements to specific angles. This process is called "beam steering".

There are two different ways for performing beam steering with multibeam systems using either direction of arrival (DOA) or time of arrival (TOA). Two different algorithms are using this information to analyze incoming signals and to relocate the beaming direction. "Bearing direction indicator" (BDI) is locating the direction of arrival while "Weighted Mean Time" (WMT) uses arrival times of the signals at every hydrophone. BDI can only be used mainly for beams from outer swath regions arriving at large swath angles, WMT also allows locating beams from the central part of the swath. Wave fronts arriving more or less parallel to hydrophone array must have been reflected from areas below the ship. This is called the specular regime and the incoming signal are very strong and of short duration (Figure 9a). Beams from the non-specular regime have a shallow grazing angle to the sea floor. This will be detected as a longer signal with smaller amplitude (Figure 9b).

BDI

BDI focuses on precise angle estimation using phase differences between adjacent hydrophones. Phase differences will either lead to constructive or destructive interference when summing signal traces of adjacent hydrophones. This can be used to identify the beam angle but

only if phase differences are large enough. Small angles do not allow exact estimation of the incoming signal. Therefore BDI processing is used mainly in the non-specular regime.

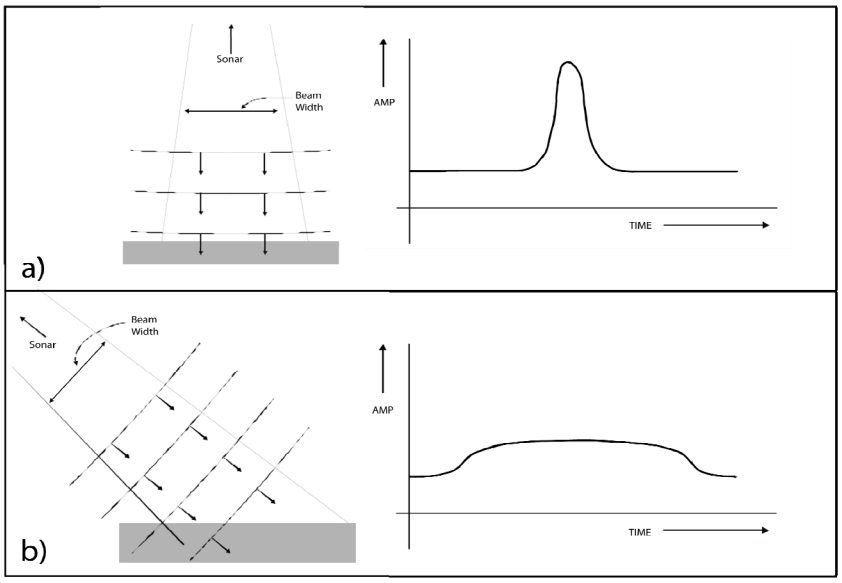

Figure 9: Specular (a) vs non-specular (b) regime and recorded signal amplitudes from these regions (SeaBeam, 2000).

WMT

The WMT approach is focusing on arrival time differences and can be used also for signals from small swath angles (specular regime). Echoes from these regions show a short duration and a well defined amplitude peak which can be used for accurate calculation of arrival time.

Adjustment / Mills Cross

Usually projector and hydrophones are adjusted in a so called Mills Cross system. Projector array is arranged parallel to vessel direction and hydrophone array is placed perpendicular (Figure 10). This causes that the part of the sea floor covered with the transmitted wave intersect with the part observed by the hydrophones. Generated beams of multibeam systems are rather narrow in along track direction (in general about 2°) and have a large opening angle in the across track direction. The opposite is the case for the receiving area. Beam steering results in numerous narrow stripes in across track direction. The overlay of transmitted and received beams resulted in numerous depth values recorded from small and well defined areas at the sea floor.

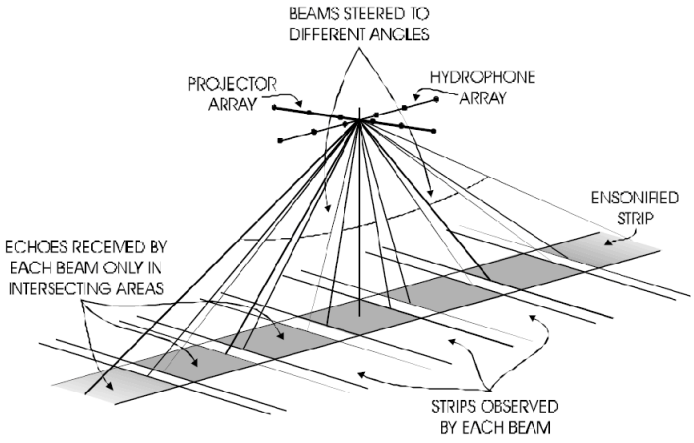

Figure 10: Mills Cross adjustment for multibeam systems (SeaBeam, 2000).

Resolution

Resolution of multibeam measurements is mainly influenced by the system configuration and water depth. The number of separated beams through beam steering process affects distance between two adjacent depth points at the seafloor. Water depth of course plays a major role for resolution of bathymetric data. In shallow water distance between adjacent depth points is smaller than in deep water. This leads to a higher resolution in across track direction for shallow water than for deep water. For example with common multibeam systems that have resolution angles of about 2 degrees the footprint at the seafloor (directly under the vessel) will be ca. 3.5 m for water depth of 100 m but 7 m for 200 m water depth. Lake Ohrid shows water depths down to 290 m with a mean depth of about 150 m resulting in across track resolution of about 5 meter. Along track resolution is affected through ping rate and ship speed. In general the next acoustic pulse will be transmitted when all returning beams of this signal were detected at the hydrophone array. After that a next swath is generated and hydrophones wait for returning signals. Meanwhile the ship has moved along the profile so that the next series of returning beams are coming from an area along the profile. Slow ship speed will therefore lead to a higher along track resolution because along track distance between two successive swathes is closer together than at fast ship speed. A high ping rate will also keep this distance smaller and lead to better resolution. Though ping rate is a function of depth because travel time varies with depth. This means that shallow depths are equivalent with faster ping rates because travel time is shorter and therefore also along track resolution is higher than in deep water. The multibeam system deployed for the BLOSSOM campaign in Lake Ohrid had a maximum ping rate of 25 pings per second.

Coverage

As mentioned above coverage of multibeam measurements mainly depends on water depth. Swath angle is limited through system configuration and cannot be changed during the survey. In principle large water depths lead to a larger area that will be covered through transmitted signal. But this also means longer pathways for travelling beams especially for outer beams. Energy of these beams can be too weak for being detected at the hydrophones. Therefore large water depth in terms of greater distances for the beams can also reduce coverage. Figure 11 shows a mean coverage plot depending on water depths for an ELAC SEA BEAM 1180 multibeam system, as used for bathymetric measurements at Lake Ohrid.

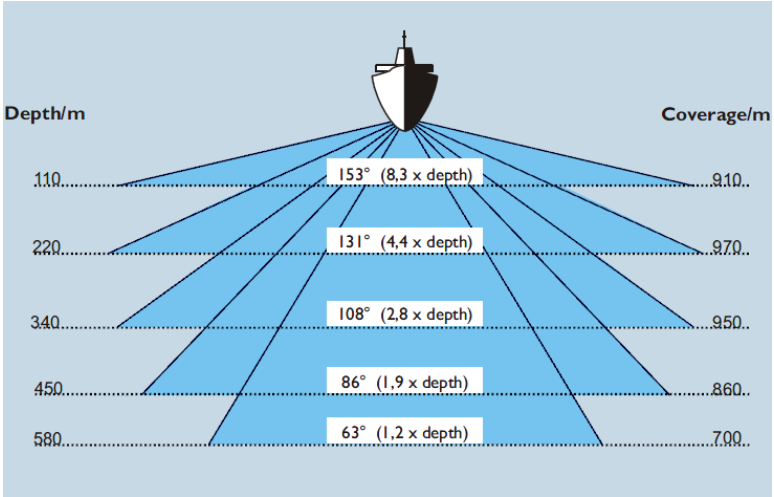

Figure 11: Depth dependent coverage of ELAC SEA BEAM 1180 multibeam system (ELAC).

The system used on the field campaign on Lake Ohrid was a SEA BEAM 1180 multibeam sonar system and consisted of two transducers arrays (each implying hydrophone and projector array) with an opening angle of 153°. A high frequency signal of 180 kHz is transmitted suitable for shallow waters. 126 single beams can be resolved by the hydrophone array allowing a resolution of 1.5°. Transducers are arranged in a "V-shaped" position perpendicular to ship direction. In this special type of multibeam sonar hydrophone and projector arrays are combined and beam forming is already performed during signal transmission. The mills-cross technique is not applied in this kind of V-shaped sonar but projectors and hydrophones are in-line. Generation of acoustic signals is achieved by the Rotating Directional Transmission method (RDT) where beamforming of transmitted pulses is obtained by offset time triggering of individual transducers. The SEA BEAM 1180 multibeam sonar is suitable for depths down to 600 m and hence sufficient for mapping Lake Ohrid with a maximum depth of about 290 m.

Ship Motion compensation

Ship motion is critical for bathymetric surveys. Roll, heave, and pitch movements affect angle and arrival time of the beams. Depth calculation from multibeam data is very sensitive to ship movements and would cause massive errors if they are not corrected. Compensation is done by means of a motion sensor which should be positioned at a central position on the ship close to the transducers thereby providing information about the relative movements of the vessel such as surge (along track direction), sway (across track direction) and yaw (rotation around z-direction) movements. Navigation is recorded by a GPS. All this information is used to correct data measured by the hydrophones before position and depth of points on the sea floor can be calculated. For the BLOSSOM campaign an IXSEA OCTANS IV Surface motion sensor was deployed on the vessel providing this information as well as a GARMIN GPS 152 for navigation. Output data of the multibeam system are then already stabilized for ship motions. The control unit saves all signals of a swath and saves them together with all swaths of a profile.

Backscatter

Along with depth calculation the multibeam system also allows visualization of backscatter strength of the returning energy. Backscatter is the amount of energy scattered from the bottom back to the hydrophone. Backscatter strength can provide information about material changes on the seafloor surface but also on the morphology of the sea floor. In general fine grained sediments have lower backscatter capacities than rocks and coarse grained sediments. Therefore this data provide additional information about surface properties.

3.2.2. CTD

It is essential to know the exact sound velocity profile of the water column in order to determine the water depth with multibeam systems. Variations of sound velocity in the water column affect bending of rays especially from the outer regions of a multibeam swath. Therefore it is important to have profound knowledge about sound velocity to relocate the received beams. Determining a sound velocity profile is done with a CTD (Conductivity-Temperature-Density). At selected positions water temperature, conductivity and density is measured by during lowering and pulling up the CTD on a wire. A linear relationship between density and depth allows transformation of measured density values into depths. With temperature and conductivity data, sound velocities can be calculated for all depths.

We used a Sea&Sun Technology CTD48M memory probe (Figure 12) during the bathymetric campaign at Lake Ohrid to gain sound velocity profiles at four different locations within the lake (Figure 16). Inside this probe a microprocessor is located which runs from an internal battery and records received data during the CTD run. On board the data can be transferred to the computer via a multiconductor cable. Sound velocity profiles were measured down to 250m depth (maximum length of available wire) at 1m resolution.

Figure 12: CTD (48M) for measuring conductivity, temperature, and density profiles for determining water sound velocity profiles.

3.2.3. Sediment echo sounder System

The parametric Innomar echo sounder system consists of a SES-2000 "compact" transducer for sending and receiving acoustic pulses and a main unit which is connected with a computer, GPS-system and the motion sensor.

General

Parametric sediment echo sounders are transmitting and receiving signals with the transducer using the so called "parametric effect" for generating acoustic signals. Signals are travelling through the water until they hit a boundary layer. These interfaces cause reflection and transmission of incoming sound waves. Reflected waves are recorded at the transducer and provide information about depth of the reflected layer and impedance contrast of these materials. The amount of reflected energy mainly depends on the impedance contrast between two materials. Density difference between water and seafloor is a significant boundary layer and causes strong reflections. Transmitted energy will travel trough sediments and will cause further reflections at boundary layers of different materials.

Parametric effect

The transducer is transmitting two very high (finite) amplitude sound waves at slightly different frequencies. If two waves of similar frequencies are generated simultaneously, also the sum and the difference of the two primary frequencies are emitted. These secondary frequencies travel in the emission cone of the primary frequencies. The primary signals are high frequency pulses; they are used for measuring the water depth below the vessel. In contrast, the relatively low difference frequency is able to penetrate into the sediments and provide

structural information of the uppermost sediments (Figure 13). Table 1 shows examples for typical frequencies transmitted from the deployed system and the resulting low frequency.

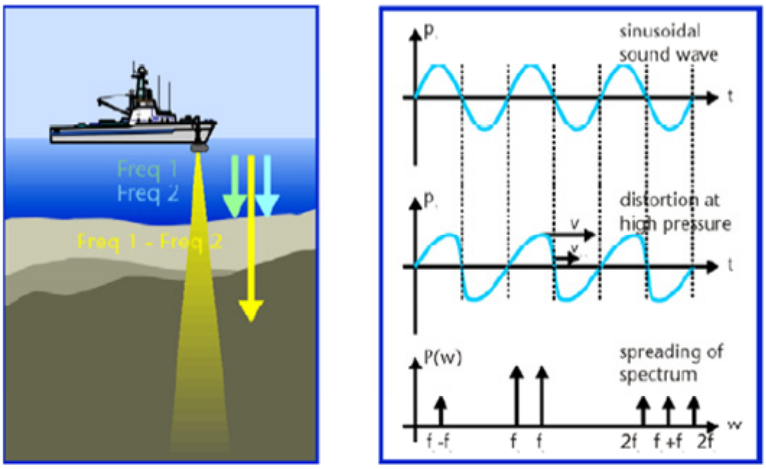

Figure 13: Parametric effect of sediment echo sounder systems. Two low frequent signals interfere to a low frequent signal able to penetrate into deeper sediment layers (Innomar, 2005).

Freq1	Freq2	Freq1-Freq2
102 kHz	98 kHz	4 kHz
103 kHz	97 kHz	6 kHz
104 kHz	96 kHz	8 kHz
105 kHz	95 kHz	10 kHz
106 kHz	94 kHz	12 kHz

Table 1: Typical transmitted frequencies of sediment echo sounder systems (Freq1 and Freq2) and the resulting frequency (Freq1-Freq2), (Innomar, 2005).

The Innomar echo sounder is making use of the parametric effect. As the secondary frequencies travel in the emission cone of the high primary frequencies, a narrow beam sediment echo sounder system can be realized even with small transducer sizes. This allows transmitting pulses with small aperture angles resulting in a small footprint, which means high lateral resolution. Figure 14 shows comparison of aperture angles between a parametric system and a linear system where deep frequent signal is transmitted directly. Direction of transmitted signal is constant for different frequencies and no side lobes and ringing effects are generated.

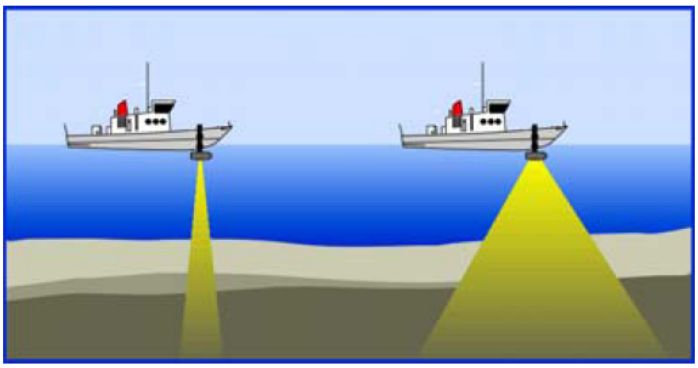

Figure 14: Comparison of aperture angles between parametric (left) and linear (right) systems (Innomar, 2005).

Resolution and penetration

Transmitting short signals allows to measure sediment layers with a high vertical resolution. Using a 10 kHz signal will be able to differentiate layers with a thickness of 7.5 cm (Innomar, 2005). Horizontal Resolution depends on aperture angle, pulse rate and ship speed. The small aperture angles (3.6°) of the parametric Innomar system lead to higher resolution. Pulse rate determines how often sound pulses are transmitted and therefore also affects horizontal resolution. The Innomar echo sounder system provides a pulse rate of up to 50 pulses per second. Slow ship speed will cause a higher coverage of the seafloor with transmitted and reflected signals. Standard electronic beam steering will also integrate ship movement information provided by the motion sensor. Every reflection from interfaces decreases energy of the traveling signal in addition to the normal signal attenuation. Energy loss depends on frequency but also on material properties. Thus, maximum penetration into the sediments will vary during a survey.

The Innomar system allows several additional adjustments for improvement of data quality. Detection sensitivity for transducers can be changed or ping rate can be increased for better lateral resolution. Recorded data can be visualized directly on board with a computer linked to the control unit. For onboard visualization the recording software converts measured travel time into actual depth using a fixed velocity of 1470 m/s. Not the whole received signal will be stored but only data in a specified window. Range of this window can be modified (varying during the cruise between 30 and 50 m) and start position must be adjusted permanently according to water depth. Innomar echo sounder system uses "ses"-output data format containing information about amplitude data, time, pulse length and depth values of high and low frequencies, as well as navigation. During the field campaign in Lake Ohrid high frequencies Freq1 and Freq2 of 105 kHz and 95 kHz were used resulting in a difference frequency of 10 kHz. With this signal a mean penetration of about 30 m was achieved and sometimes even sedimentary structures down to maximum 50 m could be resolved.

3.2.4. Instrument setup during the bathymetric campaign

Multibeam echo sounder

The multibeam transducer was placed at the bow of the vessel. The two transducers in a V-shaped configuration were attached to an especially designed frame at the bow of the vessel (Figure 8). Depth of the multibeam transducer was ca. 70 cm below water level.

Connection cables were leading from transducers to the control unit on the vessel and from there data was transferred to a data acquisition station, consisting of a Windows based personal computer. Movements of the vessel were recorded using an IXSEA OCTANS IV Surface motion sensor positioned on the vessel. This motion sensor was sending information about heave, roll and pitch to the data acquisition station. A sound velocity profile was imported and written to the swath files. The data acquisition station was also connected to a Garmin GPS 152 to get the exact position of the vessel. On the acquisition computer the software Hydrostar 3.5.3 form ELAC Nautic was used for operating. Sound velocity data stored on the CTD48M memory probe could be transferred to the computer. Electricity was provided by two generators. To ensure a continuous power supply a UPS was used.

Before multibeam measurements were taken out a calibration of the transducers had to be arranged because the precise adjustment needs to be known for accurate data acquisition. For

calibration one profile was measured with the multibeam systems in both directions. Usually this is done on relatively plain sea floor. Difference of measured data on both tracks allows determining the alignment the transducers. This information is used by the multibeam system during operation.

Sediment echo sounder

A frame built by colleagues from Cologne University was used to attach the sediment echo sounder to the vessel. Data was transferred to a personal computer with operation software ("SESWin") which served as recording and operating station for the sediment echo sounder. A complete overview of the used equipment can be seen in Figure A1 (appendix).

3.2.5. Profiles and Tracks

An already existing general bathymetric map of Lake Ohrid helped to define tracks for the multibeam survey. Using depths and calculating swath widths multibeam tracks were planned with the aim to achieve good coverage between adjacent profiles but also map a large part of Lake Ohrid in the time available. Greater depths allow much faster mapping of the lake floor because distance between adjacent profiles can be larger than in shallow water regions. However it must also be considered that great depths lead to lower resolution of the bathymetric data. Mean coverage of the seafloor for Lake Ohrid campaign was about five times the water depth.

During the entire BLOSSOM campaign nearly 300 km² of the lake floor was covered by multibeam echo sounder which is about 85% of the lake surface and more than 600 km of sediment echo sounder profiles were recorded nearly without interruption. Tracks of multibeam and sediment echo sounder profiles are presented in Figure 16 and sound velocity profiles were recorded at four different locations within the lake. An example of a velocity profile can be seen in Figure 15 representing the measured velocity distribution at the northern part of Lake Ohrid (Figure 16, d). All CTD measurements during the cruise are presented in the appendix (Figure A2).

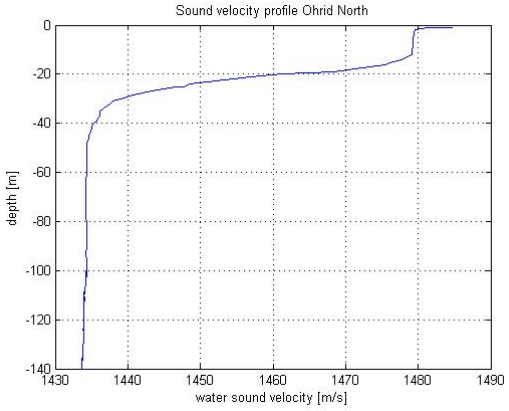

Figure 15: Sound velocity profile from the northern part of Lake Ohrid (Figure 16, position d).

Particularly in the area around Ohrid Bay a very good coverage of multibeam data was achieved as this region was crossed each day when leaving and returning to the harbor in Ohrid. Time shortage did not allow further mapping of the north western part near the Albanian/Macedonian border. During processing it turned out that the distance between

adjacent tracks in some parts of the Central Basin was too large hence leading to small gaps in the bathymetric map.

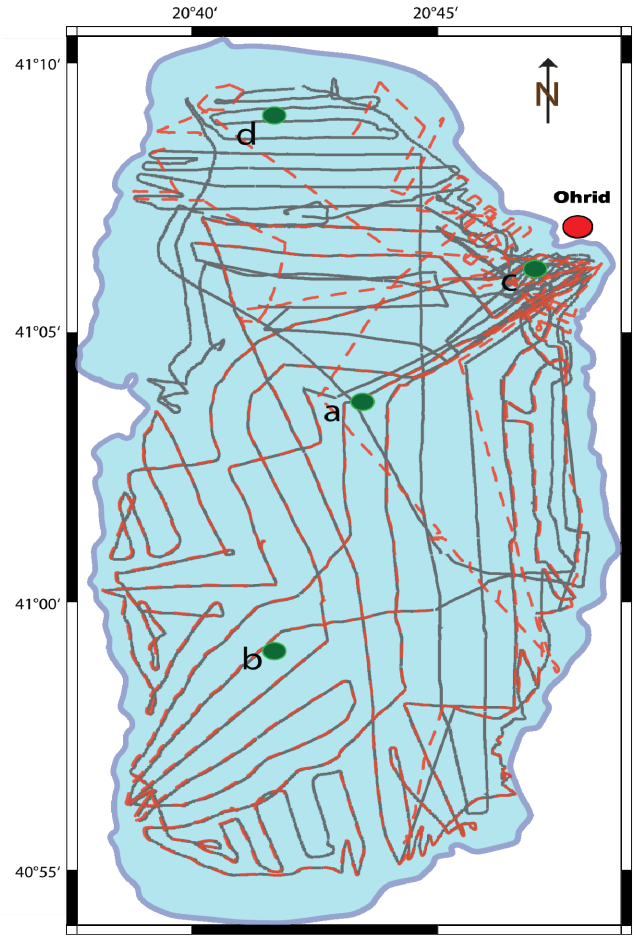

Figure 16: Multibeam (black line) and sediment echo sounder (dashed red line) profiles during BLOSSOM campaign in Lake Ohrid. CTD locations are marked with green dots (a-d).

For this thesis bathymetric data from the BLOSSOM campaign is used for studying morphological structures of mass wasting processes on the western and southern part of Lake Ohrid. Sediment echo sounder from this campaign as well as sediment echo sounder and multichannel seismic data from previous field measurements (2004, 2007 and 2008) are used to investigate composition of deeper sediments in these areas.

3.3. Data Processing

Sediment echo sounder data were already processed and were ready for further interpretation. In contrast bathymetric data needs several processing steps in order to generate a bathymetric map. These processing steps include clearing swath data from erroneous beams, adapting water velocity profiles and interpolating individual depth points to finally calculate bathymetric grids. In the following the processing approach for the bathymetric data will be explained in detail.

3.3.1. Bathymetric data

For bathymetry and later backscatter processing the software package MB-SYSTEM was used. This is an open source software package running under Linux/Unix environment. The software

holds several different programs for converting data, processing and editing data, showing statistics for collected data, etc.

MB-System can create grids presenting bathymetry, side scan or backscatter data. Generation of grids with MB-System is based on GMT (Generic Mapping Tools). GMT is also an open source software package for creating maps. Commands have to be written in text scripts that run under Linux/Unix. Output format of GMT scripts are generally specified as grids or postscripts.

Creating a data list

Multibeam data are stored as individual files in "xse" format (176 in total for the BLOSSOM campaign). First of all a text file is created containing all file names of the "xse"-files in the current working folder. This is done with the command **mbm_makedatalist**. Most of the MB-System commands are based on data lists which makes it easier to apply commands to many profiles at once. An extract of the data list can be seen in Figure A4 in the appendix.

Plotting preliminary results

Preliminary plots can be generated showing unprocessed bathymetric data of all files in the data list (Figure A6, appendix) using the command **mbm_plot**. By adding the name of the data list after MB-System commands they are applied to all profiles that are written in the data list. Additional options allow plotting contours or shaded relief images and can also show navigation tracks of all profiles.

Generating ancillary data files

For further processing of the bathymetric data ancillary data files have to be generated for every profile. These data files contain additional information like navigation, area of profile, ship speed, etc. and offer faster reading of swath data (Table 2). The command **mbdatalist** creates some of these additional files automatically (inf, fbt, fnv) for every mb94 file in the data list while others are generated if changes are made on single profiles such as navigation correction or editing of flags.

File extension	File description	Contained information
.inf	*file statistics*	metadata: geography, ship track information, numbers of flagged or zero beams
.fbt	*fast bathymetry*	provide faster acces to swath bathymetry data
.fnv	*fast navigation*	provide faster acces to navigation data
.par	*parameter files*	specify settings and parameters about processing swath data files
.esf	*bathymetry edit flags*	information about edited flags of swath files
.nve	*edited navigation*	information about edited navigation of swath files
.svp	*sound velocity profile*	information about vertical sound velocity distribution

Table 2: Ancillary data files used in MB-System

Creating sound velocity profiles

For processing bathymetric data it is essential to have proper information about sound velocity in the water column in order to calculate accurate depth and position of every target point at the sea bottom. We collected sound velocity profiles on four different locations using the CTD (Figure 16). As a first step all bathymetric data were processed using the deepest reaching sound velocity profile that was collected on the cruise (Figure 16 position: a; Figure A2, appendix, "Ohrid Deep"). This approach caused major problems and showed that the sound velocity distribution in Lake Ohrid is more heterogeneous than expected. Figure 17 shows an

example of mismatches between adjacent bathymetry profiles. Especially for the outer beams sound velocity profiles play an important role because of ray bending. Offsets between outer beams of adjacent profiles are very likely due to wrong sound velocity profiles. Using the other collected sound velocity profiles did not improve the situation significantly.

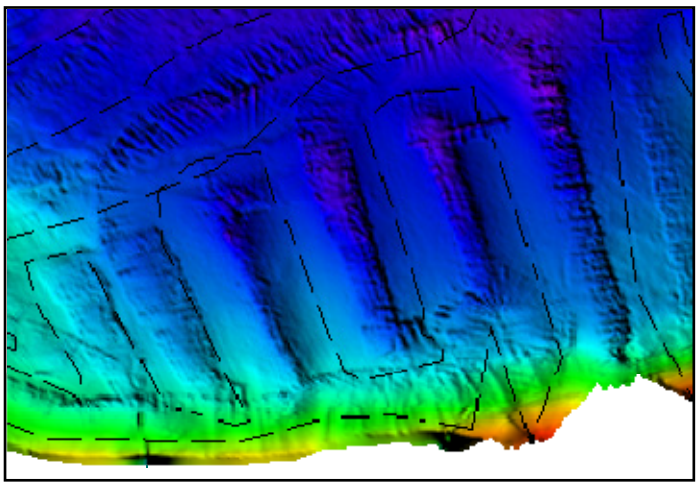

Figure 17: Example of mismatches between swath data of adjacent multibeam tracks (dashed lines) for bathymetric data that was generated by wrong sound velocity profile.

Sound velocity is varying significantly at different positions in the lake. The measured sound velocity profiles show clear depth dependence (Figure A2, appendix). As mentioned before our CTD measurements could only reach depths down to 250 m because of the length of the wire. Therefore no data of water layers in the deep central part of Lake Ohrid could be obtained. A cold current is floating through Lake Ohrid from south to north. Water of this current enters the lake at sub-aquatic springs near Sveti Naum (Figure 4). Due to high density it sinks under warmer water masses and was not detected by the CTD at the deepest parts of Lake Ohrid. However, this water mass has significant effects on the velocity and ray bending of the multibeam signals. Probably this cold water mass is one of the main problems during processing.

Mbsystem provides a program called **mbvelocitytool** which allows interactive generation of sound velocity profiles that can be adapted to data of bathymetry profiles. Every swath profile can be loaded individual with **mbvelocitytool**. Sound velocity can be adapted interactively and the effects of changes on the bathymetry are plotted. The residual view helps modifying the water sound velocity profile to determine best fitting profiles for the following processing steps. Figure 18 shows examples of well and poorly adjusted sound velocity profile in the **mbvelocitytool** environment.

Several different sound velocity profiles were generated with **mbvelocitytool** to determine a profile that sufficiently fits all data. This approach, however, was not successful and the major parts of the data still showed offsets between two adjacent tracks. For this reason five different sound velocity profiles were generated representing different parts of the lake (Figure 19). This approach allowed accounting for regional variations in sound velocities.

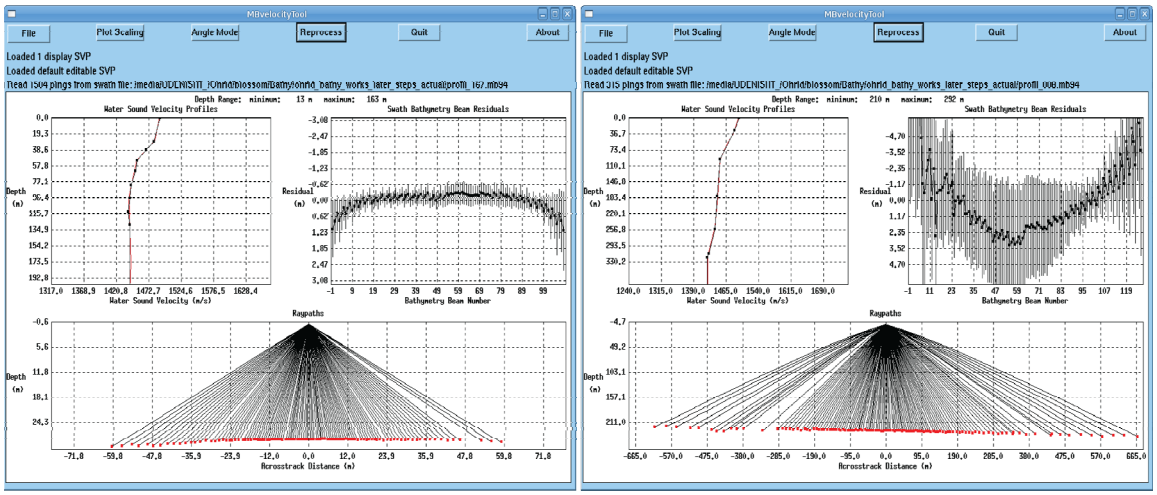

Figure 18: Swath data opened with mbvelocitytool. Examples of well adjusted (left) and poorly adjusted (right) swath data characterized by the swath bathymetry beam residual view in the upper right window. Upper left window shows actual sound velocity profile.

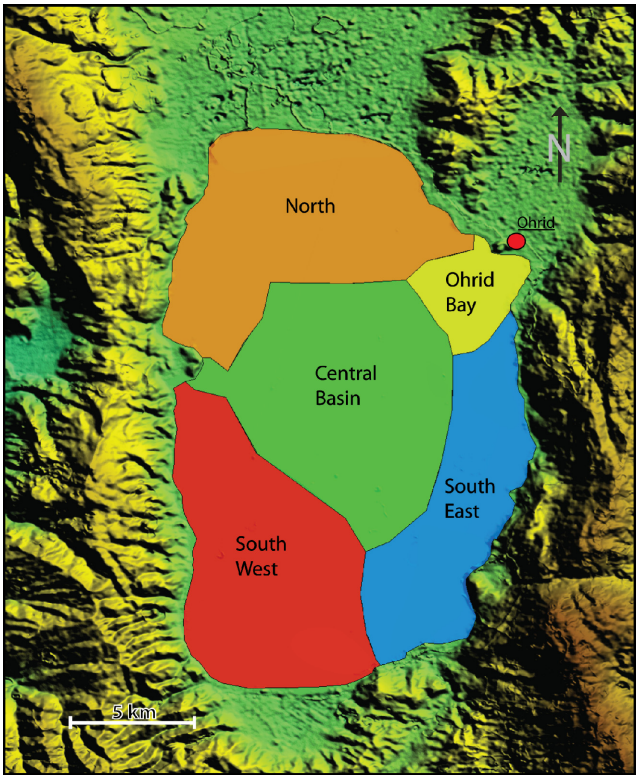

Figure 19: Sound velocity zones used for processing bathymetric data of Lake Ohrid. Profiles demonstrating velocity-depth distribution of every zone are presented in Figure A3, appendix.

Figure 19 shows the division of Lake Ohrid in five regions. Every region stands for one sound velocity profile generated with **mbvelocitytool**. Hence five new data lists were generated containing only profiles of a distinct region. An example of an artificial generated water sound profile can be seen in Figure 20 representing the velocity profile used for the northern part of the lake the remaining ones can be seen in the appendix (Figure A3).

The representative sound velocity profile that shall be used for the later processing was written in the ".par"-files of the corresponding data file.

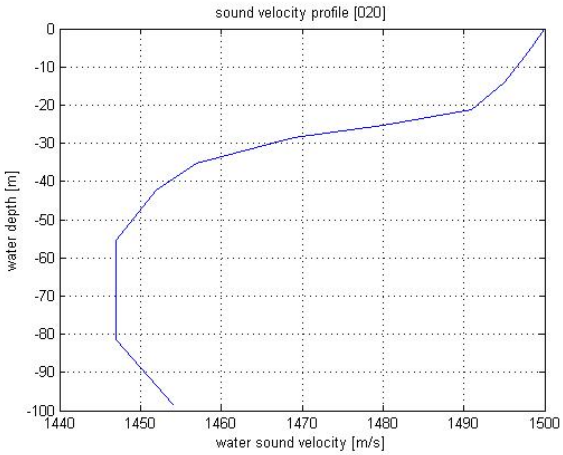

Figure 20: Representative sound velocity profile of the northern part of Lake Ohrid generated with mbvelocitytool.

Cleaning and editing bathymetric data

A first look at the bathymetric map shows several features which do not reflect actual seafloor topography. Instrument noise or strong movement of the vessel can produce artificial peaks in the bathymetric data that must be corrected. The **mbclean** tool provides a filter mechanism for removing single beams in every swath file. This is a useful tool for automatic flagging of errors in the bathymetric data. **Mbclean** provides a large variety of options for adjusting the filter mechanisms, like flagging outer beams, flagging beams outside defined depth ranges, etc. In general the outer beams of a swath do not provide very reasonable data. The signal to noise ratio from these beams is rather high and errors from the sound velocity profile are amplified here. While Ohrid Bay Zone and North Zone contain rather shallow bathymetry and the outer beams provide more reasonable information in shallower than in deeper water less of the outer beams of every swath are flagged in these zones. A cleaning option that flags so called "bad rails", single swaths that seems to be mirrored with respect to the previous and later swaths was helpful as they appeared often in the Lake Ohrid data. These swaths are probably due to data errors and do not reflect actual topography changes. Another option removes beams that exceed a certain slope. This command reduces spikes (either across track or along track) in the data that are unlikely to occur in nature. Large variations from mean value of a swath can be flagged by an additional option but was not necessary for our data. Actual used commands for cleaning and editing bathymetric data of Lake Ohrid can be seen in the appendix. Choosing strict filter options with **mbclean** could lead to removing real features on the lake floor. Smaller blocks may be deleted because they exceed for example the spike filter value of **mbclean**. But even with a strict filter settings, not all data errors can be flagged. Therefore the **mbclean** command was used rather conservative which made it essential to have a manual look at every single swath of all profiles using **mbedit**.

The tool **mbedit** allows opening every single profile and to flag or restore single beams. Every ping is shown as a line combining all beams of this ping. Beams that were flagged by the previous **mbclean** command are marked in green. Red beams represent additional manual flagging. Only the black data points are used for later processing. Figure 21 shows an example of the **mbedit** program with opened swath files. Additional examples of rather poor quality swath data can be seen in the appendix (Figure A7).

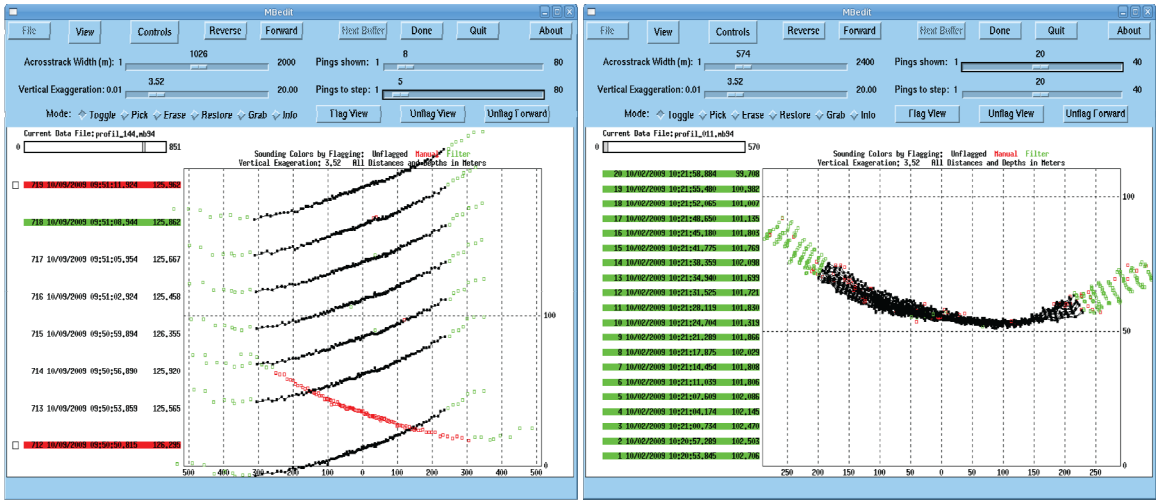

Figure 21: Example of several pings of an opened swath file with mbedit showing different viewing options. Black dots represent depth points used for later processing; green and red dots represent flagged depth points either with mbclean or mbedit. Outer beams are flagged due to high noise ratios in these areas. Left: waterfall view showing example of a "bad rail" (red dots). Right: across track view of a series of pings without significant errors.

The number of pings that are displayed in the window can be adapted as well as the across track width. Different viewing options are possible to change between waterfall view (where single pings are presented separately, one after the other) of along or across track view (following pings are shown at the same time). Vertical Exaggeration can be modified for better investigation of the data with respect to artificial spikes. Unrealistic depth values can be removed if they were not already flagged already by the **mbclean** filter. For some cases it is rather difficult to distinguish between real and artificial. Also sometimes the **mbcelan** filter erased beams that are obviously no artificial depth soundings but real structures on the lake floor. These beams can be restored so that they will be included in the calculation of the bathymetry. Changes regarding flagged or restored beams are written into the "esf"-files of every profile.

Processing bathymetric data

After applying filter mechanism and manual editing the swath data of all profiles are processed with the **mbprocess** command. All changes that are made so far will be taken into account. Sound velocity profiles will be used to recalculate the depth for individual beams taking ray bending into account. **Mbprocess** uses the "par"-files for general information of every profile like sound velocity, etc., and the "esf"-files for information about flagged or edited beams. The command will be applied on all profiles listed in the data list and will generate new swath files with the extension "p.mb94" instead of ".mb94". These files now contain the processed and corrected swath bathymetric data which can be used for creating a bathymetric map.

Creating bathymetric grid

Calculating a grid is the last step in the processing flow. Before calculating the grid a new data list must be created now listing all the filenames of the processed swath files ("p.mb94"). The **mbgrid** tool is based on GMT commands. A variety of settings are available like extracting areas, applying different gridding algorithms or interpolation methods and output formats. For the interpolation method it turned out that the best results were achieved by using a weighted Gaussian mean algorithm. On the Lake Ohrid data an **mbgrid** command was used generating a

topography grid as output with a grid cell size described in meters. One option in **mbgrid** commands is a clipping option. For Lake Ohrid data this options was used in a way that all grid cells with no swath data will be filled by interpolation within a distance of 15 times the grid cell size. Grid cells farther away are set to NaN (Not a Number). Four different bathymetric maps were generated with grid cell sizes of 5x5 m, 10x10 m, 20x20 m and 50x50 m.

The compilation of all MB-commands used for Lake Ohrid data processing can be seen in the appendix.

3.3.2. Backscatter data

MB-System also provides tools for processing and visualization of backscatter data. The procedure is similar to processing bathymetric data. First amplitude data is corrected by averaging over a specified angle before amplitude data can be processed and plots can be generated using MB-System commands that will produce a GMT script. For backscatter processing a data list is generated containing the original "xse"-files of all profiles. The "esf"-files containing information about flagged beams are also in the same folder. Again the exact commands used for backscatter processing are listed in the appendix.

Correction for amplitude data

Every swath sonar data file contains bathymetric data but also amplitude data. For making use of the amplitude data the first step is a command called **mbbackangle** which reads out these amplitude data and generates tables of average amplitude values. The angle over which average amplitudes shall be calculated can be specified. For calculating backscatter data from Lake Ohrid data an **mbbackangle** command was used where amplitude data were selected from the files listed in the data list. An additional option allows setting number of grazing angle bins and the maximum angle that is considered (here: 63 bins were summarized and the maximum angle was set to 75°, 150° for the whole swath). For each profile a correction table is generated by the **mbbackangle** command. This correction table with the suffix ".aga" contains relation between amplitude and grazing angle for each series of averaged pings. The amount of individual pings averaged for each amplitude-against-grazing-angle table was set to 50.

Processing backscatter data

Processing the amplitude data of all profiles in the data list is done by **mbprocess**. **Mbbackangle** has also created modified parameter files (".par") for every profile so that the **mbprocess** command now uses amplitude data for processing. The **mbprocess** program will read the correction tables (".aga"-files) of every swath file and will generate processed files with the suffix "p.mb94".

Creating backscatter mosaic

Processed backscatter data can now be visualized with the command **mbmosaic**. Several parameters can be added to the **mbmosaic** command to specify the output mosaic like grid spacing and different interpolation algorithms. As for the procedure of bathymetric data processing a new data list must be created now containing all the processed files. The **mbmosaic** command allows numerous options. Most important ones are specifying the grid cell size for the amplitude data that creates a mosaic of all profiles in the data list. In this case a 5x5 meter grid was adjusted. Spline Interpolation was applied and clipping dimension for spline interpolation

was set to fill data gaps within five times the grid spacing (grid cells farther away are set to NaN. A Gaussian weighted mean mosaicing filter was applied. This allows determining which data points are used for the mosaic. Only points with priorities greater than the priority range value are taken into account. Format of the output grid can be modified. Grid formats like ascii tables, binary files, ArcView format etc. can be given as output. Here grid format was set to netCDF file for reading with GMT. Longitude and latitude can be specified and boundaries of the output grid can be set. Using a prioritization table gives the possibility to define the priority of data points with respect to the grazing angle. Priority can vary between 0 and 1 for all single angles of a swath. A priority table used to amplify the beams in the center of the swath is shown in Figure A5 (appendix).

Running the GMT script that is generated by the **mbmosaic** command will now produce a postscript-file picturing backscatter data of the requested area allowing to adjust additional options like color tables.

3.3.3. Sediment echo sounder data and Seismic data

The Innomar System used during the BLOSSOM campaign 2009 produced "ses"-files from every profile that had only be converted to "segy" (using the program "SES-convert") for visualization. Multichannel seismic profiles from previous campaigns were already processed as well as sediment echo sounder data from these surveys.

3.4. Software for imaging and interpretation

Global Mapper

For visualization of the processed bathymetry and backscatter data the software Global Mapper was used. It allows to load grid data and to geo-reference image datasets, to perform measurements and display elevation data also in 3D. A lot of additional options like generating shapefiles or interpolating point data were used for analyzing and imaging datasets.

Fledermaus

Fledermaus software was used for imaging elevation data sets and is especially suitable for generating 3D perspectives. Grid data has to be converted into SD files (using the program "DMagic") before importing into Fledermaus.

Kingdom Suite

Seismic and sediment echo sounder data were analyzed using the software Kingdom Suite, which allows examination and interpretation of acoustic data sets by detection of horizons, fault structures or mass movement deposits.

4. Results

4.1.Bathymetric map of Lake Ohrid

Results of the processed multibeam data are visualized in a bathymetric map of Lake Ohrid. A first overview can be seen in the 20x20 m grid cell size map in Figure 22. Several artificial features are still visible in the map either due to bathymetry processing errors or interpolation between non-overlapping adjacent tracks. A small strip of rather smooth and plain bathymetry at the coastal limit of the acquired bathymetry is caused by grid cell spacing and resulting interpolation artifacts. Beside some remaining errors several real features can be identified on the bathymetric map; these features will be described in the following chapter:

- The deep central basin and Magic Mountain

The central part of the lake is characterized by a large and rather flat basin enclosing an area of about 100 km² (28% of total lake surface) with depths around 230 m (Figure 22). Two slightly deeper areas are located at its edges. A northeast – southwest elongated depression is located at the north western edge with a length of 6 km and depths of up to 260 m. The deepest part of the Lake can be found at the southeastern border of the central basin with a maximum depth of 293 m. The overall basin has a relatively smooth topography without any blocks or significant changes in morphology. The only exception is the so called "Magic Mountain", a basement high in the southeastern corner of the central basin (Figure 22). Steep flanks of more than 23° characterize this structure which rises up for more than 120 m from the deepest region of the lake. It has a north-south orientated elongated shape with a total length of 1.6 km and a width of about 600 m. An additional smaller local high is located south of the Magic Mountain rising ~40 m above the surrounding lake floor but showing similar steep slope angles (marked by MM2, Figure 22).

-Steep slopes along the eastern and western boundary margins

The eastern and western margins show rather steep slope angles. Especially northwest of the central basin a step of over 100 m height difference occurs. Slope angles have average values of about 6° but locally exceed 20°. The southern part of the western slope area has a more or less constant slope angle of 3-4° except for the deepest part of the slope (transition to the Central Basin), where a prominent step of about 20 m occurs (Figure 22). In contrast the Eastern slope area shows more variations. Several small plains are situated next to small depressions and steep scarps of 30 to 50 m height. In general the transition from steep flanks into the central basin is very abrupt on both sides.

-Shallow areas in the southern and northern parts

The northern and southern areas are defined by more shallow regions than the eastern and western flanks. Slope angle is usually decreasing with increasing depth and the transition to the Central Basin is very smooth. A steep shelf break with an adjacent smoother area is observed at the southern margin of the lake. Slope angles of about 5° occur close to the coastline while values of 0.5-2° are found towards the Central Basin. Both shallow areas in the north and south show numerous channel-like structures close to the coast (Figure 22).

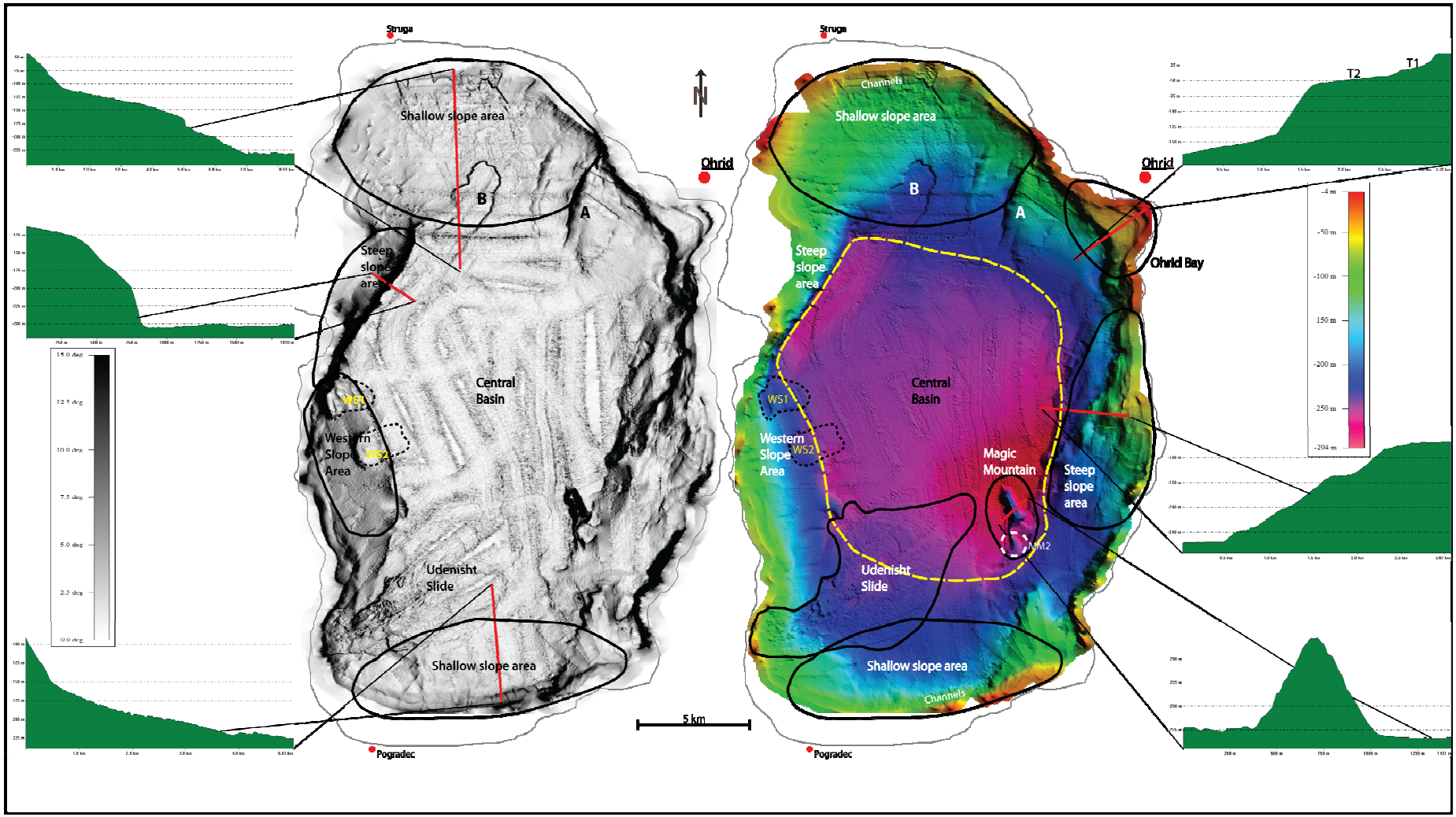

Figure 22: Bathymetric overview map of Lake Ohrid based on multibeam survey with a grid size of 20x20 m. Multibeam tracks are still visible especially in the Central Basin. The grey line marks the shore of Lake Ohrid. Highlighted are areas of special interest together with a cross section profile of their topography; Mass movements along the Western Slope Area are marked with WS1 and WS2 the large graben-like structure in the north with B. The elongated ridge is illustrated by A, MM2 shows a smaller elevation south of Magic Mountain. (see text for detailed description).

-Terrace structures at Ohrid Bay

Two terraces running parallel to the coastline mark the area around Ohrid Bay. The first terrace (**T1**, Figure 22) is located at about 30 m water depth and drops down to about 55 m to the second terrace (**T2**). With a width of about 1 km the gently dipping (< 1°) area of the second terrace is followed by another distinct morphological step of about 75 m from where on the lake floor continuously deepens into the Central Basin with a slope angle of 1.5.

- Large ridge structure northwest of Ohrid Bay

Northwest of Ohrid Bay a large north - south elongated ridge like structure can be traced along a distance of 4 km (marked as A in Figure 22). The morphological step (>10°) from this ridge results in a height difference of more than 50 m.

- Graben like mass wasting structure in the northern part

A prominent graben like mass wasting feature (marked as B in Figure 22) can be seen running from the northern shallow area of the lake to the transition between the steep western part and the Central Basin. Steep sidewalls of up to 10 m in height open up a ca. 1.5 km wide depression which is elongated in northeast to southwest direction and extends for about 3.5 km with decreasing height of the sidewalls towards its southwestern end.

- Sliding structures Udenisht

Within the southwestern part of Lake Ohrid a large area is characterized by a hummocky topography. Sidewalls are clearly visible constituting the boundaries of this area that was allocated to the major Udenisht Slide Complex (Figure 22). The Udenisht Slide Complex is the main objectives of this study and will therefore be discussed in detail later in this thesis.

-Sliding structures along the Western Slope Area

Beside the large Udenisht Slide two other structures along the western slope can be detected on the lake floor indicating mass movement events (Figure 22, WS1 and WS2). Their dimensions are much smaller than the Udenisht event and their effects on the lake floor are not that obvious. The appearance of additional mass wasting structures along the western slope can be used to study mass wasting deposits with similar characteristics and hence comparable trigger mechanism as for the large Udenisht Slide Complex. Closer investigation of this special area will be done in the next chapter.

4.2.Western slope area

Within the western slope area the bathymetric data allows to identify two mass movement deposits (Figure 23, WS1, WS2). Sediment echo sounder and seismic data will provide closer determination of the internal structures of these deposits. The large Udenisht Slide at the south-western part of the western slope area will be described in a separate chapter.

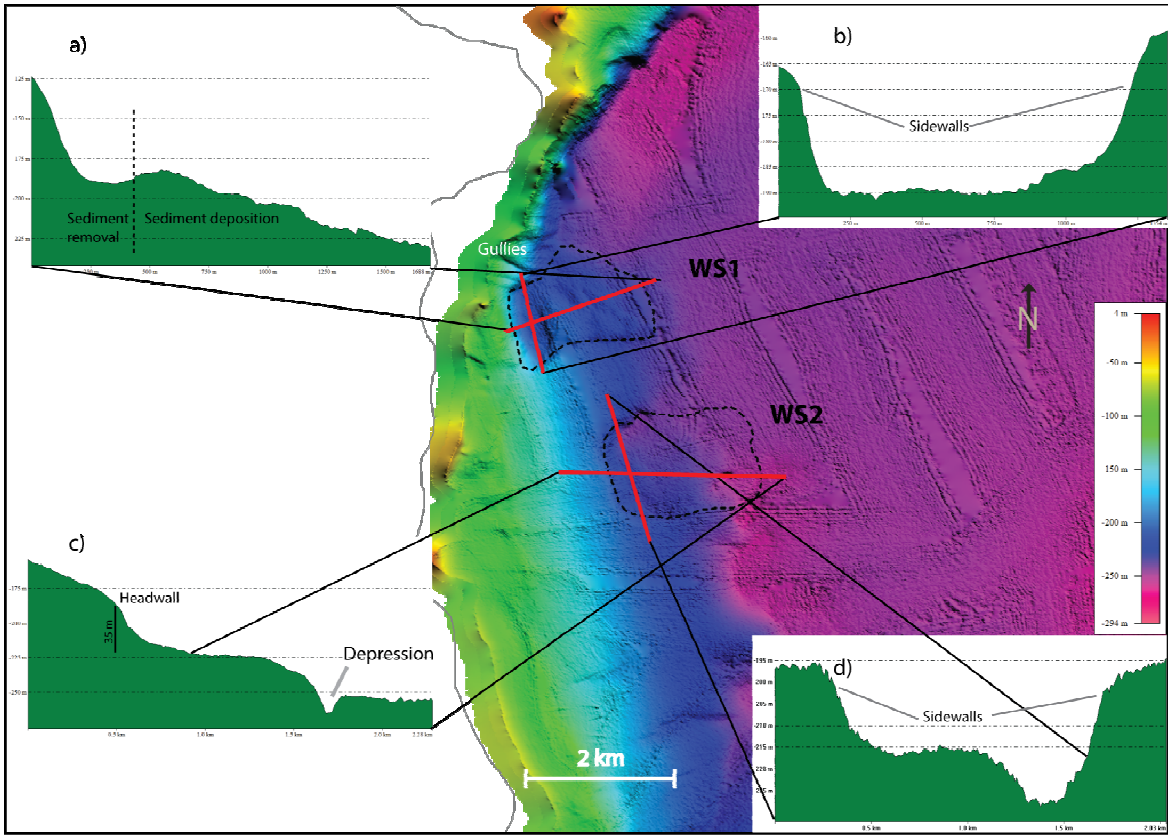

Figure 23: Bathymetric map of WS1 and WS2 mass wasting areas (grid size: 10x10 m). Steep head and sidewalls are imaged for WS1 in profiles a) and b) with channel structures north-west of WS1. Steep sidewalls appear also along WS2 (profile d). A circular depression is visible at transition to Central Basin in WS2 (profile c).

4.2.1. WS1

The WS1 mass movement structure is characterized by a steep headwall and sidewalls along its up-slope area as well as sediment accumulation at the transition zone between western slope and Central Basin (Figure 23, profiles a and b). The bathymetric data allows separation of WS1 into an area of erosion (0.3 km²) and an area of accumulation (1.2 km²), (Figure 23, profile a). These two areas are divided by a north south elongated ridge of nearly 10 m height that is dipping towards the headwall. At the up-slope part of WS1 steep and high (max. 30 m) sidewalls appear running parallel from west to east and defining the width of WS1 to nearly 1 km. The headwall cannot clearly be identified because of overall extreme steep flanks (>16°) of the western slope area in this region. The area of accumulation is elevated higher than the surrounding lake floor of the Central Basin allowing relatively good estimation of the down-slope extension of WS1. North of the WS1 area three gullies more than 500 m long can be traced from the coast (where bathymetric data is available) towards WS1 (Figure 23). They have widths in between 50 and 90 m and incision depths of 3 to 7 m. It seems that they are cut by the northern sidewall of WS1.

Seismic and sediment echo sounder profiles crossing the WS1 slide (Figure 24) image the internal structure of the WS1 slide. Unfortunately only those two seismic/sediment echo sounder data are available from this mass deposition structure and imaging of the mass transport deposits is poor. Several layers of rather undisturbed sediments can be detected beneath the lake floor with a thickness of about 0.1 - 0.2 sec two-way-travel time (TWT) on the north south sediment echo sounder profile of Figure 24a. Below these layers no further reflections can be imaged and a transparent unit of the WS1 deposition can be seen. However, interface between well stratified reflectors and WS1 unit beneath (dashed line in Figure 24) shows an irregular topography especially at the northern edge of WS1. Penetration of sediment echo sounder data is too low to highlight deeper reflections within or below the transparent body. The lateral extension of the WS1 deposition coincides with an elevation at the lake floor. A small part of the depositional area is displayed in a west to east running multichannel seismic profile (Figure 24b) crossing the northern part of WS1. A thin layer of undisturbed sediments (~0.1 ms TWT) is underlain by disturbed and deformed reflections. These depositions also show lower amplitude values. To the west this deformed body is limited by a steep eastward dipping reflection which more or less parallels the western slope. Although seismic data allows detecting deeper reflections, it is still difficult to determine the base of the chaotic unit representing WS1. Just below WS1 deposition again deformed reflections of low amplitudes can be seen alternating with areas of high amplitude reflectors. This setting does not allow identifying a well defined base of the mass transport deposits. While the western slope is characterized by only few reflecting layers lying above the acoustic basement, the transition to Central Basin shows increasing amount of undisturbed sedimentary successions. Sediment packages can be traced down for more than 0.1 sec TWT where they are lying on top of the acoustic basement with increasing thickness of undisturbed reflectors east-wards. A striking basement high is located in a subsurface depth of ca. 0.15 sec TWT about 1 km east of WS1. At the eastern end of the seismic profile the parallel reflections are disturbed by a fault (dashed line Figure 24) which affected almost the entire sediments except the uppermost layers.

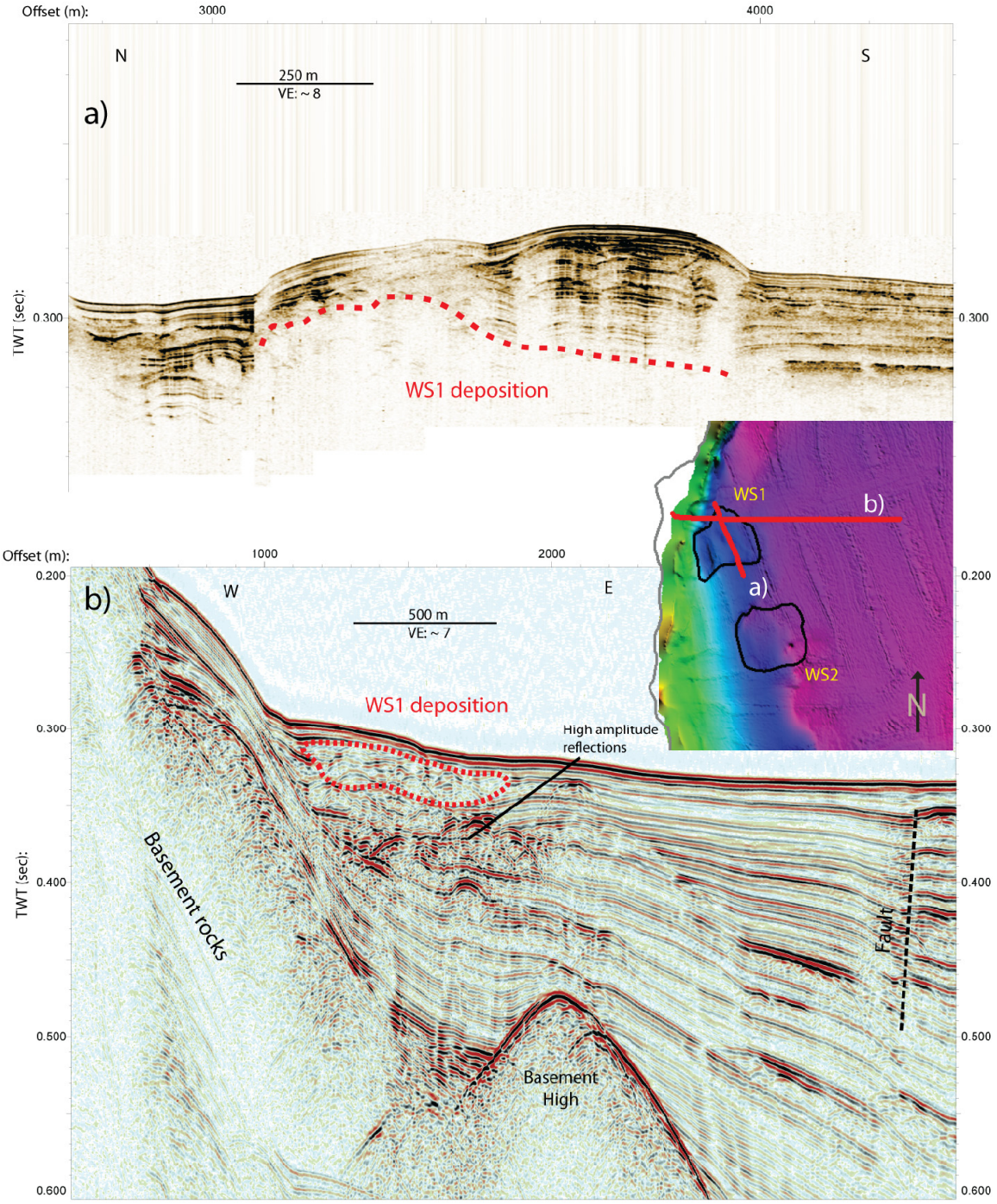

Figure 24: (a) Sediment echo sounder- and (b) multichannel seismic profiles crossing WS1. Area above the slide deposits shows local elevation at the lake floor (a). WS1 deposits are marked by the red dashed line. Beneath WS1 deformed zones of low amplitudes as well as high amplitude reflections can be seen; at the eastern part of the profile a large fault zone is located. See inset map for locations of profiles.

4.2.2. WS2

The upper part of the WS2 mass movement can also be clearly detected within bathymetric data (Figure 23). Its down-slope extension was defined using sediment echo sounder and seismic data (Figure 25). With an areal coverage of 1.8 km² WS2 slide has similar dimensions as WS1. With respect to its area the WS2 mass movement shows relatively high sidewalls (20 m, Figure 23, profile d) in the upper part and a huge headwall of 35 m (Figure 23, profile c). The slope perpendicular west-east crossing profile c) shows significant differences in gradient along the slide. Gradients of 3.5° above the slide are followed by a steep headwall (>13°) and a rather horizontal plateau of about 500 m length (Figure 23, profile c). In the lower part of the slide area (in transition to the Central Basin) a circular depression (130 x 140 m) with a depth of about 20 m is visible in the bathymetry. The depositional area of WS2 is not marked by significant sediment accumulation at the lake floor as it was seen for WS1. Therefore only seismic and sediment echo sounder data provide information on the extent of this mass movement.

Figure 25 shows two acoustic profiles along the WS2 structure pointing out the steep headwall and the different slope angles in slide direction. Several parallel and undisturbed sediment layers can be observed up-slope the headwall while the headwall itself is characterized by low reflections and penetration (Figure 25a). Layered sediments (with a thickness of about 0.02 sec TWT) are found on top of a rather transparent unit (marked by the green dashed line in Figure 25) further down-slope the headwall. The uppermost part of this transparent body of the WS2 mass movement still shows some small deformed reflections. This unit can be traced for nearly 1.5 km in slide direction. The base of the transparent unit can only be detected in the multichannel seismic profile (Figure 25b, dashed green line) resulting in a mean thickness of approximately 0.02 - 0.03 sec TWT. Similar to seismic profiles from WS1 (Figure 24b), Figure 25b shows that sediments along the western slope are deposited more or less parallel above the acoustic basement. A thickening of these parallel layers can be seen in direction to the Central Basin. Some high amplitude reflections within this sedimentary succession are visible in the multichannel seismic data. The WS2 deposition clearly contrasts the mainly undisturbed reflections of the western slope area as well as the Central Basin. A bright spot (an area of spatial limited high amplitude values) is visible within sediment successions above the transparent unit of WS2. The location of the bright spots coincides with the position of the depression that was found in the bathymetric data.

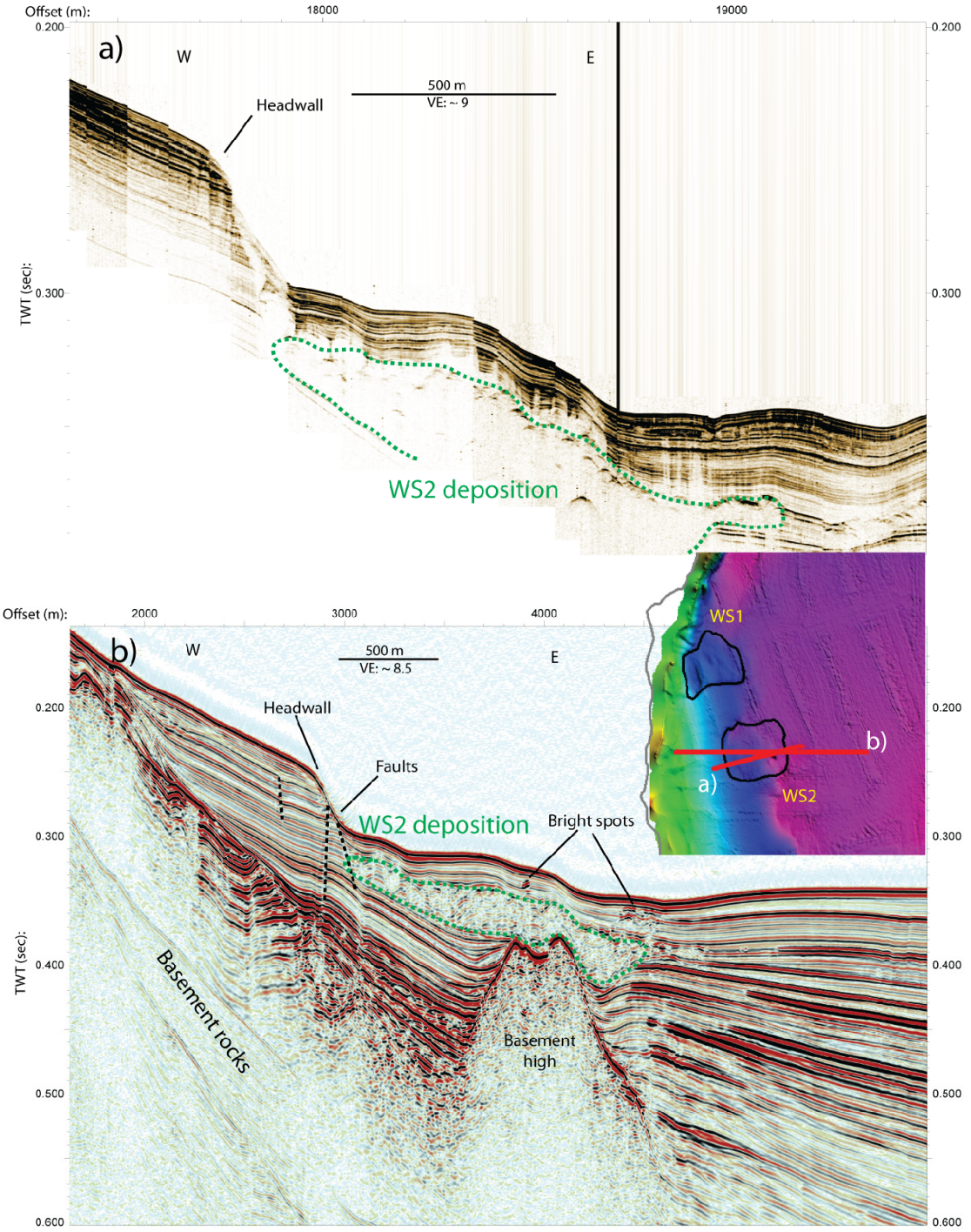

Figure 25: Sediment echo sounder (a) and multichannel seismic (b) profiles crossing WS2. Undisturbed parallel reflections are visible above the transparent WS2 deposition body (marked by the green dashed line). A basement high is located just below WS2 (b). Faults close to the steep headwall are visible as well as bright spots in uppermost sediment layers above WS2 deposition. See inset map for locations of profiles

4.3. Udenisht Slide Complex

The Udenisht Slide Complex is one of the largest mass movement events that occurred in Lake Ohrid. Figure 26 shows the area affected by the slide either by removal or deposition of sediments during the mass movement process. The amounts of removed or accumulated material were obtained using bathymetry and sediment echo sounder data. The affected region covers an area of more than 28 km² representing nearly 8% of total lake surface.

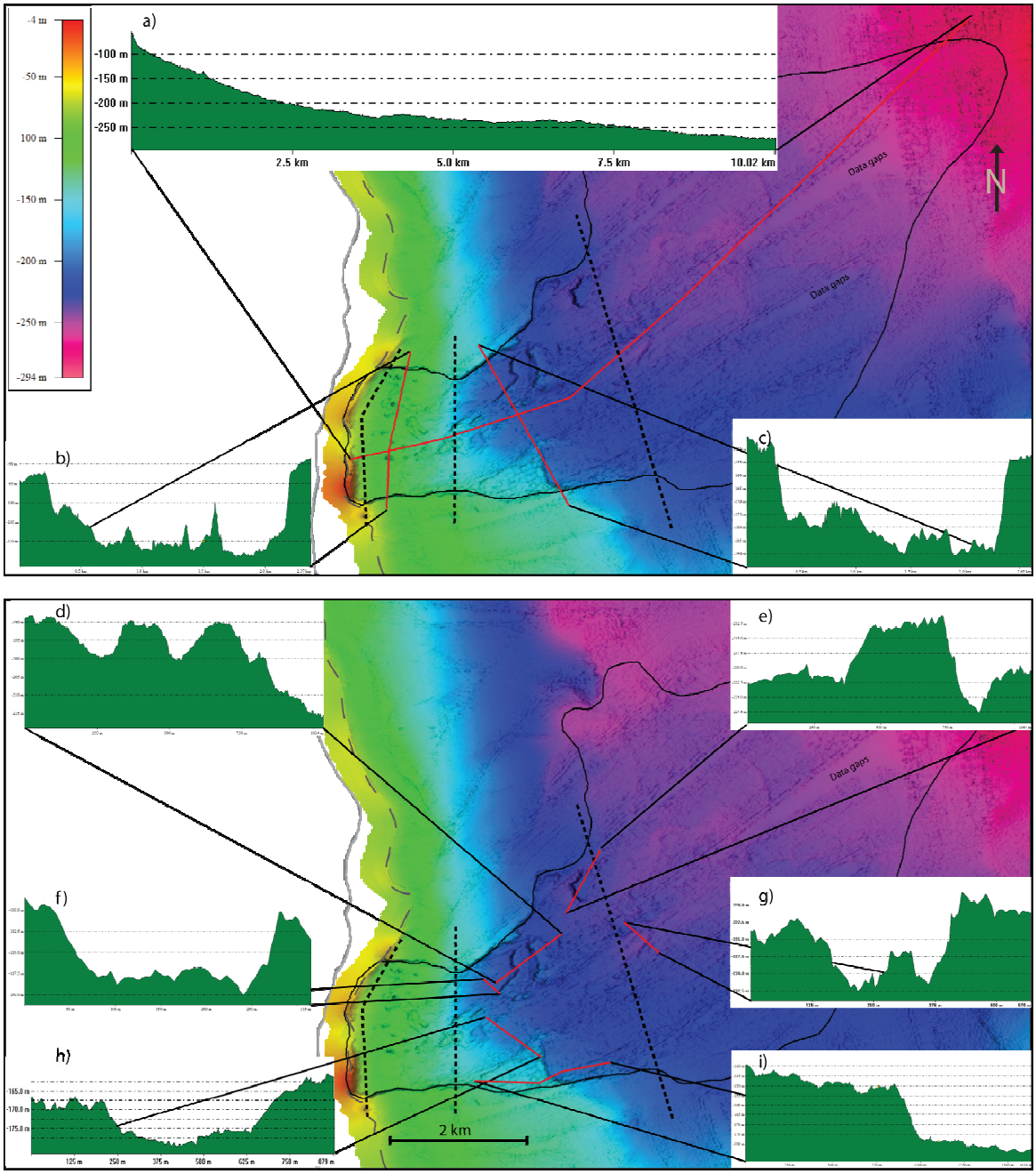

Figure 26: Bathymetric maps of Udenisht Slide area (grid size: 10x10 m). Thin black line indicates extension of the region affected by Udenisht Slide. Dotted lines mark different segments (Headwall area, Upper, Middle, and Lower Segment). Lake floor profiles (a-c, red lines) present the general morphology of the slide. Profiles d-i mark specific structures detected in the slide area. Bathymetric maps have same scales while bathymetric profiles show different scales. Grey line demonstrates the shoreline, dashed brown line mark extension of bathymetric data and indicate zones of interpolation. Areas of data gaps are filled by interpolation as well.

4.3.1. Morphology of the slide

Bathymetric data mark the outline of the slide especially in its upper part (less than 160 m water depth) because several deformation features related to the sliding process can still be observed on the lake surface. In the lower part especially sediment echo sounder and seismic data were used to determine extensions of the slide. In order to characterize affected areas of the slide complex it has been divided into four segments by means of difference in slope angles: (1) extremely steep headwall area, (2) the blocky Upper Segment (ca. 3° – 5°), (3) the heterogeneous Middle Segment (ca. 1.5° – 3°), and (4) the Lower Segment with its smooth topography (< 1.5°) (Figure 26). A detailed map of the Udenisht area is shown in Figure 26 and Figure 27 including profiles and prominent structures which will be described in the following paragraphs.

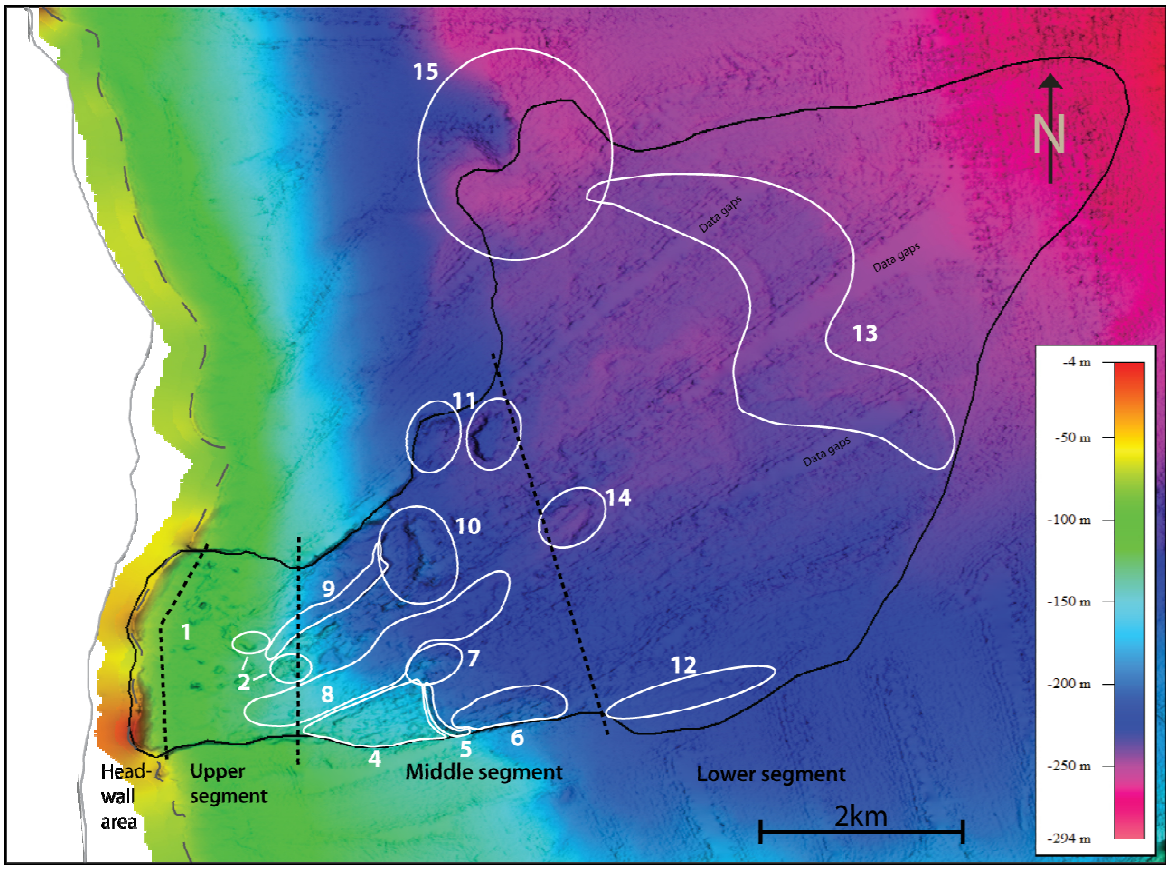

Figure 27: Detailed bathymetric map of Udenisht Slide (grid size: 10m x 10m) showing prominent structures detected in the slide area. Structures (1-15) are described in the text. Grey line demonstrate the shoreline, dashed brown line mark extension of bathymetric data and indicate zones of interpolation. Areas of data gaps are filled by interpolation as well.

Headwall area

The headwall area is characterized by steep slopes of 10° - 30° (Figure 27, profile a) but no distinct head scarp can be found. Unfortunately, multibeam measurements could not be continued closer to the coastline because the lake floor is too shallow to obtain a reasonable coverage of multibeam tracks. Therefore bathymetric data was collected from the Udenisht Slide area not shallower than about 25 m. Within the measured area no distinct headwall of the slide

could be imaged. Nevertheless, the southern part of the assumed headwall area shows an extremely steep zone that might represent a part of the headwall. A morphological step of nearly 45 m and a slope gradient of more than 25° can be observed in this area. Artifacts caused by interpolation at the edges of the bathymetric data are present and subsequently influence the analysis of data along the outer beams of the tracks. This can easily lead to misinterpretation of the headwall area and hence makes it difficult to locate the exact origin of the mass movement.

Upper Segment

The sliding area in the upper segment is characterized by nearly vertical sidewalls with heights of 10 to 25 m (Figure 26, profile b). Width of the slide restricted by the sidewalls remains relatively constant between 2 and 2.2 km resulting in an eastward course of the slide in the Upper segment before it shifts to a north-eastern direction (falling together with the start of the Middle Segment). Highest sidewalls (about 20 m) of this section are located on the northern side in water depth of less than 100 m. Lake floor topography of the upper section is marked by numerous smaller and some larger blocks (Figure 27, 1). Most of these blocks have heights of around 5 m except for two blocks that even reach heights of almost 10 m. Average dimensions of blocks in the upper part of the sliding area are about 25-35 m in width and 40-60 m in length. Among these blocks there are several elongated chunks; some are arranged with their long axis in slide direction. Others have a more cone shaped appearance. For those close to the northern sidewall it is difficult to distinguish single blocks because several blocks seem to be connected or are interacting with each other. No blocks are found in the southern part of the upper segment. Two extremely large blocks with dimensions of 320 m x 130 m and 340 m x 180 m, respectively, are determined in the upper segment; both have heights of about 5 m (Figure 27, 2).

A map highlighting the slope angles is shown in Figure 28. Single blocks in the upper segment are clearly exposed (Figure 28, 1) as well as the steep northern and southern sidewalls. In addition, Figure 28 shows a small edge on the eastern part of the upper segment defined by a change in slope angle from 3° to locally up to 7° towards the middle segment. This edge forms a lineament that is crossing the upper segment and continues about 1 km northwards of the sliding area indicated by strong changes in gradient (Figure 28, 3). In the middle part of the upper segment this line almost disappears but can clearly be observed again at the southern margin of this segment. The height of the northern sidewall is decreasing towards the middle segment and even disappearing at approximately the same position where the north south elongated lineament is reaching the slide area (Figure 28, 3).

Middle segment

In the middle segment (water depth of 150-220 m) a widening of the sliding area coincides with a slight change in direction. The widening results from an opening of the northern sidewall towards the north-east direction while the southern sidewall is still aligned in east-west direction. The southern part of the sidewall is characterized by steep and high (30 m) scarps (Figure 26, profile c) with decreasing heights down-slope (10 m). Only in more than 160 m water depth their height is again increasing to 20 m and more.

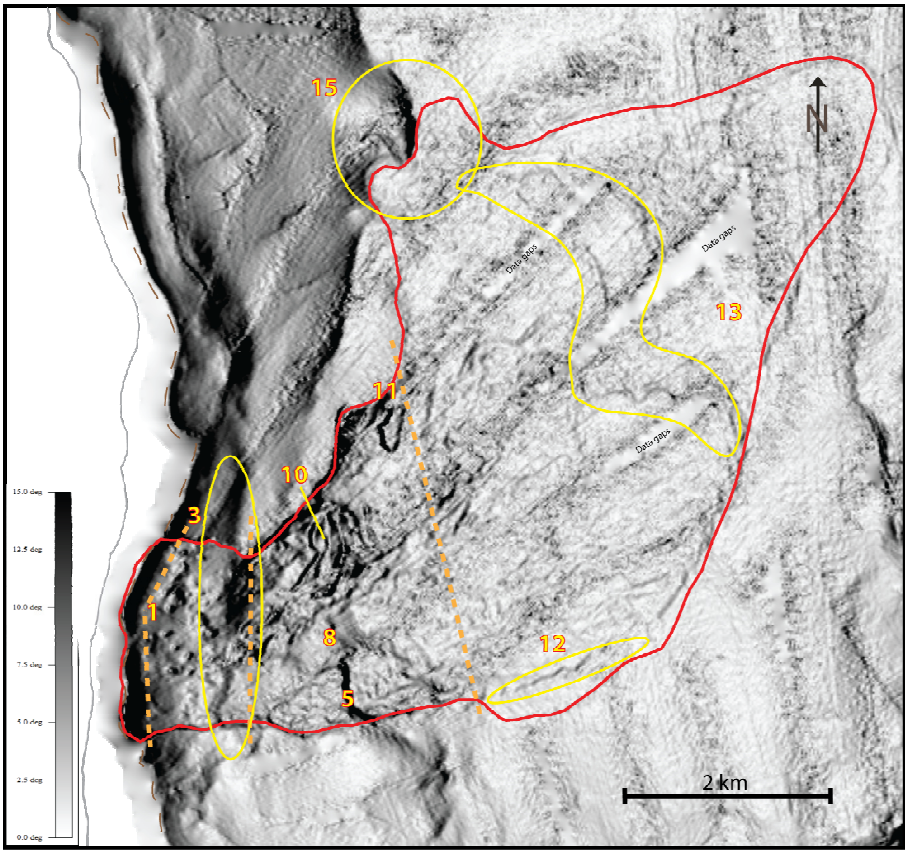

Figure 28: Slope view of Udenisht Slide area based on 20x20 m grid cell size. Red line marks extension of the slide. Yellow numbers correspond to structures described in the text. Grey line demonstrate the shoreline, dashed brown line mark extension of bathymetric data and indicate zones of interpolation. Areas of data gaps are filled by interpolation as well.

A small plateau with a rough topography is found along a shallower region of the southern part of the Middle segment (Figure 27, 4) followed by a steep north-south directed morphological step (Figure 27 and Figure 29, 5) in down-slope direction. This elongated step has a length of 750 m, with maximum step heights of 30 m and slope angles of about 20°. Further down-slope sidewalls are getting higher again but less distinct. Here, they interfere with strong morphological changes and block structures. In this relatively chaotic region single blocks cannot be separated but are bound together to large irregular blocky structures (Figure 27, 6). Profile i) in Figure 26 shows the change in lake floor topography along the small plain and across the morphological step. North of the step another large blocky structure can be observed, extending in east west direction with a length of 500 m, a width of 140 m, and maximum height of 10m (Figure 27 and Figure 29, 7).

Further north a west – east oriented channel-like structure of rather smooth topography can be traced for more than 2 km which already started in the upper segment (in 140 m water depth) and proceeds down-slope until 200 m water depth. No larger blocks can be found within this structure over a width of about 150 m (Figure 27 and Figure 29, 8). The channel is incised several meters in the surrounding lake floor. The central area of the middle segment is characterized by a rough topography. Single blocks cannot be distinguished in this area although the lake floor shows an overall hummocky character.

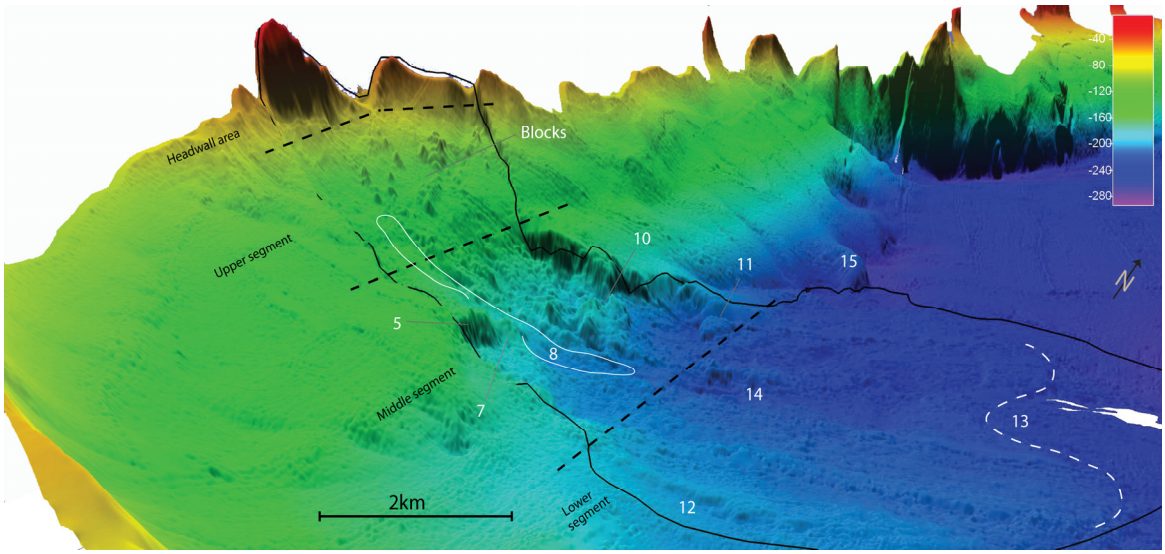

Figure 29: 3D-View of the Udenisht Slide area. Steep slopes of the headwall area are visible together with blocks in the Upper segment. Main structures within the Middle segment are marked such as the morphological step (5), an elongated channel (8) with a depression at transition to the Lower segment (14), the amphitheatre structure (10), and a large block at the northern sidewall (11). A sinuous lined step can be seen at close to the toe the slide (13). See text for detailed description.

Another channel-like structure runs parallel to the northern sidewall in north-east direction (Figure 27, 9). Cutting 5-10 m into the surrounding surface this channel starts at ca. 150 m water depth and continues for nearly 1 km down to a water depth of 200m depth. The width of about 130 m remains quite constant (Figure 26, profiles f and h). A large semi-circle shaped structure is situated at the end of this channel (Figure 27 and Figure 29, 10). Not directly connected with the sidewall this amphitheatre-like feature consists of two larger connected mounds of 10-20 m height and a smaller elevation in up-slope direction. With a length of 750 m and a width of 600 m it covers an area of 0.45 km². Steep incisions of more than 10° gradient are delimiting the mounds (Figure 26, profile d). North of this structure the northern sidewall shows a bulge towards the end of the amphitheatre-like structure (Figure 27, 10). In the north eastern margin of the middle segment another morphological high is located about 320 m away from the sidewall (Figure 26, profile e and Figure 27, 11). This large block structure (500x200 m) of 10-12 m in height is situated close to an obvious indentation in the northern sidewall. This indentation is cutting in the sidewall for nearly 250 m over ca. 700 m, hence showing similar dimensions as the large block (Figure 27, Figure 28, and Figure 29, 11).

Lower segment

The lower segment is characterized by relatively plain topography. Being already at the transition to the Central Basin this segment shows only low slope gradients (< 1.5°, Figure 26, profile a). No significant elevations or mounds can be detected in this area and bathymetric data does not allow defining small blocks in this area because elevations are nearly in the same order as signal noise. The southern sidewall disappears fully from 190 m down-wards and is replaced by a small west – east elongated bulge of about 3 m in height (Figure 27, 12). This sediment accumulation is aligned with the sidewall and continues down-slope for nearly 2 km before it runs out. But sediment echo sounder profiles show that actual extension of the slide is found south of the accumulation, therefore it does not describe the continuation of the sidewall. Also the northern sidewall disappears completely within the Lower segment. Only few patterns can

be identified on the lake floor in this segment that are likely to be real structures and not due to errors in the bathymetric data. Detected mainly by means of the slope view two elongated structures of 1 – 2 km in length are located in the lower segment marked by a downward step of 3 – 10 m in direction towards the Central Basin (Figure 27 and Figure 28, 13). Figure 29 shows that this down step is elongated rather sinusoidal. The step disappears at some locations or cannot be detected anymore because data quality is too low. An elongated depression oriented in slide direction is located at the transition from the Middle to Lower segment in the central part of the slide covering an area of 0.13 km²; it has a maximum depth of 12 m (Figure 26, profile g and Figure 27, 14). It is situated at the prolongation of the larger channel structure that was detected in the middle segment (Figure 27, 8).

In the lower segment the area that was affected by Udenisht Slide was mainly determined using multichannel seismic and sediment echo sounder data, because detecting the area by means of bathymetric data turned out to be rather difficult. Nevertheless the slope shade view of Figure 28 helps to detect some slope variations that coincide with the borders of Udenisht Slide area in the lower segment. Especially at the eastern margin it reveals a south-north directed pattern which matches with the edge of the Udenisht Slide. At the north-western margin the slide area is limited by a nose shaped elevation from the western slope that is extending towards the Central Basin (Figure 27 and Figure 28, 15).The north-western margin of the lower segment that borders this elevation also represents the deepest part of the area affected by the slide with a maximum depth of 250 m.

4.3.2. Surface structures revealed by backscatter data

Figure 30 shows a map of backscatter values of the Udenisht Slide area. Backscatter data provide additional information especially for the lower segment where no obvious morphological changes are imaged. Material changes imaged as backscatter variations help to locate the accurate extension of the slide. Also structures that could not be imaged with bathymetric data alone might be detected using backscatter information.

Interpretation of backscatter data obtained from a multibeam device has to be done carefully especially in areas where slope angles are higher because variations in backscatter data can also be a result from different angles of incidence. Therefore not all information provided by backscatter data gives useful information about material changes but can also be related to steep flanks or due to elevation changes. Material changes can be identified especially in areas with a smooth topography based on backscatter data.

Many white and black areas can be seen on Figure 30 resulting from missing or incorrect data. Along the rim of overlapping tracks backscatter signals show smearing effects that are not related to any geological or morphological feature. Local backscatter minima in the upper part of the slide probably represent the shadow zone for backscatter signals due to larger blocks that are situated on the steep slope that implies high backscatter values for the whole Upper segment (Figure 30, 1 and 2). Here backscatter data does not provide additional information because variations are primarily influenced by morphology as seen for example along the steep flanks of the large amphitheatre structure in the Middle segment (Figure 30, 10).

Extremely high backscatter from the headwall area let assume that here different material is exposed on the lake floor because no similar backscatter values are found along surrounding slope areas (Figure 30, 16). But morphology may play a significant role as well as this area is also

characterized by extremely steep slopes pointing out the difficulties of backscatter data derived along steep flanks.

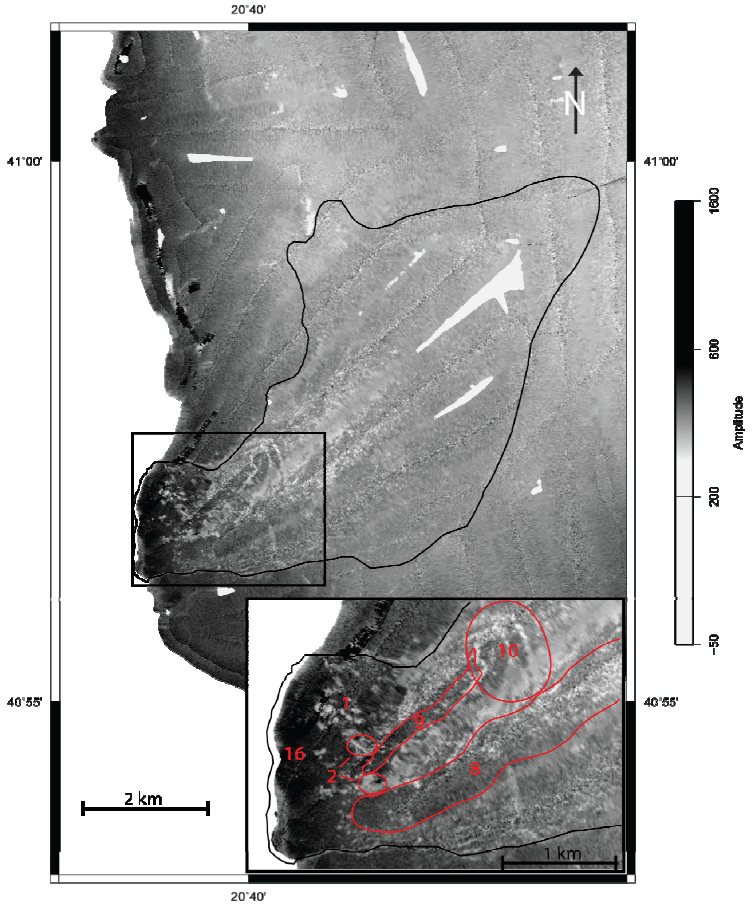

Figure 30: Backscatter map of Udenisht Slide area (marked by black line). Light areas represent zones of low backscatter values. White regions are due to data gaps. Smearing effects of outer areas of adjacent multibeam tracks are visible. Inlet shows a detailed part of the upper part of the slide. Structures detected by backscatter data are marked with red numbers. See text for description.

Along the two channel structures (Figure 27, 8 and 9) high backscatter can be identified probably due to different material on the surface of these elongated structures. Comparison to surrounding areas infer that backscatter variations are due to difference in surface material as high backscatter of the channels can be traced over various slope angles and hence is probably not only an effect of morphology.

Unfortunately, other areas of the slide do not show obvious variations in backscatter compared to unaffected slope areas. For example, within the rather smooth lower segment where the backscatter data should give the best results no significant change in surface composition can be observed. Unfortunately, even not at the boundary between reworked and undisturbed sediments gives a clear backscatter signal.

Most of the backscatter variations over the Udenisht Slide Complex coincide very well with morphological highs or varying slope gradients, which are already described based on the bathymetric data. Backscatter variations caused by varying sediments are hardly visible; hence backscatter data of Lake Ohrid does only provide limited amount of new information.

4.3.3. Internal structure of the south-western slope area

Sediment echo sounder and multichannel seismic data allow imaging sedimentary structures within the area of the slide complex. Furthermore depositional thickness and areal extent of the slide can be estimated based on seismic data. First I will describe the internal structure and main characteristics observed within the Udenisht Slide by means of sediment echo sounder and seismic profiles. The second part deals with sediment structures and older slide bodies at greater burial depth beneath the main Udenisht sliding area that are visible in several seismic profiles.

The key seismic and sediment echo sounder profiles demonstrating the internal structures of Udenisht Slide and the western slope area are presented in this chapter and will be described in detail. Additional profiles providing further information about the composition of the south-western part of Lake Ohrid and the depositional body of Udenisht Slide can be found in the appendix.

4.3.4. Sedimentary characteristics of the Udenisht Slide Complex

First I will present two sediment echo sounder profiles that allow detailed classification of the slide area and the main deposition unit of the Udenisht Slide, before seismic profiles provide additional information about the mass movement deposit as well as closer investigation of sedimentary structures beneath the slide.

Imaging internal structures within the headwall area is difficult for two reasons. First of all distinct identification of a headwall by using the morphological data was not possible because a clear scarp could not be detected. Secondly, due to the steep slope within that area the penetration of sediment echo sounder data is very limited and mostly reflections from the lake floor were detected. Nevertheless, a sudden increase in water depth within the headwall area is visible (Figure 31). Although the penetration along the upper segment is still poor massive blocks are evident in Figure 31. Within the Middle segment three distinct elevations of the amphitheatre-like structure described in the bathymetry (Figure 27, 10) without any penetration are detectable. A small sediment wedge characterized by a transparent to blocky facies is found immediately up-slope of the blocks but no infill can be found between the elevations (Figure 31). Transition of Middle to Lower segment marks the beginning of the main Udenisht Slide deposition unit indicated by a rather transparent body in the sediment echo sounder data (Figure 31 and Figure 32). This main deposition body can be divided into four sections based on internal structures, thickness, and surface morphology (Figure 31, I-IV).

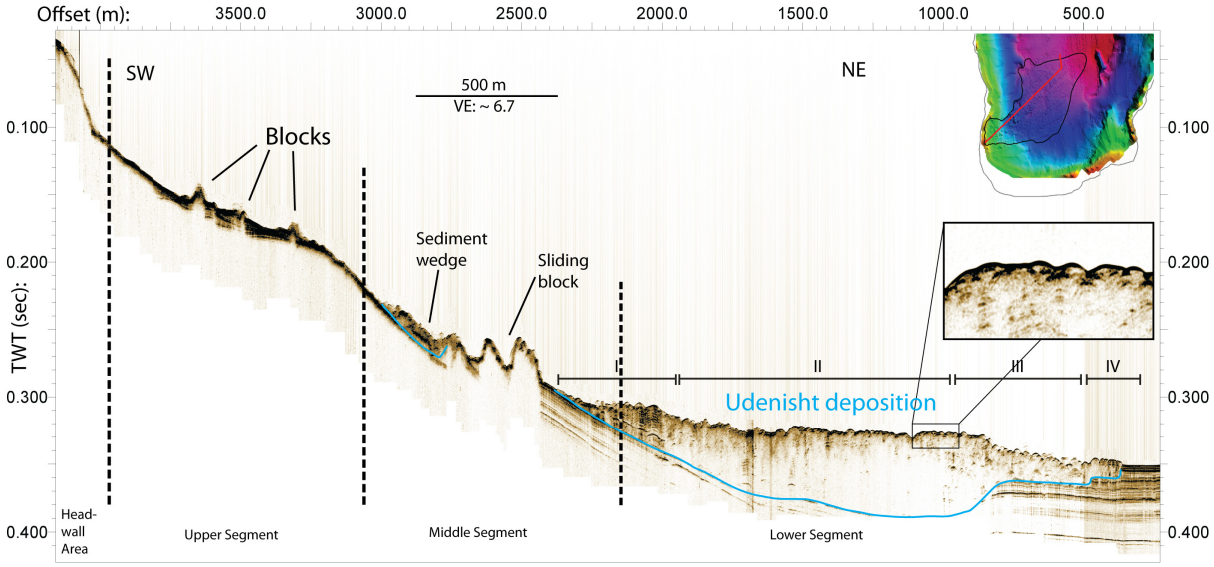

Figure 31: Sediment echo sounder profile across the Udenisht Slide area imaging the headwall, large blocks within the Upper segment, sliding block in the Middle segment (with sediment wedge up-slope) and main depositional area further down-slope. Sections (I-IV) show different characteristics within the main depositional unit which is marked by the blue line. Inlet shows close up of the surface of the main depositional slide area. See inset map for locations of profiles

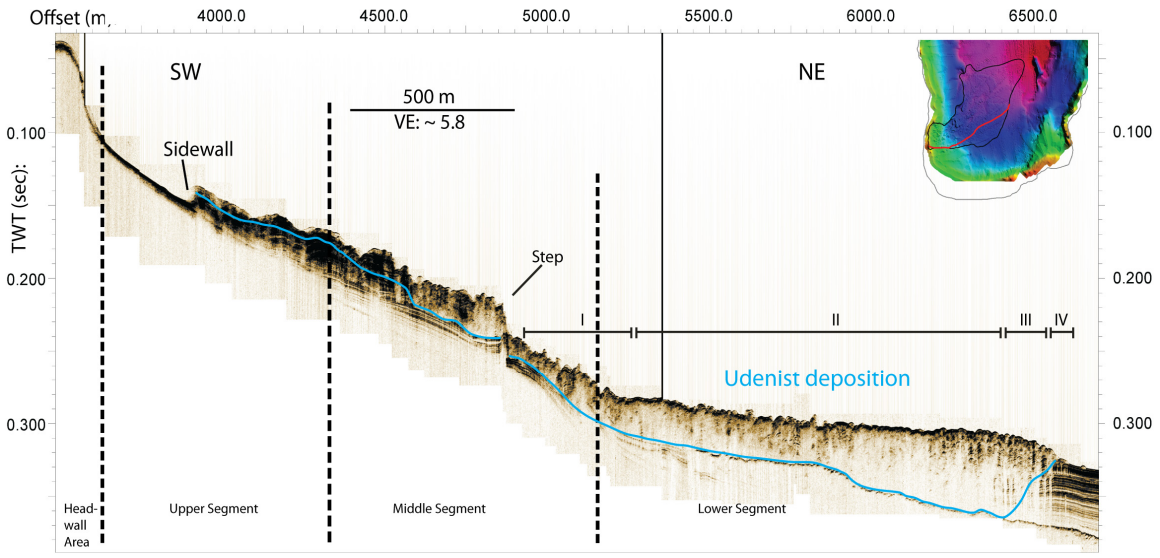

Figure 32: Sediment echo sounder profile showing main parts of Udenisht Slide including a steep headwall and slide deposits on the upper and middle segment. Note that the track on the upper segment was in close vicinity of the sidewall hence some reflections are most likely side effects. A morphological step is visible in the middle segment. The main depositional area is characterized by a thick transparent body (blue line). A high amplitude reflection beneath the transparent body indicates the top of a second slide. The transition to undisturbed sedimentation towards the central basin is very sharp. See inset map for locations of the profile.

The first section (I) shows higher amplitudes in comparison to the other three sections, some sediment layers with one prominent horizon (Figure 31 and Figure 32). The base of the deposition is imaged by an east dipping high amplitude reflector The hummocky surface of section I shows similar roughness as the deposition up-slope the morphological step in the

Middle Segment (Figure 31). The largest part of the main depositional unit (II) is made by a thick transparent sedimentary body. Slide thickness is largest in this section. Base of the Udenisht deposit is marked by an irregular interface that is most likely the top reflection of an additional transparent unit, an older, buried mass wasting event underneath (Figure 31). A sudden decrease in thickness of the slide deposits is noticeable within section III (Figure 31 and Figure A9 in the appendix). Undisturbed sediments are evident beneath this section as well as a morphological step at the boundary to section II (Figure 32). The surface roughness seems to be higher compared to section II as the lake floor is not one single horizon but show rather patchy reflections. In section III layered sediments are visible below the transparent body. Section IV is characterizes the toe of the Udenisht Slide at the boundary to the undisturbed sediments deposited within the central basin. An additional decrease in depositional thickness can be recognized in Figure 31. The rough reflector indicating the base of the Udenisht deposition (section II-IV) can be traced further east underlying also areas where no material from Udenisht Slide was deposited.

Before seismic profiles of the Udenisht deposition will be shown, main seismic units that can be found within the south western part of the lake will be illustrated briefly.

4.3.5. Seismic units within the south western part of Lake Ohrid

Sediment successions of the south-western part of the lake can be divided into three different seismic units: The acoustic basement is covered by a unit of high amplitude reflectors of partially deformed sediments (labeled Unit A on Figure 33), overlain by well stratified and undisturbed sediment packages showing moderate amplitudes of Unit B. Alternations of higher amplitude reflections and low reflective zones can be seen again in Unit C with parallel sediment layers as well as areas of slightly deformed sediments (Figure 33 and Figure 34). Unit C is characterized by several mass wasting deposits. The large Udenisht Slide deposit is mainly located within Unit C as well.

Figure 33 shows a seismic profile running from west to east along the southern part of the slide. Acoustic basement can be seen along the western slope overlain by slightly deformed reflectors of Unit A. Undisturbed parallel reflectors of Unit B can be distinguished clearly only in the Middle and Lower segment, while the alternating high and low reflective zones of Unit C are found only further down-slope within the Lower segment. The main Udenisht Slide deposition is marked by rather transparent body down-slope a morphological step (Figure 33) coinciding with the elongated wall already described in the bathymetry (Figure 27, 5). A small transparent deposition can be detected at the back of this step. Bending of sediments below the step affects the entire underlying sediment layers (down to the basement rocks) and is related to a vertical zone of low amplitudes. Increasing in deposition thickness of the slide deposit can be seen within section I and II while stepwise decrease characterizes section III and IV. Additionally to the three seismic units described earlier Figure 33 shows vertical zones of extremely low amplitude values. One of them is situated beneath the morphological step while another wider zone of low amplitudes is located further down-slope in between section I and II where amplitudes of reflections within the deposition unit as well as the underlying sediments of Unit B and C are particularly low (Figure 33).

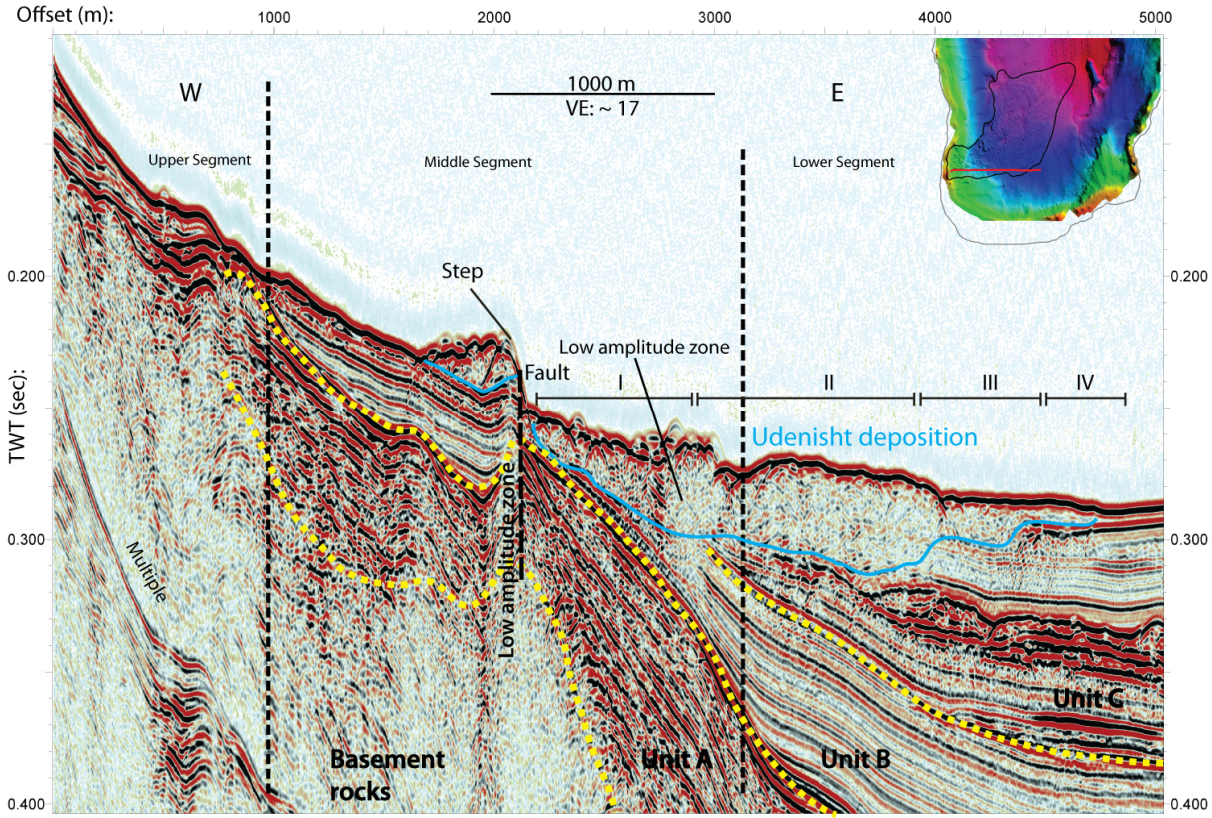

Figure 33: Multichannel seismic profile across the slide area imaging structures up to a depth of 0.4 sec TWT. The basement is covered by seismic Units A-C (see text for further explanations). Udenisht Slide deposits are imaged as transparent unit (marked by the blue line) with stepwise increasing slide thickness. Deposition above a morphological step can be seen with a zone of low amplitude reflections along a fault zone beneath the step. Another low amplitude zone is situated within the main Udenisht deposition (section I-II). See inset map for locations of the profile.

A south north crossing seismic profile is presented in Figure 34 showing significant differences in thickness within the slide deposit. The acoustic basement is located in about 0.1 - 0.2 sec TWT below the lake floor. Seismic Unit A directly above the basement is characterized by high amplitude reflections of moderate continuity, which are overlain by clinoforms within Unit A. About 0.05 sec TWT of well stratified sediments with lower amplitudes of Unit B follow on top of Unit A. Higher amplitude reflections are again visible in Unit C representing the uppermost 0.5 sec TWT below the lake floor. At the southern part of the profile a transparent vertical zone disturbs the sediment layers rising up from the basement to almost the lake floor causing a slight upward bending of the layered reflections. The uppermost layers of Unit C are disrupted by chaotic to transparent body assigned to the Udenisht Slide deposition showing deformed internal reflections and rough lake floor topography. Thickness of Udenisht deposition is decreasing towards its northern margin where the steep northern sidewall limits the extension of the slide (Figure 34). The central part of the slide deposit illustrates a cone like incision of the deposit into underlying sediments for more than 0.02 sec TWT. Position of this graben-like feature coincides with the large channel structure visible in the bathymetric data (Figure 27, 8). The southern margin of the deposit again shows increasing thickness to about 0.03 sec TWT before sudden transition to undisturbed sediments occurs.

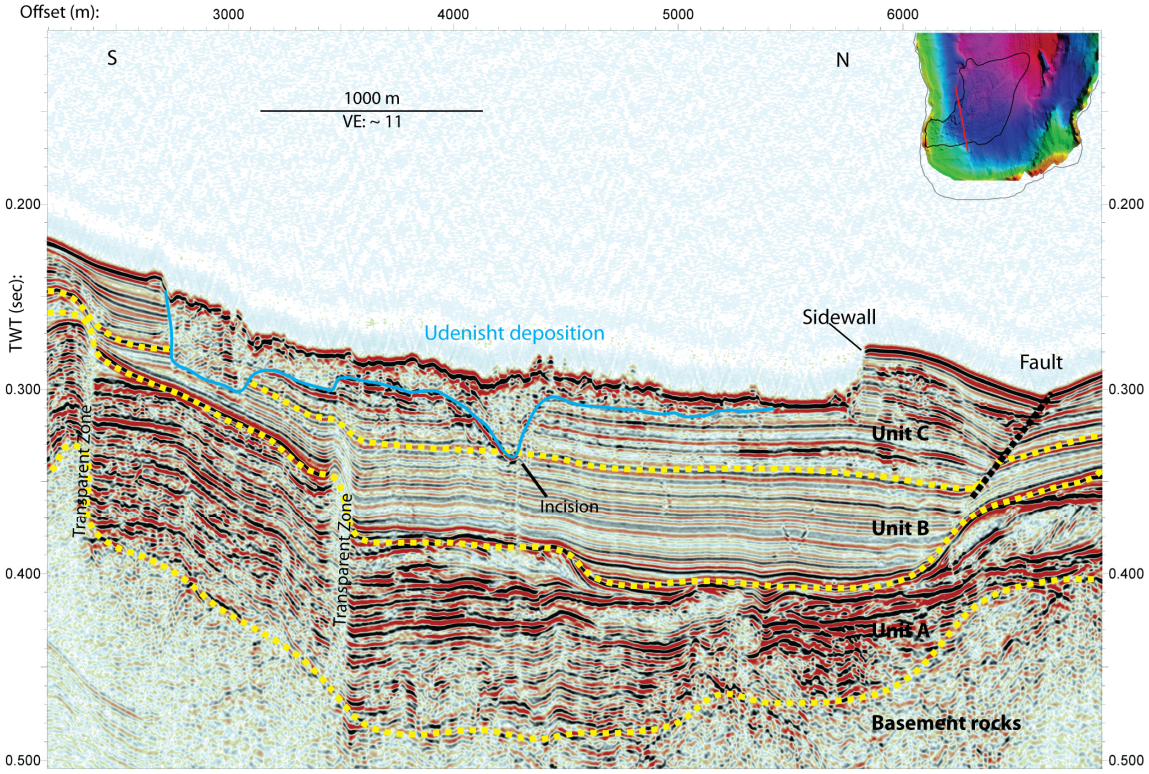

Figure 34: Multichannel seismic profile crossing the Udenisht Slide in a S-N direction at transition of Middle and Lower segment. Seismic Units A-C are covering basement with clinoforms in Unit A. Undisturbed sediment layers containing blanking zones. Udenisht deposit (marked by the blue line) on top of parallel reflectors, shows cone like incision with infill of transparent material. Steep sidewall and a large fault structure characterize the northern margin of the profile, vertical transparent zones in the middle to southern part. See inset map for locations of the profile.

Nearly one kilometer north of the northern sidewall a fault is imaged coinciding with a deepening on the lake floor (Figure 34). The fault is located above a large clinoform structure of Unit A and displaced all of the overlying sediments even the uppermost layers beneath the lake floor. Between the fault and the northern sidewall sediments of Unit C show numerous small areas of high amplitude reflections alternating with lower amplitude zones.

4.3.6. Seismic evidences for older mass wasting within the southern part

In addition to the chaotic to transparent deposition body of Udenisht Slide additional seismic profiles (Figure 35) show at least four other deposition structures within the southern part of Lake Ohrid that are due to mass wasting processes. Just below the bottom reflection of the Udenisht Slide another transparent to chaotic body is situated ("Naum") characterized by low amplitude values and internal deformed (Figure 35). The top of this slide unit was already seen in sediment echo sounder data as a strong and irregular reflector at the base of Udenisht Slide (Figure 31 and Figure 32). High amplitude reflectors mark the bottom of this unit. At some locations the bottom reflection shows an irregular topography and is partially even not visible anymore. The extension of the Naum slide body can be traced over a large distance of more than 7 km northwards although bottom and top reflections are not always easy to define. The Naum unit is located more to the east compared to the Udenisht Slide. Based on numerous sediment echo sounder and multi channel seismic profiles the closest location to the coast (about 700 m away from the coast) of this depositional body is found off the small coastal town Sveti Naum, where it is visible at ca. 160 m water depth (Figure 35). Thickness of the Naum unit varies between 0.01 and 0.035 sec TWT. In contrast to the rather transparent Udenisht body the Naum unit is characterized by generally higher amplitude reflections and several alternations of only slightly deformed areas and zones of chaotic deposition (Figure 35).

The areas where the base of the Naum unit shows an irregular topography result from another mass movement deposit ("Tushenisht 1") that is located directly below Naum (Figure 35). With a south - north extension of about 2 km this body shows more internal reflections than the Udenisht unit and folded and deformed structures are alternating with more transparent zones within the deposition. The interface between Naum and Tushenisht 1 is marked by a thin horizontal layer of a high amplitude reflection that sometimes disappears and hence is only difficult to detect. Another high amplitude reflection representing its base separates Tushenisht 1 from underlying horizontal and mostly parallel sediment layers revealing a maximum thickness of this deposition of 0.05 sec TWT (Figure 35b).

Below Tushenisht 1 an additional chaotic depositional structure can be imaged ("Tushenisht 2", Figure 35) showing much larger dimensions compared to Tushenisht 1 with respect to its length of more than 7 km (Figure 35). In contrast to the upper three mass movement deposits this slide body shows no direct contact to an overlaying slide unit. About 0.01 sec TWT of undisturbed sediment layers are deposited between Tushenisht 1 and Tushenisht 2. Deposition unit of Tushenisht 2 has nearly no internal reflections and shows similar transparency as the Udenisht unit. The base of this depositional body cannot clearly be identified because sediment layers beneath have very low reflectivity.

South-east of Magic Mountain another small slide unit can be found ("Trpejca") showing low amplitude reflections and internally deformed sedimentary layers (Figure 35a). This unit is characterized by relatively large thickness of up to 0.04 sec TWT but small lateral extension of ca. 1 km.

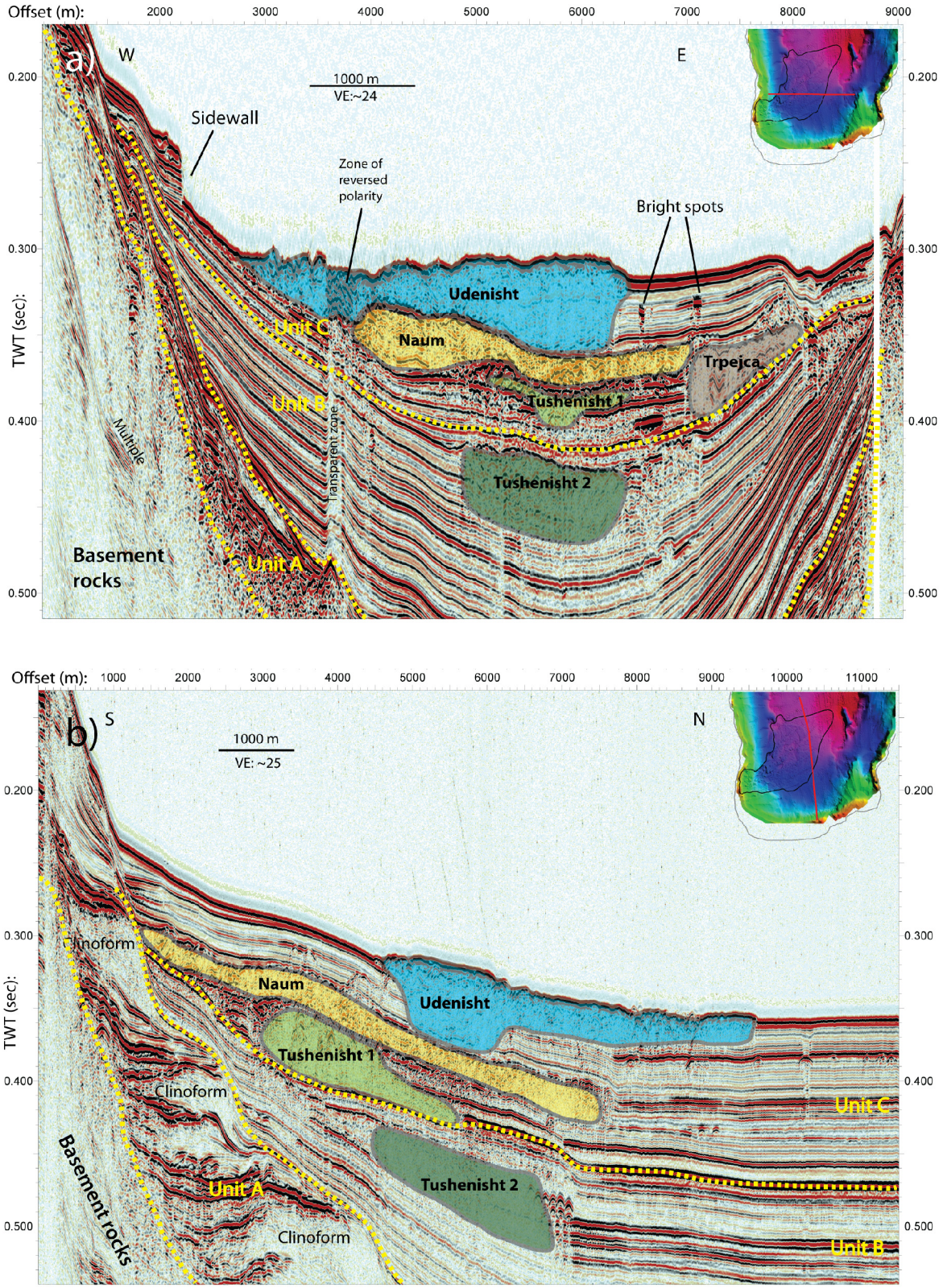

Figure 35: West-East (a) and South-North (b) orientated multichannel seismic profiles showing that mass movement events are a common feature not only in recent times. Mass movement deposits are located in seismic Units B and C together with a steep sidewall from the Udenisht event (a). Unit A shows high amplitude reflectors including clinoforms (b) covering basement rocks. A vertical low amplitude zone from basement through the overlying units is visible in a) as well as bright spots in the uppermost sediment layers. See inset map for locations of profiles

5. Discussion

In this chapter the results from multibeam, seismic, and sediment echo sounder data will be discussed with the aim to understand slide processes and associated hazards. In a first step interpretation will result in possible scenarios for slide evolution; later I will address the tsunamigenic potential of the Udenisht Slide.

As seismic and sediment echo sounder profiles show travel times and not depth, travel times must be converted into depth. Therefore a depth-sound velocity profile is needed, which is a rather difficult approach. No reliable velocity information was determined during seismic processing because the short streamer did not allow a proper velocity analysis. Best estimation would be to derive such values from acoustic measurements of lake sediments cores or through borehole data. Unfortunately only some short cores (max 20 m in length) are available from the Ohrid region so far. Hence other studies dealing with seismic velocities of comparable sediments are used.

Anselmetti and Eberli (1993) measured seismic velocities from 210 minicore samples from different areas and illustrate sound velocity range from 1700 to 6500 m/s for v_p. These velocity variations are controlled by depositional lithology and post depositional processes like cementation or dissolution. Furthermore they demonstrate that velocities for unconsolidated sediments range from 1550 to 1800 m/s at the time of their deposition. They conclude that porosity must be seen as the primary factor affecting seismic velocity and that burial depth or age alone cannot be taken as an indicator for velocity distribution. According to the study of Anselmetti and Eberli (1993) an average velocity of 1675 m/s was used for shallow sediments in Lake Ohrid (up to ca. 0.15 sec TWT below the lake floor) because these sediments are likely unconsolidated. An average velocity of 2300 m/s was used for depth calculation of deeper sediments (below 0.15 sec TWT) (Anselmetti and Eberli, 1993). However, depth calculation of seismic profiles within Lake Ohrid must consider that the values of Anselmetti and Eberli (1993) are not derived from the Ohrid region: The actual seismic velocity for the study area may differ. After depth conversion of the acoustic profiles it is possible to estimate deposition age of sediment layers by means of available sedimentation rates for Lake Ohrid from Wagner et al., 2009. It also needs to be considered that sedimentation rates have most likely varied over time. Hence all ages needs to be regarded with great care. Nevertheless, better age estimation cannot determined be without information from a drill site.

5.1.Western Slope Area

On the Western Slope Area two small mass movement events are described in the result section (WS1 and WS2, Figure 23). Both landslides can be clearly detected in the bathymetry although they are already buried under 7 m (for WS1) respectively 15 m (WS2) of sediments. In the following these two events will be discussed in terms of their structural geometry such as lateral and vertical extend and their age. Results from the available data will be interpreted with respect to the sliding processes in order to discuss trigger mechanisms of these events. Those two relatively small events contribute to gain knowledge about landslides in Lake Ohrid especially along the western slope area.

5.1.1. Volume and Thickness

Simplified volume estimations were done for both landslides using segments of average thickness in the slope area where material was removed. This led to a volume of removed

material of ca. $8.5 \cdot 10^6$ m³ for WS1 and $10.7 \cdot 10^6$ m³ for WS2 showing that the two events not only have similar extensions but also removed similar amount of sediments from the western slope. Determining the thickness of the deposited material is difficult especially for WS1 where sediment echo sounder data does not allow clear detection of the base of the sliding material. Nevertheless, at the northern margin of WS1 a thickness of 30 m was assumed (Figure 24b). Thickness of the WS2 deposition body is about 25 m (Figure 25). Due to the poor coverage with seismic and sediment echo sounder profiles in the region of WS1 and WS2, it is not possible to determine a representative thickness of the entire depositional area. This makes it impossible to estimate the actual amount of redeposited sediments for both events. In a simplified case the removed volume on the slope equals the amount of transported and deposited material further down-slope. However, most likely additional material was mobilized due to erosion activity during the actual sliding process.

5.1.2. Age

Well layered sediments are found above both mass movements. While ca. 7 m of sediments were deposited on top of WS1, WS2 is buried under more than 15 m of well stratified sediments, implying that WS2 is older than WS1. Wagner et al. (2009) report relatively constant sedimentation rates of about 0.6 mm/yr in Lake Ohrid during the Holocene which corresponds to the uppermost ca. 7 m of sediments. For deeper sediments no individual data for sedimentation rates are available why 0.6 mm/yr must be applied also for age estimation of deeper sediment layers. Sedimentation on top of the WS1 deposition body shows that the WS1 event occurred ~12000 yrs BP in contrast to the older slide WS2 that probably took place ~25000 yrs BP. These values are only rough estimates keeping in mind that these numbers may contain large errors mainly caused by converting TWT into depth and possible lateral and temporal variations in sedimentation rate. Small hiatuses may be another error source. No obvious unconformities were detected in the sedimentary succession deposits on top of the mass transport deposits, but acoustic systems are not able to detect small hiatuses due to their limited resolution. Nevertheless, age estimations and the fact that these mass depositions are still visible in bathymetric data shows that both events occurred in younger Pleistocene times.

5.1.3. Processes and trigger mechanisms

Both mass movement events occurred in similar depth (WS1: 145 m – 225 m, WS2: 175 m – 255 m) and close to the transition of the Western Slope area into the Central Basin. Strikingly the shape of both affected areas show relatively short extension in slide direction (1.5 – 2 km) compared to their width (ca. 1 km). Additionally, the run-out area of both mass movement events is rather short. WS1 and WS2 took place in the transition region between Western slope area and Central Basin characterized by a prominent change in slope gradient from 3-4° on the slope to the almost flat Central Basin. Both slides occurred in rather deep water depth which limits the length of the slides because the distance to the flat Central Basin is small. Therefore energy of both landslides is assumed to be relatively low as the material was not transported over long distance.

Geometry of the rupture surface and the shape of the slide body suggest that the WS1 event was as a rotational slide or a slump (Hampton et al., 1996). The westward dipping north south elongated ridge of the WS1 event is interpreted as a rotated block of the slumped body where the sediments were compressed and bended upward. However, the landslide aspect ratio (ratio between initial height of the slide body, h and length of the slide body, l) of WS2 (h/l = 0.03) is

larger than usual ratios for observed slumps (0.05-0.15) (Watts et al., 2005). Nevertheless, with respect to the observed morphology, the WS1 event might indeed be a slide with strong rotational character.

Figure 36 shows a simplified example of how the WS1 event might have developed to reach the present stage. The northern part of the WS1 depositional area (Figure 24) shows deformed internal reflections but the overall structure of deposited material is not destroyed completely. This observation indicates that sliding process of WS1 was similar to a low energetic rotational slide or slump because internal structure of the deposition body might not be totally destroyed during such an event.

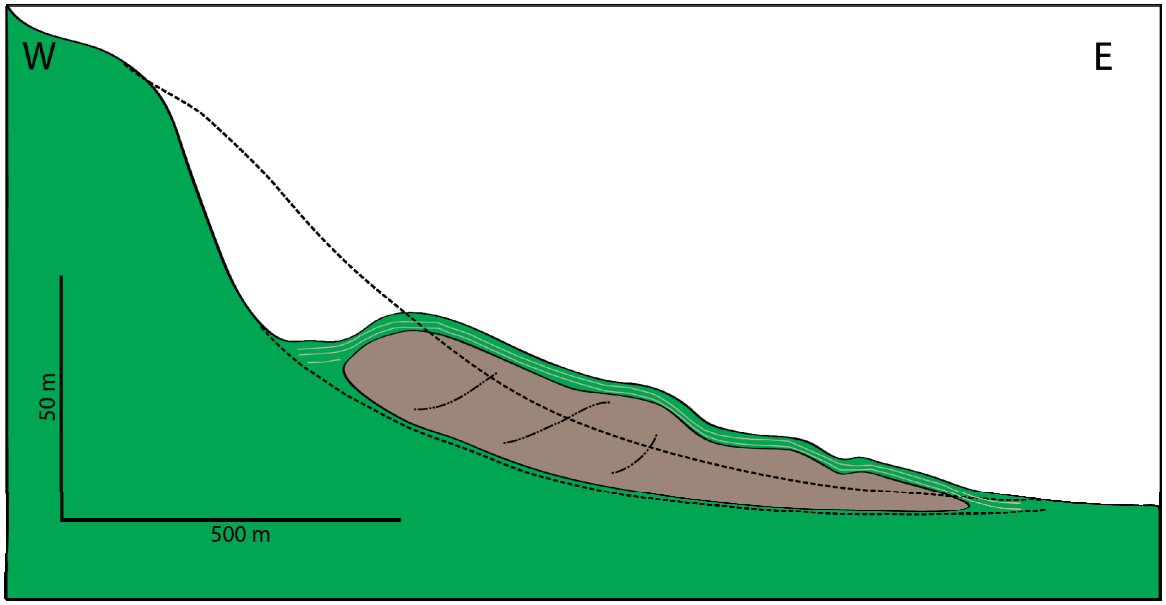

Figure 36: Simplified drawing of WS1 mass movement event based on a bathymetric profile along WS1 and a seismic profile. Note that shape of the former slope and actual position of the deposition body is only estimated. The rotational character is inferred from the existing lake floor morphology.

Likewise the WS2 event can be interpreted as a rotational slide because rupture surface is curved and run-out distance is relatively short. Seismic data on the other hand shows only few internal reflections indicating that the sliding body has been strongly deformed during the process. Based on the short run-out distance of both mass wasting events duration of the sliding processes is assumed to be relatively short and the process ended abruptly mainly due to the transition to the flat Central Basin where more initial energy would be needed to transport material over long distances.

North-west of the WS1 area three channel-like structures are cut off by the sidewall. Lack of bathymetric data in direction to the western coast does not allow determining how close these channels approach the coastline. These channels, however, most likely transported sediments from the coastal area or even from onshore into the area where the WS1 event occurred. High sediment input at this relatively steep part of the lake is considered as important factor contributing to the slope failure resulting in the WS1 event. Syvitski (1989) points out that overloading of sediments is a major factor for local slope instabilities.

Figure 37 shows a slope view of WS1 pointing out that the depositional area shows clear deformation structures on the seabed. Although the depositional body is buried under 7 m of sediments, the morphological pattern at the lake surface can still be related to the mass

transportation. Rotational sliding tends to create hummocky and irregular surface topography by processes such as breaking and buckling (Coleman and Prior, 1988). Irregular lake floor structures within the WS1 area may also be due to sporadic sediment input from the channels north of WS1 (Figure 23) indicating that the channels were still active after the slide occurred. WS2 shows a much smoother morphology at the lake floor, probably because of it is older age and the resulting thicker sediment cover on top of the slide. But also the absence of sediment input though channels might be a reason.

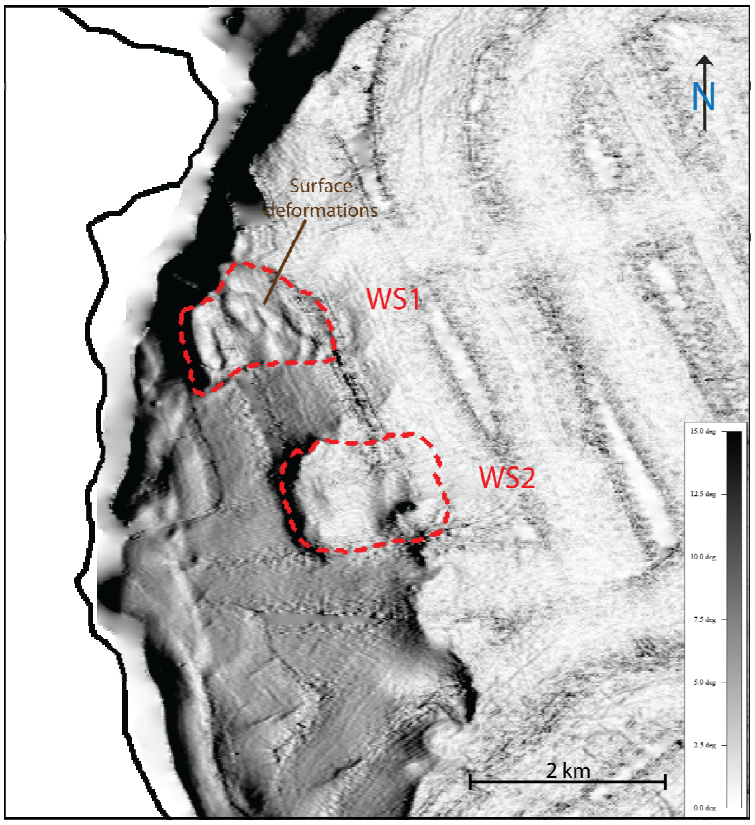

Figure 37: Slope view of WS1 and WS2 mass transport deposits. Irregular surface of the WS1 depositional area trace deeper deformations resulting from deformation during sliding which are still traceable on the lake floor despite a 7 m thick sediment cover on top of WS1. WS2 shows less deformed surface sediments

A northeast - southwest elongated fault zone is located north of WS1 marked by an extremely steep slope within the north western part of the lake (Figure 22). WS1 is positioned where this extensive and still active fault interfere with faults of the western slope area. This suggests that in addition to an intense sediment load displacement along this fault can finally have triggered the mass movement on the already instable slope. The headwall area of WS2 is characterized by two nearly vertical fault zones that emerge close to the lake floor indicating that both faults must have been active recently (Figure 25). They affect the whole sediment layer overlying the basement rocks (here approximately 60 m) (Figure 25). The fact that the faults are located very close to the headwall of WS2 suggests that they initiated the slide. It is likely that energy released by an earthquake along one of the faults caused a displacement within the unconsolidated sediment package and subsequently triggered the mass wasting event.

An interesting feature of the WS2 slide is the remarkable depression at the transition zone to the Central Basin (Figure 23). Unfortunately the seismic profile of Figure 25 does not cut this structure directly but it still illustrates that the depression is located above a basement high. It is only possible to speculate about the origin of this depression but numerous depressions are

found in Lake Ohrid but with smaller dimensions. These more or less circular shaped depressions (ca. 50 - 100 m in diameter) of about 4 -7 m in depth are comparable to pockmarks that could represent possible gas seepages (Iglesias et al., 2009). Especially in the northern part of the lake such pockmarks can be observed clearly at the seabed suggesting that they are a common feature along the western side of Lake Ohrid (Figure 22). Formation of pockmarks can be described by fluids that are escaping through the sea floor along migration pathways and thereby lift the finer sediments into suspension. Redistribution and local slumping of these sediments then leads to depressions at the seabed (Høvland et al., 1984). The depression within the WS2 deposition area might also be a pockmark although it has an astonishing depth of nearly 20 m. This feature exceeds the usual pockmark dimensions that are observed within the northern area of Lake Ohrid. Although the seismic profile (Figure 25b) does not cross the depression directly, a small bright spot is observable above the basement high suggesting the presence of fluids and/or gas within the sediments. Even though the depression on the WS2 area is extraordinary large compared to similar structures in the lake it is likely related to fluid migration. The location of this pockmark directly above a basement high let assume that fluid migration is associated with the basement high. The appearance of such a large pockmark structure at the base of the slope also influences stability of slope sediments. Softening of the sediments by gas seepage destabilizes and hence generates conditions where up-slope sediments cannot be kept on the slope and subsequently starts to slide. Probably the current shape of this remarkable pockmark was formed after the WS2 event occurred. Otherwise it would have been buried by the slide material. Nevertheless, the appearance of such a huge pockmark structure suggests that this location is characterized by large amount of rising fluids and/or gas. It is likely that sediments at the base of the western slope have been softened by gas seepages already prior to the occurrence of the WS2 mass failure. Therefore seepage is considered as an additional pre-conditioning factor for slope failures at the western slope. West - east directed acoustic profiles (Figure 24b and Figure 25b) image the basement high as a south north elongated structure rising towards the south that is finally exposed at the lake floor (Figure A10, appendix). Connected to the basement high is an extensive fault zone running parallel to the basement high along the western slope. This slightly east-dipping fault marks the transition from the western slope area into the Central Basin. The widespread morphological step visible on the bathymetric data (Figure 22) most likely represents a surface expression of this fault. Such an active fault can be an important trigger mechanism for slides that occurred in close vicinity to the transition between the western slope area and the Central Basin.

The two detected mass movements (WS1 and WS2) on the western slope show similar dimensions suggesting similar sliding processes such as short duration of the slide and relatively low energy resulting in short run-out distance. Fault displacement in combination with high sediment input and slope destabilization due to fluid escape structures (large depression, WS2) most likely caused the failures along the western slope.

5.2.Udenisht Slide

The results from bathymetric data, multichannel seismic and sediment echo sounder data of the Udenisht Slide will be discussed in the following in order to achieve a better understanding of the processes and mechanisms of this mass movement event. A pre-slide slope reconstruction was done in order to estimate the volume of removed material from the slope during the event. Comparison with transported volume (derived from thickness calculation of the slide deposits) will be used to discuss the evolution of the slide during different stages of the sliding process. I will address the question of the origin of the slide and will present age estimations of the Udenisht event as well as for older mass movements, which have been detected on the southern margin of the lake. Discussion of trigger mechanisms shall finally clarify why the Udenisht Slide occurred.

5.2.1. Pre-slide slope reconstruction

The evacuation area of Udenisht Slide is well defined through sidewalls along the southern and northern part of the slide and by the assumed headwall at the western side. On the eastern side this area is constrained by an imaginary line connecting both sidewalls at the point where they disappear (Figure 38b, white line).

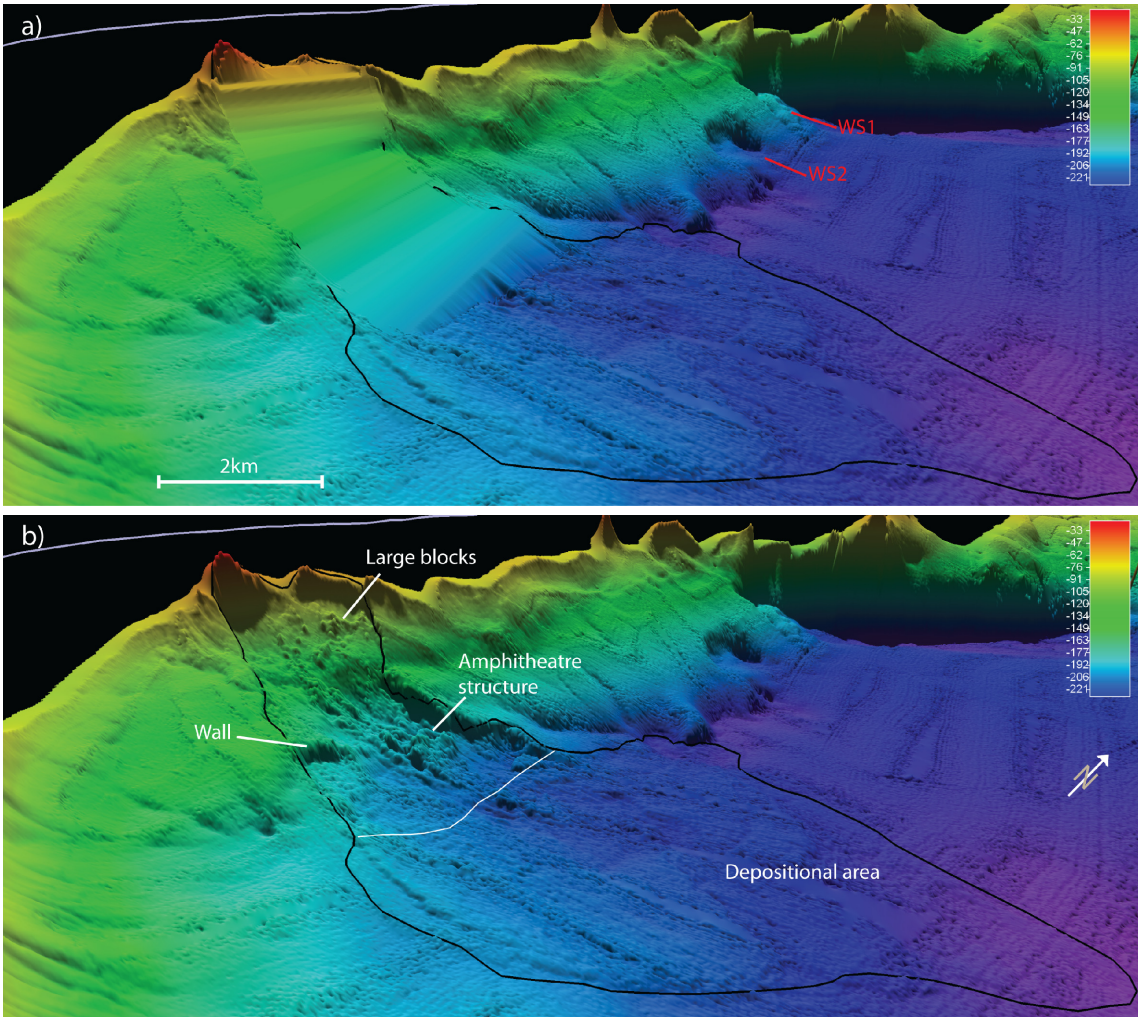

Figure 38: 3D View of Udenisht Slide area showing the reconstructed pre-slide morphology (a) and the present day measured bathymetry (b). Note that only the morphology of the evacuation area was reproduced and not the deposition area. Mass movements from western slope (WS1 and WS2) are seen north of Udenisht. The white line in b) indicates the basin ward extension of the evacuation area of the slope.

Hence an area of about 8 km² was calculated for the evacuation area. For the slope reconstruction several profiles running perpendicular to the slide direction and cutting the southern and northern sidewall were extracted using the software Global Mapper. In a specific file longitude, latitude, and depth values were saved. The locations of these profiles were chosen as such that depth values for the northern and southern sidewall are the same and in a next step all points were set to the respective sidewall depth in each profile. A detailed description of this reconstruction approach is described in the appendix (Figure A12, A13, appendix). The result, a "pre- and post-slide" view of the Udenisht Slide area is shown in Figure 38. The difference between the reconstructed grid and the measured bathymetry grid was calculated with the Kingdom Suite Software resulting in an approximate volume of 0.11 km³ for the evacuation area of the Udenisht Slide event.

5.2.2. Age

The clear occurrence of obvious mass movement structures on the bathymetric map reveals that Udenisht Slide is not buried under a thick layer of sediments. Seismic and especially sediment echo sounder data actually allow determining the thickness of deposited sediments on top of the slide body, which can be used for an age estimation of the slide. Figure 31 shows a detailed section of the depositional area of Udenisht Slide highlighting only one very thin layer on top of the slide material. Sediment echo sounder pulses are high frequency signals that can already resolve sediment layers in the dimension of decimeters. The echo sounder data show drapes on top of the slide in range of 10 to 50 cm. This corresponds to 200-800 years of undisturbed sediment accumulation after slide occurrence using sedimentation rates determined by Wagner et al. (2009).

5.2.3. Dimension of the mass movement

Extension

The depositional area of Udenisht Slide was estimated from seismic and sediment echo sounder data to be about 24 km². The area of removed material from the slope was calculated to 8 km² and the overall area of Udenisht Slide to 28 km². These numbers illustrate an overlap of evacuated and depositional regions. This implies that slide material has been deposited also on regions where material was removed before (Figure 39, area between red and blue dashed line).

Material transportation proceeded into the deepest part of the lake demonstrating a relatively long run-out distance of about 7 km. Mazzanti and Blasio (2009) investigated sub-aquatic landslides in numerous lakes where a sudden change in slope angle occur and found that the depositional area shows a so called horseshoe shaped structure characterized by semi-circular rims at the toe of the slide and short run-out distances. They further suggest that this shape results from a flipping back of the landslide at its front that would then explain the short run-out distance. The Udenisht Slide exhibits similar characteristics as the examples studied by Mazzanti and Blasio (2009) but it is defined by a long run-out distance with a tapered shape of the depositional area in direction to the deep parts of the Central Basin. Deposition around the nose shaped elevation (Figure 27, 15) at the north-western margin of the Udenisht Slide is caused by a 250 m-deep local depression supporting transportation and deposition of slide material.

Thickness

The thickness of the depositional body varies significantly over the slide area (Figure 39). Together with eastern dipping reflectors (at the transition from slope to Central Basin) that probably served as a glide plane for the moving sediments (from acoustic profiles in Figure 31 and Figure A9) a steady increase in depositional thickness can be observed (Figure 39, black dashed line: 1). A small zone of relatively constant thickness is followed in down-slope direction where largest thickness occur (45 m, Figure 39, black dashed line: 2). An upward step of the base of the slide deposit correlates with abrupt decrease in slide thickness (Figure 39, black dashed line: 3) from 40-45 m to ca. 10-15 m. The toe of the slide is characterized by relatively constant thickness of about 10 m (Figure 39, black dashed line: 4).

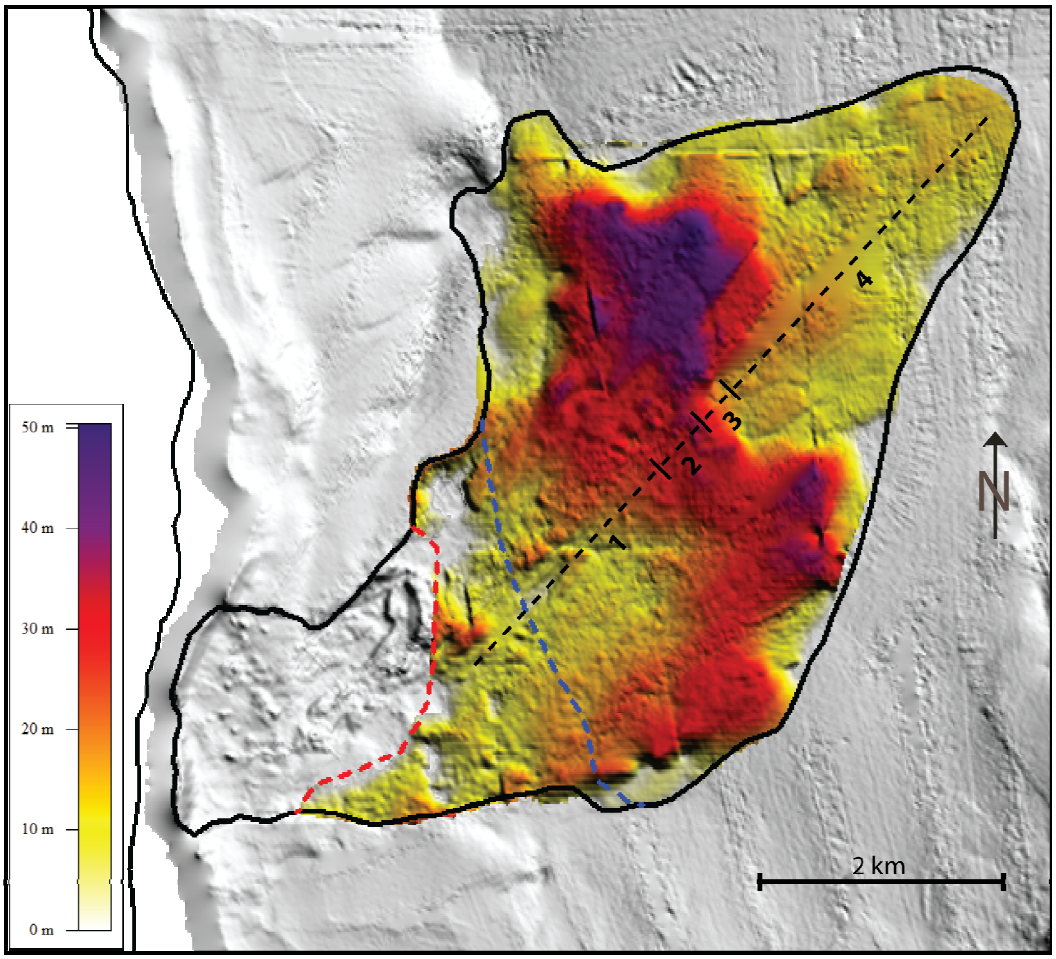

Figure 39: Thickness distribution of Udenisht Slide deposits. Steady increase in thickness is followed by sudden decrease from ca. 45 m to 10 - 20 m. Red dashed line show upward limit of the depositional area of Udenisht Slide, while the blue line marks the downward limit of the evacuation area. The area between the red and blue dashed lines shows the region of slide deposition in the evacuation area.

One explanation of this sudden thickness decrease is based on the paper of Bull et al. (2009) where similar features are described as ramps. They represent variations in deposition thickness where the basal shear surface cuts up to new stratigraphic levels and thereby connects parallel segments of the base of the slide deposits in different stratigraphic levels. Either down-cutting or up-stepping ramps are possible. Bull et al. (2009) give an example of the Møre Slide south of the Storegga Slide (Northern Atlantic) where several down-cutting and up-stepping ramps can be observed showing steps of about 40 m. Frey-Marinez et al. (2006) demonstrate that ramps are

often connected with an accumulation of deposited material behind up-stepping ramps, so that the thickness decrease of the deposited material is smaller than the actual height of the ramp. This is the case especially for frontally emergent landslides where the toe of the slide is further away from the ramp (Figure 40). Ramps are relatively common features in major slides and are easily to detect in seismic data (Bull et al., 2009). However, due to their similarity to faults, headwalls or even sidewalls one has to be careful to avoid misinterpretations. Different explanations are discussed for the genesis of ramps such as variations in mechanical properties as friction along the glide plane, variations in mechanical properties of the transported material or a combination of both (Bull et al., 2009). In general ramps are aligned perpendicular to the slide direction but they are also observed parallel to the transportation direction. These kinds of ramps are referred to as slots but Bull et al. (2009) also admits that there is no satisfying explanation by now to describe development of such slots.

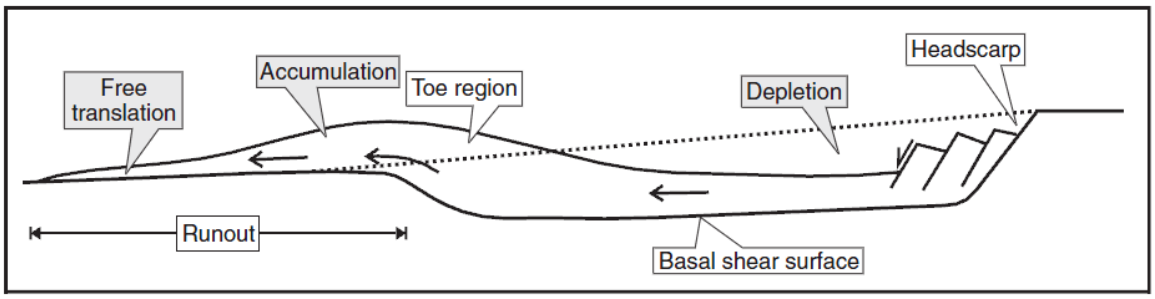

Figure 40: Schematic depiction of frontally emerged landslides. Material ramps out the basal shear surface onto the seabed and is free to travel considerable distances over the undeformed slope position. From Frey-Martinez et al.

Thickness decrease in the Udenisht depositional body may also be interpreted as an up-stepping ramp as its orientation is perpendicular to the main transportation direction and it lies within the observed dimensions of ramps. The bathymetric data shows a basin wards morphological downward step of a few meters at almost the same location as the in the slide body. As the morphological step more or less follows the supposed ramp, these two features are very likely to be related. This observation, however, is in contrast to the observation that ramps tend to lead the transported material to overflow this obstacle and thereby generate sediment accumulations at the lake floor. For the Udenisht case, step like decrease in slide thickness correlates with a downward step at the slide surface. Erosion processes after slide deposition cannot explain this step observed on the bathymetric map. As mentioned in chapter 3, cold water current is flowing from the southern margin along the deep Central Basin northwards. Deposits further down-slope might be affected by strong erosion due to this current and therefore create a deeper located toe of the slide deposits. The alignment of the morphological step at the lake floor and the thickness decrease of the slide deposits cannot be explained simply by an erosive current at the lake floor.

A two-phase Udenisht Slide event offers an alternative interpretation for the sudden decrease of the slide thickness. A first slide cut deep into the underlying sediments and deposits of this first event are found up to the area, where the sudden decrease in slide thickness is observed. A later second slide deposited sediments on top of the previous slide but the run-out distance for this second slide was longer. Deposits of the second slide are overlying the deposits of the first event with more or less constant thickness conserving the shape of the previous slide deposit. This scenario will be discussed in more detail in the following chapters.

Volume

Volume estimations were done for the transparent depositional body of the Udenisht Slide. Therefore the base of the Udenisht Slide body was picked using the Kingdom Suite software package and a 3D-depth grid with depth values converted from travel times of seismic data was created. For this purpose an imaginary well was placed in the study area containing a Time-Depth chart with a velocity model as explained before.

The Kingdom Suite software now allows calculating the difference between bathymetric grid and the depth grid of the base of the slide limited by a polygon encircling the area of deposition (Figure 39). Another polygon was created representing the area where material was deposited but excluding the evacuation area (Figure 39, dashed lines). Calculated volumes of deposited slide material are presented in Table 3:

	Area (km^2)	**Volume (km^3)**
Whole Udenisht deposition unit	**24**	**0.42**
Slide deposits not including the evacuation area	**20**	**0.38**
Evacuation area	**8**	**0.11**

Table 3: Dimensions of Udenisht Slide

Volume calculation demonstrates that the slide deposits almost exceed the volume of the evacuation area by a factor of four. At first glance this is an amazing discrepancy. However, slide material, which was already deposited in the evacuation area distort the estimation of evacuated and deposited sediments. This is illustrated in Figure 39 where an overlapping zone (between red and blue dashed line) represents an area deposition in the evacuation zone. On one hand this leads to an increase in the total deposited volume but on the other hand it also leads to an underestimation of the volume of the evacuation areas. To overcome this problem an additional polygon was generated that only calculates deposits outside the slope area (east of the dashed blue line in Figure 39). This leads to a volume of 3.8 km^3, which is still more than three times the volume of the missing slope.

The mismatch between missing material and deposited material might have various reasons. One possible explanation falls together with a topic which will be discussed in the next part: the origin of the slide. As mentioned earlier, the exact position of the headwall area of Udenisht Slide still remains speculative. Hence, it is possible that the actual failure scar of the slide is situated further up-slope and subsequently the estimation of the missing material would be too small.

Besides the possibility of higher located failure, basal erosion during the slide process is very likely and would explain the volume discrepancy. Erosive processes within large submarine landslides are a common process observed and reported by several authors (Klaucke and Cochonat, 1999; Pratson and Coakley, 1996). Gee et al. (2007) show an example of the Brunei landslide where about 80% of transported material was mobilized by basal erosion during the slide. They also point out that landslide induced erosion is capable to remove hundreds of meters of seafloor sediments. Explaining the volume discrepancy only by erosional processes during the landslide would imply that about 70% of transported material during the Udenisht Slide was mobilized during the slide event by basal erosion accompanied by a migration of the

landslide base deeper into the underlying sediments. Such huge amount of additionally activated sediments implies immense energy contained in the moving landslide body. This can be seen as an indicator that Udenisht Slide was a high-energy event not only transporting sediments from the slope but also activating sediments while the slide was over-running them. Surprisingly, mobilization of underlying sediments took place in rather flat regions with slope angles of about 0.5° and continues for several kilometers indicating that the slide still was highly energetic when it entered the flat Central Basin. This is in accordance with the long run-out distance which also testifies the power contained in the mass movement.

As seen in bathymetry and backscatter data an elongated channel-like structure is located at the central part of the Udenisht Slide (Figure 27, Figure 29, and Figure 30, 8). Seismic data (Figure 34) shows that this area is also characterized by down cutting of the basal glide plane in a V-shape form. While no comparable channels are found in such depth ranges in Lake Ohrid it is likely that this structure is related to the sliding process of the Udenisht Slide. Seismic profiles show that infill of the channel is similar to Udenisht Slide deposits suggesting that sliding material concentrated at the central part of the slide resulting in deep erosion of underlying sediments. Energy of the slide is assumed to be highest along this area. Considering the entire width of the slide at around 150 to 180 m water depth, it stands out that two large morphological highs structures are located at the northern (Figure 27, 10) and the southern (Figure 27, 5) margin. In the central part no such morphological features are visible on the bathymetric map. In contrary the central part even shows incision into the underlying sediments. Not only most of the slope sediments were transported in the central part; it also seems to represent the part with the highest energy regime. It is likely that previously existing obstacles were removed by the massive force of down-sliding materials. Next to the channel structure an elongated rather irregular and blocky part is located (Figure 27) indicating that this zone was mainly used for deposition of huge blocks during the slide event. In contrast, the channel acted as a pathway for fully disintegrated material causing deep erosion into underlying layers. Deep erosion in front of the slope was probably facilitated by the presence of gas seepages (Figure 33, Figure 34, and Figure 35a). Liquefaction of sediments due to migrating fluids supports erosion of softened material during the sliding process.

Sediment echo sounder data shows a relatively homogenous transparent slide body with hardly any internal structures in the deposition unit. This is the result of complete mixing of mobilized sediments during the sliding process where even the stratification of former undisturbed and layered sediments was fully destroyed by the erosive character of the mass movement. The toe of the slide depositional area is characterized by rough topography but no larger blocks are observed assuming that the material transported furthest away from the slope was rather fully disintegrated and therefore easier to move.

5.2.4. Slide Processes

Slide Origin

A major question in order to understand the slide process of the Udenisht Slide is the location of the origin of the sliding process. As shown in the Results chapter this is a quite difficult task because bathymetric data from the headwall area does not show a clear failure scarp. The defined headwall area indeed shows steeper slopes than adjacent areas in the north and south

but the exact starting position of the mass movement remains uncertain. Two main contrasting hypotheses can be made with regard to its origin:

The failure occurred on land and the slide propagated into the lake or the failure scarp is located within the lake but shallower than 25 m water depth and hence was not completely imaged by acoustic data. In the second case the steep flanks mapped during the multibeam survey represent part of the headwall area.

The absence of a well defined headwall suggests that is in any case further up-slope maybe even on land. Lake Ohrid is surrounded by steep mountain chains especially at the eastern and western margins. The distance between the available bathymetry and the coastline is only about 240 m. Hence the small volume of the evacuation area indentified in the lake may point to a land origin of the slide. Unfortunately no detailed images of the onshore area between the small towns of Udenisht and Memelisht are available. Only satellite images and Aster elevation data can be used to search for onshore evidences of a mass failure or a headwall (Figure 41).

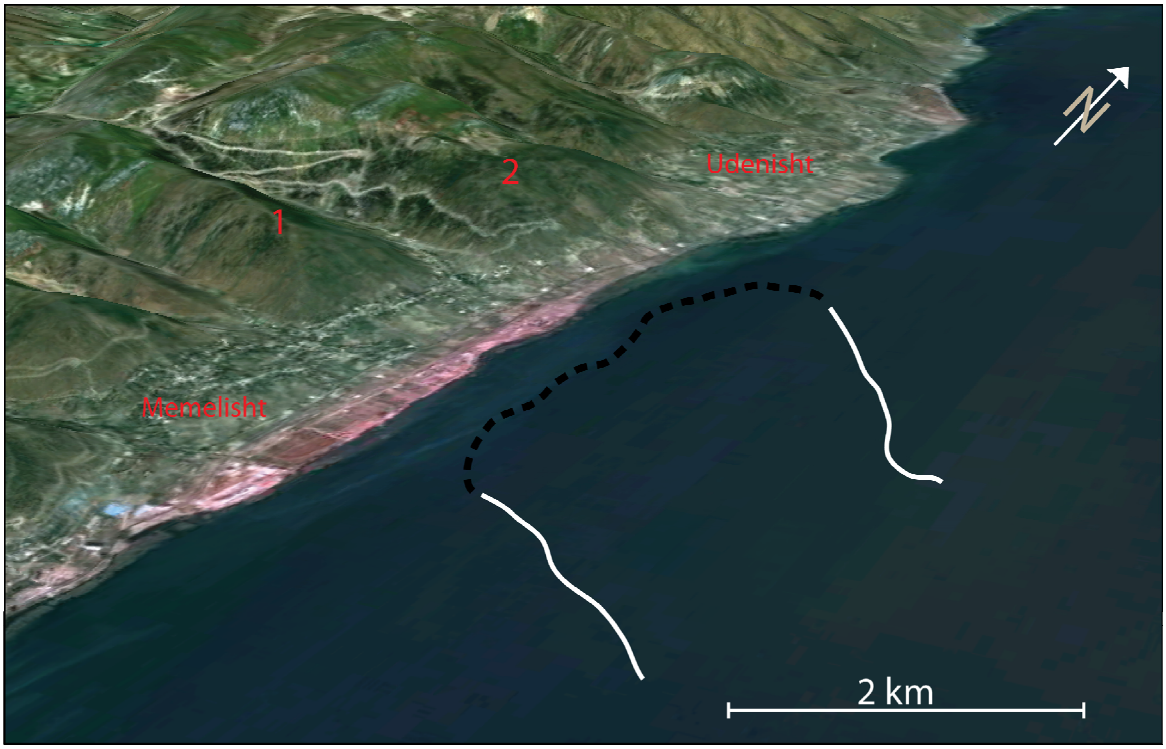

Figure 41: 3D-View of the headwall area of Udenisht Slide. The dashes line shows the assumed headwall based on bathymetric data. White lines show position of sidewalls. Two mountain ridges (1 and 2) are located between the small villages of Udenisht and Memelisht which are potential locations for a sub-aerial origin of Udenisht Slide.

Analyses of these images illustrate that two west - east elongated mountain ridges with steep slopes of more than 15° directed towards the lake are found at the onshore extension of the slide area. A narrow (50 - 450 m) plain is situated between lake and mountains on which the two villages are located. The mountain number 2 (Figure 41) reaches very close to the coast (ca. 50 m). This area coincides with the closest mapped sub-aquatic position of the Udenisht Slide at the western coast line and hence would be the most-likely candidate for a sub-aerial failure. Steep mountain flanks can be prone to mass failure events, but nevertheless the Udenisht Slide probably did not had its origin on land for the following reasons.

First of all no obvious headwall can be found in the elevation data as well as in satellite images. With an age of less than 800 years this event should have left noticeable traces on the

flanks of the mountains even though erosion is considered to be high. No historical report about a landslide was found in chronicles of the Albanian coastline of Lake Ohrid although information about the history of the two villages is very poor. Nevertheless a significant headwall scarp or sidewalls similar to the ones inside the lake should be expected after such a large mass movement.

Secondly, the narrower mountain (Figure 41, number 1) is located several hundreds of meters away from the coast separated from the lake by a flat coastal plain. A slide starting so far away from the coast must have had enormous initial energy to travel across this flat area into the lake. No evidence of such a large event is found on the flanks of this mountain. The only mountain that can come into consideration is the one south of Udenisht (Figure 41, number 2) because of its proximity to the lake. The width of the mountain, however, is relatively small compared to the slide width inside the lake. If the slide would have started on this mountain flank it must have widened extremely fast from the size of the mountain (ca. 1 km) to the width of the slide area (2 km) in the lake.

It is more likely that the origin of Udenisht Slide lies within the lake. Probably the very steep part of the assumed headwall area is in fact part of the headwall but lack of bathymetric data closer to the shoreline typical headwall morphology is not imaged. Maybe one additional multibeam profile a little closer towards the coast would have revealed the failure scar. Typical slope angles for headwall areas of sub aquatic landslides are within 10-30° (McAdoo and Watts, 2005; Strasser et al., 2007; Sayago-Gil et al., 2009; L'Heureux et al., 2010). These values are in good agreement with those observed in the headwall area of Udenisht Slide. Steep slopes with heights of 25-45 m compared to sidewall heights of max. 20 m support the fact that they belong to a headwall area. Bathymetry profiles from areas north or south of Udenisht Slide show that continuous slope prolongation towards the coast would result in slope angles of max. 10°. This is already quite steep but less than values within the Udenisht Slide area indicating that this is the beginning of the headwall. Hence even though the headwall scar is not resolved in the data it is likely that the steep part parallel to the coast already shows the beginning of the headwall. The actual position of the failure scar remains insecure but probably lies within 150 - 250 m offshore.

Temporal development of the Udenisht Slide

The main transport direction of Udenisht Slide is north-east. While in the upper part (above 150 m water depth) it is directed only towards the east, the slide direction changes to a north-eastern tendency which also comes along with a widening of the slide. Based on the results presented earlier in this thesis several scenarios for the development of the sliding event can be discussed. In the following three scenarios will be presented that are visualized in Figure 42 assuming that the Udenisht Slide occurred as

-one large slide,

-two slides (first one originating at ca. 160 m water depth, second one at the present headwall),

-two slides (first one originating at ca. 130 - 140 m water depth, second one at the present headwall).

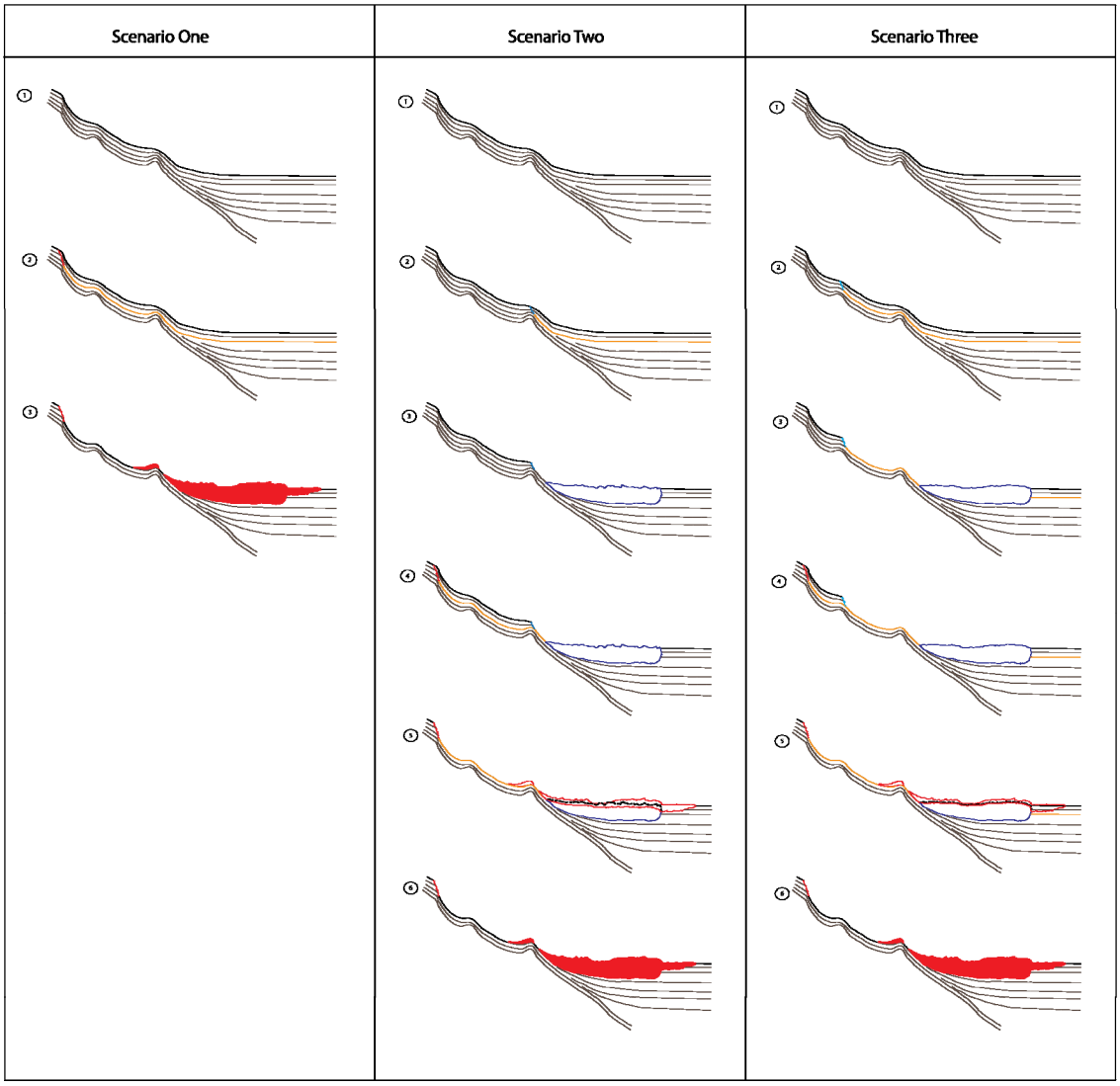

Figure 42: Different stages of the evolution of Udenisht Slide based on three different scenarios described in the text. As a basis for these sketches, the seismic profile of Figure 33 as well as the lake floor morphology of the reconstructed and present day slope were used. The last stage of every scenario shows the present situation of lake floor morphology and slide deposits.

Scenario One: A single large slide

If the Udenisht Slide is considered to be a single phase event this failure must have been started at the present day headwall area. As one reason for the failure to start here the steep slope of this area can be mentioned. Adjacent areas north and south of the Udenisht headwall area show slope angles of more than 10°. After the onset of the mass failure an enormous amount of slope sediments were mobilized over a width of 2 km and started to move down-slope. The enormous sediment package of partially more than 20 m in thickness was released and transported eastwards. Following the largest gradient the slide direction shifted northwards towards the Central Basin in ca. 140 m water depth. No major slide deposits are found in the headwall area as well as in the Upper and partially Middle segment of the slide.

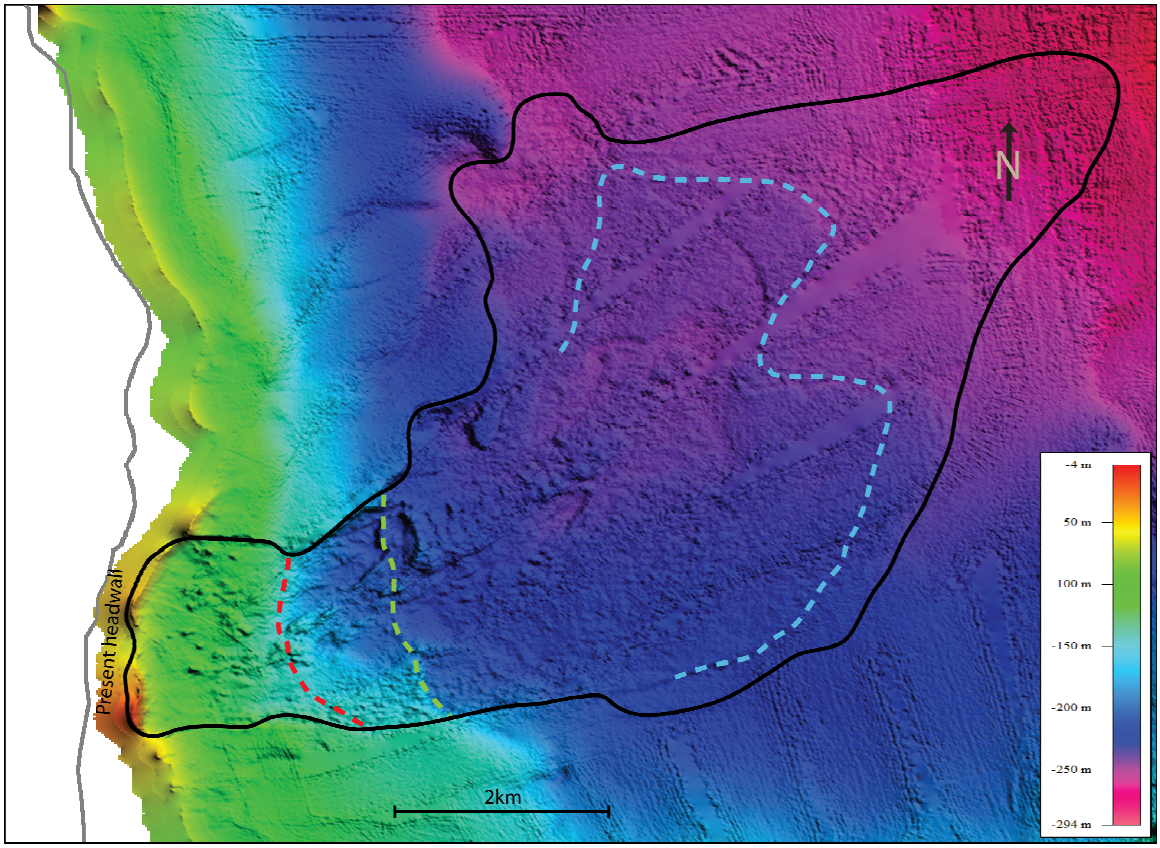

Figure 43: Bathymetric map of Udenisht Slide showing assumed headwalls for the first slides described in scenario two and three (dashed green line indicating failure scarp of scenario two, dashed red line marks area of assumed headwall of the first slide in scenario three). Dashed blue line shows extensions of slide deposit of the first slide based on the sudden change in thickness of Udenisht Slide body and on a morphological step at the lake floor. Total area of Udenisht Slide is shown by the black line.

Therefore the lake floor in these areas represents the exposed glide plane except for some small post slide drapes, which are imaged in the acoustic data. As the sliding body entered the lower segment it already gained enormous kinetic energy and hence was able to erode massive amounts of undisturbed sediments. The basal shear plane was cutting into deeper sediments, in some areas nearly as deep as the top of the "Naum" unit which partly makes up the base of the Udenisht Slide. Eroded sediments were mobilized, transported as part of the whole sliding body and completely mixed. At around 200 m water depth deposition of the transported sediments began but the main slide body was still in motion. The material was moving on for several kilometers into the plain Central basin. In about 3 km distance from the outer toe of the present deposits, energy of the slide had decreased that much that it was not possible to erode the underlying sediments any more. Increased friction along the basal shear plane resulted in an up-stepping ramp. The slide had still enough energy to transport sediments for another few kilometers until finally the kinetic energy of the slide reduced so far that the slide came to a stop.

Scenario Two: Two slides

A second scenario includes two mass movement events that produced the observed sliding structures. In this scenario Udenisht Slide can be seen as two relatively independent events or as a retrogressive slide, which is very common for sub-aquatic mass wasting. The large Storegga

slide that affected the Norwegian margin is the most famous example of retrogressive sliding where first failures are located down-slope and the following failure scarps migrated further up (Haflidason et al., 2004; Kvalstadt et al., 2005). Gardner et al. (1999) demonstrated that the Humboldt slide (offshore California) consisted of several retrogressive failure episodes where each failure undercut the sediment sequence of the up-slope area and thus decreased its resistance and subsequently failed (Gardner et al., 1999).

In this second scenario for the Udenisht mass movement, a first failure took place at about 160 m water depth at the location where a north south elongated morphological step can be seen in the bathymetric data (Figure 27, 5). This morphological step would be part of the ancient headwall of the first event. This ancient headwall probably extended over 2 km in north-south direction across the entire width of the slide. The position of the assumed first headwall can be seen in Figure 43. Activity along a fault system running along this headwall acted most likely as a trigger. Sediments were mobilized from ca. 160 m water depth on and were transported in north-east direction. Massive erosion during the slide activated additional undisturbed sediments and caused down stepping of the basal shear plane. The slide material was transported between 3 and 4.5 km away from the headwall towards the Central Basin. The border of the deposition body consisted of an accumulation of slide material creating a bulge at the lake floor. The areal extent of the first slide deposition is marked in Figure 43. The second failure took place at the present headwall area and caused down sliding of sediments along the Upper and partially Middle segment. The role of the missing material (from the first slide) for subsequent failure of the second slide cannot be determined clearly; hence it is not possible to distinguish whether an additional trigger like an earthquake was needed to initiate the second event or if it started due to decreased resistance at its base through material removal from the first slide. Therefore it is not possible to define if both slides occurred individual or are part of a large retrogressive sliding process.

After the second mass failure was released the activated sediments were sliding down-slope overriding the headwall of the first event. Small amounts of sediments have been deposited at the back of the first headwall where an up sloping area can be seen (Figure 33), but most of the first headwall was eroded during the second slide. On the way down, the moving sediments also overrode the deposited material from the first event. Since the second event had its origin at around 30 m water depth, the moving sediment body gained immense kinetic energy and hence was able to erode material from the slide body of the first event. The interface between slide deposits from both events is not visible in the acoustic data because the contrast in seismic impedance is non existing or very small. Both slide events have similar sedimentary composition at the interface. Heterogeneities assumed at the interface of both slide deposits are at very small scales and cannot be resolved by the acoustic systems resulting in transparent reflection-free slide bodies. Deposition of the second event not only covered the complete deposition area of the first event it also propagated further into the Central Basin. By overflowing the accumulations at the end of the first deposition this step was also conserved at the top of the second deposition. Therefore the extension of the first deposition is still visible at the lake floor. The time delay between first and second slide cannot be determined because the interface between the two events was eroded or the time was too short to accumulate enough sediments.

Scenario Three: Two slides

The third scenario is similar to the second one except that the first failure started at about 130 - 140 m water depth in an area, where a change in sliding direction from east to north-east is observed in the bathymetric data. The position of the first failure also falls together with a change in slope angle at the present lake floor from about 4° to a small area of nearly 8° gradient in down-slope direction (Figure 43). In this scenario the morphological step described as being part of the headwall in scenario two is explained as part of a large displacement along a prominent fault system which already existed before slope sediments were removed by the mass movement. The first slide transported material down-slope similar as the first slide in scenario 2 but exhibiting more energy because the failure started further up-slope. In addition the first event consisted of more material compared to the first event of scenario two. Higher position of this event let assume that it was an event with a higher energy potential and subsequently erosion of undisturbed sediments was greater compared to scenario two. Down-stepping migration of the basal shear plane proceeded as described in the previous scenarios. Deposition of this first slide body started ca. 1 km away from the failure and continued for another 5 km. A bulge was created at the northern and eastern margin by this slide unit. A second slide starting at the present day headwall area was overriding the deposited material of the first slide. Since the second slide had a higher starting position it was able to propagate further into the Central Basin. At the margin of the first deposition body the second deposition is overlying and adopting the bulge that is now seen at the lake floor, marking the extension of the first event (Figure 43, dashed blue line). Material from the second slide was deposited until it reached a maximum distance of 9.5 km from the headwall.

As already mentioned in the second scenario, the time between first and second slide cannot be determined because the whole depositional area of the first slide is covered by the deposits of the second slide. The estimated age of 200-800 years of the Udenisht event only applies for the second slide. Furthermore it is not possible to distinguish if both slides are independent slides or retrogressive events. But it is likely that such a huge event as the first slide had enormous implications on the slope stability of the remaining slope. Therefore this critical condition probably could not be maintained over long time and failure of the second slide occurred relatively shortly after the first slide. The exact timing, however, remains still unclear and shortly after the first slide might be minutes, days, weeks or even years.

These three scenarios could explain the slide deposition unit as well as headwall and sidewall structures which are observed at the present lake floor. As mentioned before the explanation of ramps is in contrast with the observed deepening at the lake floor in slide direction. Therefore Scenario 1 suggesting one large slide is less likely. Also the second scenario has some shortcomings. Since the first failure is described at ca. 160 m depth it is difficult to image that this event had gained enough energy to erode more than 20 m of undisturbed sediments only a few hundred from the headwall. Furthermore this event must have started at rather low slope gradients (2°), which makes it even more difficult to gain enough acceleration energy to transport material for nearly 5 km. In my opinion the most favorable scenario is the third one where the first slide started further up-slope and the headwall is located at a steeper environment (4-6°). Therefore it is more likely that this event caused deep erosion because of its higher kinetic energy. It also seems plausible that this event was able to transport sediments

that far away from the starting position. The change in slide direction which starts at about 160 m water depth can be explained by the second event with distinctive slide characteristics.

The second and smaller slide in this case started further up-slope and therefore could transfer enough potential energy into kinetic energy in order to transport material over a distance of 9 km although the initial sliding volume of this second event was comparatively small.

A volume calculation of the initial sliding masses from scenario three (based on a headwall of the first slide as seen in Figure 43) is presented in Table 4. Taking into account that position of the headwall from the first slide is relatively uncertain these volume estimations must be regarded carefully. Only estimations about the removed slope sediments (evacuation area) can be given but within the slide deposit it cannot be distinguished how much material was deposited from the first or second slide.

	Area (in 10^6 km^2)	**Volume (in 10^6 m^3)**
Slide 1	**5.5**	**80**
Slide 2	**2.5**	**30**

Table 4: Dimensions of the two initial slide bodies of Udenisht Slide discussed in Scenario Three. Values based on an assumed failure scarp in Figure 7 (dashed red line).

The large sliding block at the northern part of the Middle segment (Figure 27, 10) was probably released after or during the second slide as only small amounts of slide deposit are found at the back of this massive structure. The blocks in the Upper Segment (Figure 27, 1 and 2) were also affected by the second slide. They could not have been located at their present day position already before the occurrence of the second slide because the large amount of overriding slide sediments surely would have moved these blocks, too. Their present day's position along the steep Upper segments might be a result from transportation during the second event, indicating that disintegration of the failed sediments was not complete and large and heavy blocks were deposited close to the headwall. But it is also possible that parts of the steep headwall remained instable after the second slide and blocks were breaking off the headwall and toppling down into the Upper segment. Some of these blocks are found more than 500 m down the headwall area; hence indicating that they were not only falling from the headwall but also sliding before they stopped. Accumulation of these kinds of blocks close to the northern sidewall points to a larger part that was breaking off the headwall and gliding down. It is possible that the blocks were falling down even in the recent past and that this is still an ongoing procedure which is proceeding further to the coastline. This would keep an important threat for the coastal areas between Udenisht and Memelisht suggesting that the slope in vicinity to the shoreline is still instable and sliding, which even may affect parts of the coast, must be considered for the future.

5.2.5. Frequency of mass failures

As seismic profiles of the southern part of the lake illustrate, Udenisht Slide was not the only mass movement event that occurred in this region (Figure 35). At least four older slides on the southern margin of Lake Ohrid can be detected buried under several layers of sediments. The occurrence of several mass transport deposits within the south-western part of the lake

evidence that this region was a very active region for mass failures in the past. It indicates that these parts of the slope are rather unstable and prone for slope failures. Analysis of older mass failures can give a hint about reoccurrence rates of landslides.

Dating of older mass movement events is more complicated than for Udenisht event. Uncertainties in the grade of erosion and about long term sedimentation rates make it difficult to estimate the age of the deposited sediment layers on top of the mass deposits. Additionally resolution of multichannel seismic is poorer for greater depth and discrepancies from the actual velocity profile are amplified for deeper events.

The Naum mass movement could be traced in several seismic profiles (Figure 35, Figure A11). Large areas of the Naum deposition are overlaid by Udenisht Slide deposits. Most of the sediments above the Naum unit have been eroded by the Udenisht event leaving only one prominent irregular reflector that marks transition between those two events. Based on acoustic profiles origin of the Naum event is assumed to be south-east of Udenisht Slide. Areas where the Udenisht Slide did not affect the sediment layers on top of the Naum deposit demonstrate 25 to 30 m of sediment deposition after the Naum event resulting in an age of ca. 40 to 50 kyrs.

It must be taken into account that this age calculation is based on sedimentation rates during the Holocene (Wagner et al., 2009). Wagner et al. (2009) further demonstrates differences in sedimentation conditions between Pleistocene and Holocene, hence the estimated ages of the older mass wasting events contain large uncertainties. Age of the Tushenisht 1 event located below the Naum landslide could not be estimated because the top of the deposition area is covered by the Naum unit. Erosion due to the Naum event must be considered here because no undisturbed sediments were found on top of Tushenisht 1 unit and hence only a relative age can be given showing that Tushenisht 1 event must be older than the Naum event. It is also difficult to determine an age for the Tushenisht 2 event. Overlying reflections can be traced into the Central Basin, where they are found in ~140m burial depth corresponding to n approximate age of 230 kyrs. The Tushenisht 1 slide as well as the Tushenisht 2 slide is assumed to have their origin at the southern margin. Trpejca located southeast of the Udenisht deposit is buried under 30 - 35 m of sediments. This rather small event has an estimated age of 50 to 58 kyrs (Figure 35b). Table 5 summarizes the ages of five mass movement deposits identified in the southern part of the lake.

Mass movement	Age (BP)	Origin
Udenisht	**200 – 800 yrs**	*South-western margin*
Naum	**40 – 50 kyrs**	*Southern margin*
Tushenisht 1	**> 50 kyrs**	*Southern margin*
Trpejca	**50 - 58 kyrs**	*South-eastern margin*
Tushenisht 2	**230 kyrs**	*Southern margin*

Table 5: Summary of origin and ages of large mass movement deposits within the southern part of Lake Ohrid.

The age estimates show that Udenisht Slide is the only mass movement in this area that occurred in the recent past. This indicates that mass movements occur on a relatively irregular basis and hence a reliable reoccurrence frequency for landslides within Lake Ohrid cannot be given. A thin layer of deformed reflectors lies between Naum and Tushenisht 1 deposit indicating that sediments on top of Tushenisht 1 have been affected by the Naum slide. Around

50 kyrs B.P. three larger mass movements have occurred at different locations in the lake followed by relatively long time of quiescence before the large Udenisht event took place around 800 yrs ago. It further demonstrates that conditions for slope failures remained after sliding.

Naum and the two Tushenisht events are assumed to have their origin at the southern margin of the lake. Udenisht in contrast is the only event that started at the south-western margin indicating that all parts of the southern lake provide conditions for sublacustrine slope failures. Drawing a trend for mass movements in this area would be too farfetched. The comparison of the various mass transport deposits clearly shows that the Udenisht event was without doubt the largest event in the southern part of Lake Ohrid in terms of affected area as well as with respect to its depositional thickness. It was probably the event that started closest to the coastline but also the one which transported sediments the farthest into the Central Basin.

5.2.6. Trigger mechanisms

Discussion of trigger mechanism for mass movements is a rather speculative topic because often these processes have not been observed directly and evidences like erosion at the base of the slope or temporarily increased sediment input around the headwall area are likely to be destroyed during the mass transportation process.

Earthquakes are important trigger mechanisms causing submarine landslides. Earthquakes can act as a trigger by a rupture on a fault plane directly at the site where the slide occurs or by seismic shaking from large earthquakes in the surrounding area. For being located in an active seismic region, earthquakes come in mind immediately when talking about trigger mechanism of the Udenisht Slide. Historic reports about large and devastating earthquakes are relatively rare for this particular region. Only a few historic events were found (Table 6).

Time (A.D.)	Location	Magnitude	Reference
518	Macedonia		*Ambraseys and Jackson, 1998*
896	Veria (northern Greece)	>6.5	*Stiros, 1998*
1211	Veria (northern Greece)	>6.5	*Stiros, 1998*
1395	Edessa (northern Greece)	>6.5	*Stiros, 1998*
1700	Kozani (northern Greece)	>6.6	*Stiros, 1998*
1911	Ohrid (Macedonia)	Ms=6.7	*Muço et al., 2002*

Table 6: Large historic earthquakes in the surroundings of Lake Ohrid

The most damaging documented earthquake happened in 518 A.D. and destroyed almost the whole city of Ohrid (Hoffman et al., 2010). Moernaut et al. (2007) demonstrate that even medium-sized earthquakes with M_l=4 are able to trigger landslides. The 518 A.D. event certainly had a much higher magnitude and hence the potential to trigger large mass failures. The youngest event of the Udenisht Slide, however, occurred less than 800 years ago; therefore 518 A.D earthquake can be excluded as the trigger mechanism at least for the youngest Udenisht Slide event. As discussed above, it is assumed that the Udenisht mass wasting deposits comprise two sliding events but it cannot clarified if the evolved retrogressively or rather independent. If the slide did not behave retrogressive but consists of two relatively independent events the first

slide might have occurred much earlier and then the 518 A.D. earthquake might indeed be a possibility for triggering the landslide.

For a retrogressive event of course missing resistance from removed sediments at the base (due to the first event) is most likely responsible for activating the second event. This so called undercutting process is often observed for retrogressive landslides as reported for the Skagway, Alaska (Watts et al., 2005), the Humboldt Slide (Gardner et al., 1999), or the large Storegga Slide (Haflidason et al., 2005). Undercutting thereby decreases the resistance for the up-slope sediments and enhances the potential for subsequent failure (Gardner et al., 1999).

If an earthquake triggered the second slide event, such an earthquake must have occurred between 1200 and 1800 A.D. For this reason also the strong earthquake of 1911 could not have acted as trigger. Only few larger earthquakes are reported during the appropriate time but with relatively large distance of more than 100 km to the Udenisht Slide area. Even if they have been actually felt by residents around Lake Ohrid seismic shaking of these events was probably too small to trigger a failure such as the Udenisht event. Therefore it is more likely that a smaller event (not reported in historic chronicles) but located closer to the Udenisht Slide was responsible for the onset of the mass movement. Seismic data allows no closer investigation of the assumed headwall area and therefore existence of faults at the surrounding of the headwall cannot be proofed. But several large fault structures have been identified along the entire western slope (Figure 25b) and even in proximity to Udenisht Slide area (Figure 33, Figure 34 and Figure A10 in the appendix); hence it is likely that active faults can be found within the headwall area. The morphological step in the Middle Segment is probably related to displacement along a fault (Figure 33). Although it was created before the occurrence of Udenisht Slide (causing deposition in the back of the wall, Figure 32) it shows large offsets due to active faults in direct vicinity to the slide.

Despite the frequent occurrence of earthquakes as likely triggers, only a potential instable slope will fail during an earthquake. Hence it is also important to discuss pre-conditioning factors for slope failures.

The occurrence of gas seepages at the base of the south western slope is a pre-conditioning factor which may have played a role in the failure of the Udenisht event. Bright spots (Figure 35a, Figure A11, appendix) and fluid migration paths imaged as vertical blanking zones (Figure 33, Figure 34, Figure 35a) are found in seismic data at the transition between Udenisht Slide and the Central basin. Liquefaction and softening of sediments through upcoming fluids might have caused destabilization of the Udenisht slope area. The large depression visible at transition between Middle segment and Lower segment (Figure 27 and Figure 29, 14) of the slide is probably due to gas seepage as well. The seismic profile shown in Figure 35a illustrates high amplitude reflections with reversed polarity within the Udenisht deposition unit that originate from gas migration paths through the underlying sediments reaching the lake floor at the location of the elongated depression. This is a good indicator that rising fluids have caused liquefaction of the topmost material resulting in depression structures at the lake floor similar to the depression found above the WS2 deposition unit (Figure 23). As this has been observed at the base of the former slope it must be considered as a destabilizing factor for slope sediments.

For being located close to the coast increased sediment input from land could have played an additional role. By deposition of these sediments on the steep western slope, a critical stage might have been generated where the shear stress of the slope nearly reached its shear strength (Hampton and Lee, 1996).

From the list of trigger mechanisms and pre-conditioning factors for mass movements mentioned in the Introduction several factors do not apply for the Udenisht Slide: First of all glacial loading certainly did not play a role (because of the young age of the slide); secondly evolution of salt diapirs is not observed in this region; sea level changes must not be considered because water level of Lake Ohrid was relatively stable during the last centuries; and finally human activity can be excluded as well.

For Udenisht Slide probably a combination of several pre-conditioning factors must be considered such as fluid seepages at the base of the slope, the general steepness of slopes and increased sediment input. The actual trigger mechanism was most likely a local earthquake either for both slides, or in case of a retrogressive event the second event was mainly released by missing slope sediments.

5.3.Tsunami potential

Most of the worldwide occurring tsunamis are triggered by earthquakes. The most prominent example is the Indian Ocean Tsunami from 2004 where more than 200.000 people lost their lives and numberless communities were destroyed all around the Indian Ocean (Chateneaux and Peduzzi, 2006). For earthquake triggered tsunamis the wave height is mainly determined by the dimension of the displacement at the seabed and the amplitude of the earthquake (Harbitz et al., 2006).

But also landslide triggered tsunamis are reported to have caused devastating effects on off and onshore infrastructure. In 1998 more than 2000 residents of the coast of Papua New Guinea were killed by a giant tsunami wave which was later discovered to be the effect of an underwater slump (Synolakis et al., 2002). Nevertheless, mechanisms for those kinds of tsunamis are less well understood because numerous parameters such as the volume, initial velocity, material properties, water depth, slope angle, and deceleration influence the relationship between sliding body and thereby generated waves (Watts, 2001, Murty, 2003). Sub aquatic landslides deform during the wave generating process and coupling between the slide and the surface wave must be taken into account (Fine et al., 2002).

In general, volume of the sliding body is a one of the key parameters determining the wave amplitude in a way that a large volume also creates a high tsunami wave (Murty, 2003). But several case studies prove that also relatively small but sudden landslides can generated even more dangerous tsunamis than larger but slower landslides (Driscoll et al., 2000) as observed for example after a submarine mass failure in Nice in 1979 (Dan et al., 2007), hence unfolding that prediction of landslide tsunamis is an extremely complicated field.

Tsunamis generated by landslides show some important differences to earthquake generated waves. In general the wavelength of landslide tsunamis is much shorter (1-10 km) than for those produced by earthquakes (100-500 km) (Watts, 1998) even though the wavelength of landslide tsunamis is typically much larger than the water depths where they occur (Harbitz, 1992). In terms of released energy, Watts (2001) postulated that potential energy released from landslides is in the same order of magnitude than elastic energy released from earthquakes. The available tsunami energy released by earthquakes is proportional to the uplift of the seabed; hence earthquakes in general are able to move much more material compared to submarine landslides (Harbitz et al., 2006). On the other failure heights for landslides exceed several

hundreds of meters (or may be even kilometers), hence reaching vertical movements exceeding those of earthquakes up to 100 times resulting in comparable amount of tsunami energy (Okal et al., 2003). Another difference between earthquake and landslide tsunamis is their fluid dynamic character.

Waves generated by sliding masses have differences in their spherical spreading compared to earthquake tsunamis and are usually directed with the maximum wave heights in slide direction (Driscoll et al., 2000; Harbitz et al., 2006). Radial damping plays a much higher role for submarine landslide tsunamis than for earthquake tsunamis (Harbitz et al., 2006). Beyond that they are limited more locally but can reach much higher amplitudes than earthquake generated waves (Synolakis et al., 2002). In fact the highest amplitudes of observed tsunami have not been triggered by earthquakes but are due to landslides like for example a more than 42 m wave in Unimak, Alaska in 1946 (Fryer et al., 2004), or the highest observed tsunami by now in Lituya Bay, Alaska in 1958 where a sub-aerial rockslide was propagating into a fjord (Fritz et al., 2009) causing a wave of more than 524 m when running up the coast. The local fjord setting with steep walls, however, contributed significantly to the extraordinary tsunami heights.

Most landslide triggered tsunamis occur close to the coast line (for example on continental margins or steep flanks of islands or lakes) and because of the very short propagation distances the back-going tsunami in direction to the coast is much more dangerous than the directed outgoing wave (Geist et al., 2009). Tappin et al. (2001) report that a significant amount of wave energy of landslide triggered waves is propagating back towards the shore.

The question if Udenisht landslide in Lake Ohrid triggered a tsunami wave will never be answered definitely because no historical reports about either the slide or a tsunami wave are present. With respect to the age between 200 - 800 years and the fact that the coastline at that time was even less populated as today the absence of historical reports about anomalous waves in the lake does not exclude that the slide has triggered a wave. However, the question about the tsunamigenic potential of Udenisht Slide is of great importance especially in terms of hazards related to future landslides in Lake Ohrid.

To answer this question first it will be discussed if landslides of similar dimensions as the Udenisht Slide are capable to trigger tsunamis. Then simplified volume-to-amplitude relations are applied and the slide will be classified and compared to other landslides that are known to have generated tsunami waves.

5.3.1. Classification over landslide aspect ratio

Landslides often are characterized by the landslide aspect ratio, describing the relation between initial thickness of the sliding mass and its horizontal length. Watts et al. (2005) demonstrates formulas to estimate tsunami amplitudes based on landslide aspect ratios. While tsunami amplitudes are closely related to slide thickness it is important to define the triggering event. Therefore they use aspect ratios to distinguish between submarine mass failures: sub-aquatic slides that are suspected to be a tsunami source have aspect ratios of 0.005 - 0.02 while tsunamigenic underwater slumps show values of 0.05 - 0.15. With an assumed total length of 3.7 km and an average thickness of about 20 m the initial Udenisht Slide body (material that was removed from the slope) has a landslide aspect ratio of 0.005 and lies within the interval for tsunamigenic submarine landslides after Watts et al. (2005). Taking into account that the Udenisht event was probably a two phase event also the two single events have landslide aspect

ratios within the presented interval of Watts et al. (2005): first event: 0.013 (2.4 km in length, 20 m average thickness), and second event: 0.015 (1.3 km, 20 m), well within the range of tsunamigenic slides. This does not directly imply that the Udenisht Slide(s) triggered a tsunami but it shows that they lie well within the dimensions of numerous observed landslides that generated such waves.

5.3.2. Wave estimation according to slide volume

The initial slide volume can be measured using geophysical methods like multibeam/sediment echo sounder or seismic systems. Based on various observations of landslide tsunamis, Murty (2003) obtained a linear relationship between volume of the slide and the maximum amplitude of the followed tsunami waves:

$$H = 0.3945 \cdot V$$

Where H is the tsunami amplitude in m and V describes the slide volume in 10^6 m³.

This is a simplified model only taking into account the influence of the volume on the tsunami amplitude. Moreover it is only based on eleven examples keeping a rather poor regression analysis (Murty, 2003). A comparison with numerical models of landslide generated waves also showed an extremely weak correlation (Murty, 2003).

Applying this relationship on the total Udenisht Slide volume of 110 10^6 m³ results in a tsunami amplitude of 44 m. Considering the individual volumes given in Table 4 for a two event scenario result in tsunami heights of 32 m and 12 m for the first and second slide of the Udenisht event, respectively. With respect to large uncertainties in Murty's (2003) formula this value must be regarded with great care. His formula was obtained using data from special areas also including artificially induced rock falls. In his relationship a single event with more than 100 m in wave height influences the formula significantly. Also no data was used showing similar dimensions as the Udenisht Slides. Therefore wave estimation for Udenisht event should not be solely based on this relation. Wave heights of up to 44 m are very unlikely for a tsunami caused by a slide in Ohrid Lake.

Another relation between slide volume and wave height is proposed by Papadopoulus and Kortekaas (2003). Their relation resulted from observations of ten landslide induced tsunamis and their measured wave amplitudes and slide volumes. An empirical envelope of their findings is seen in Figure 44. Volume of the Udenisht Slide body is plotted in his relationship as well as volume of the two single events of the Udenisht Slide.

It can be seen that a one event Udenisht Slide cuts the envelope at nearly 13 m wave height while a scenario with two events cuts the envelope at 10 - 11 m (Figure 44). This still has to be regarded very carefully because the high envelope results from only two exceptional cases (PNG and Skagway, Figure 44, Papadopoulos and Kortekaas, 2003). Nevertheless compared to the remaining landslides that generated smaller tsunamis Udenisht Slide shows the largest volume (even assuming a two phase event of Udenisht event). Therefore the Udenisht Slide has to be considered as a potential tsunami source.

It must be remarked that numerous submarine landslides with comparable volumes are known that did not trigger noticeable tsunamis or no wave at all, showing that landslide tsunamis are an extremely complex phenomenon.

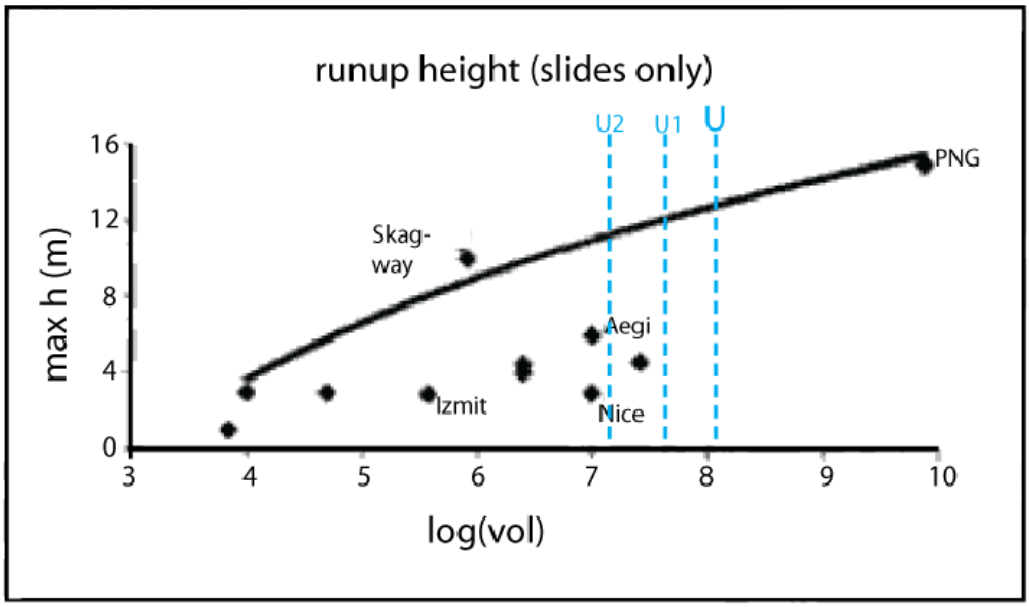

Figure 44: Empirical envelops of the maximum wave height (in m) as a function of the slump volume (in m³) (Papadopoulos and Kortekaas, 2003). Total volume of the Udenisht Slide inserted as dashed blue line (U) as well as volumes for the first (U1) and second (U2) event, based on Scenario Three.

5.3.3. Comparison with other landslide generated tsunamis

Several other observations and models provide additional data on waves generated by landslides. Table 7 summarizes data for numerous landslides with special focus on events with similar dimensions and settings as the Udenisht landslide. Most important parameters are slide volume, slope angle, setting and initial condition. It is difficult to create a data base for these kinds of tsunami waves because their reports focus on very different aspects of each event.

Table 7 illustrates that even small landslides are able to produce large tsunami waves and that slide volume alone does not explain wave amplitude.

The large Storegga landslide (Bondevik et al., 2005) in the North Atlantic is probably the best known example for the disastrous effects of landslide tsunamis where tsunami deposits are found even on the Shetland Islands that demonstrate wave heights of more than 20 m. Definitely this landslide is not comparable with the dimensions of the Udenisht Slide in Lake Ohrid. But geophysical observations revealed that Storegga slide consists of several events with different volumes. Numerical modeling of these individual events was done by Løveholt et al. (2005) with the main aim to analyze whether all partial events could have triggered a tsunami. Models of a particular relatively small block (F4, 1.3 km^3) of the Storegga Slide shows, that failure of this submarine block is still capable of generating a seiche wave of 1-2 m.

Numeric modeling of a landslide in the Santa Barbara Channel (Southern California; Greene et al., 2006) suggests that a tsunami with a height of at least 10 m was generated. Although the volume of the Goleta slide is larger than the Udenisht Slide it has comparable values with respect to slope angle or thickness of the slide. Another example of a small-scale landslide comparable to the Udenisht event that triggered a tsunami occurred in Nice, 1979 (Assier-Rzadkiewcz et al., 2000) where 0.01-0.15 km³ of material from a nearby harbor slumped down the relatively steep continental slope. This landslide started onshore but most of the transported material was mobilized underwater.

Location	Setting	Slope angle	Slide volume (in km³)	Slide dimensions (l=length, w=width, d=thickness), (in	Maximum wave height (in m)	Reference
Storregga (North Atlantic), 8150 y BP	Model of a Submarine Mass Failure (SMF) on a Continental Margin		3880		10-14 (peak heights of 30 m)	*Bondevik et al., 2005; Løvholt et al., 2005*
Storregga F4 sliding block	Model of a SMF on a Continental Margin, (waterdepth: ca. 300m)		1.3	l=2500, w=3000, d=100	2	*Løvholt et al., 2005*
Papua New Guinea (Pacific Ocean), 1998	SMF after a Ms=7.0 earthquake, (waterdepth: ca. 2000m)	12°	4	l=4500, d=600	15 (mean height: 10 m)	*Synolakis et al., 2002; Watts et al., 2005*
Santa Barbara Channel (Southern California), 6-8 kyrs BP	Model of a SMF on a Continental Margin, runout of 6 km, (waterdepth: 90-580 m)	6-10°	1.75	l=14600, w=10500, d=20-60, max. headwall of ca. 150m	10	*Greene et al., 2006*
Nice (Mediterranean Sea), 1979	SMF on a steep Continental slope	>10°	0,01-0,15		3	*Assier-Rzadkiewicz et al., 2000*
Degirmendere (Izmit Bay, Turkey), 1999	Subaerial slump after an Mw=7.4 earthquake	11°	0.01	l=300, w=75	4 (10-15 m in the bay)	*Watts et al., 2005; Tinti et al., 2006*
Lake Lucerne (Swiss Alps), 1601	Several subaquatious landslides after a Mw=6.2 Earthquake in a lake	5-15°	0.01		4	*Strasser et al., 2007*
Kitimat (B.C. Canada), 1975	SMF on a steep flank in a fjord, runout of 5 km	2-7°	0.06	d=30	8	*Prior et al., 1984*
Trondheim Bay (Norway), 1888	Submarine landslide on steep slope	12°	0.003	d=15	7	*L'Heureux et al., 2010*
Lake Ohrid (Balkan Peninsula), 200-800 yrs BP	**Subaquatious landslide in a lake, runouth of 6 -7 km, (waterdepth: 25 -**	**2-7°**	**0.11**	**l=3700, w=2200, d=20**	**?**	
First slide		***~ 2°***	***0.075-0.085***	***l=2400,w=2200,d=20***		
Second slide		***~ 4°***	***0.025-0.035***	***l=1300,w=2200,d=20***		

Table 7: Comparison of case studies (models and observations) of landslide triggered tsunamis with selected slide parameters

The Trondheim Bay tsunami, 1888 (L'Heureux et al., 2010) had a relatively small slide volume resulting in a wave of 7 m. This proves that the setting of the landslide is also particularly important for the wave generation. The 1975 Kitimat landslide in British Columbia (Prior et al., 1984) with a maximum wave height of 8.2 m shows comparable slope angle values as the south-western slope of Lake Ohrid although it has to be mentioned that this event occurred in a fjord with direct impact on the shoreline where parts of the coast subsided more than 26 m after the slide. A seiche wave in Izmit Bay, 1999 (Watts et al., 2005) was triggered by a part of the coast sliding into the sea. The preceding M_w=7.4 earthquake alone cannot explain the 3 m wave that was recorded in the Bay and even less a 12 m wave in the town of Degirmendere (Tinti et al., 2006). The extremely high tsunami waves caused by this relatively small-volume landslide point out the influence of the headwall origin on wave amplitudes. Sub-aerial slides are generating strong impulse waves when propagating into the water even if their volume is relatively small (Panizzo et al., 2005; Ataie-Ashtiani and Malek-Mohammadi, 2008). For assessing the tsunami potential of the Udenisht Slide, it would therefore be important to answer the key question whether the slide originated on land or offshore.

Landslide triggered tsunami waves are not limited to marginal seas but are also reported in lakes approved by a historical report of a 4 m seiche wave in Lake Lucerne (Swiss) in 1601 (Strasser et al., 2007) that was observed after a M_w=6.2 earthquake. Geophysical research showed that this wave must have been generated by a sub-aquatic slide within the lake with a volume of about 0.01 km³ on a 5-15° dipping slope that was released after the earthquake. With respect to the tsunamigenic potential of Udenisht Slide this case study is of great importance not only because the setting of Lake Lucerne is comparable with Lake Ohrid as both are mountain lakes with great water depth and with similar dimensions but additionally both lakes are located in seismic active regions.

The presented case studies show that there are several examples for landslides with similar dimensions and settings as Udenisht landslide capable of triggering significant tsunami waves that can destroy local infrastructure and contain a considerable threat for coastal communities. From this compilation several parameters for landslide generated tsunamis can be summarized as follow:

- mass movements with volumes as small as 0.01 km³ are able to generate significant tsunamis,
- thickness of sliding bodies can be relatively thin (15 m),
- these mass failures can occur on slopes with a relatively small slope gradient (2-7°),
- most of the observed cases are situated in active tectonic regions,
- mass failures were often connected to earthquakes,
- landslide triggered tsunamis can also occur in lakes, and finally
- headwall areas close to the coastline or even sub-aerial landslides that propagated into the water lead to higher amplitudes of the resulting waves than sub-aquatic landslides.

It must be noticed that this compilation contains only a few parameters that are important in terms of tsunami potential of sub-aquatic landslides. There are neither remarks on material properties of the sliding body nor the velocity of the sliding process even though these are also essential factors. Based on parameters presented here one can conclude that Udenisht Slide in Lake Ohrid fulfills conditions for tsunami generation and hence can be considered as a potential tsunami source.

5.3.4. Ideas about tsunamis from Udenisht Slide in particular

The compilation of landslide triggered tsunamis (Table 7) shows that every single case has its individual character and conclusion about the whole event based on comparison of single parameters needs to be regarded with great care. The Udenisht Slide shows some characteristics which might have influenced a potential wave and played a role on the effects on the shoreline.

As postulated by Discroll et al. (2002) landslide tsunamis are directed with the main wave amplitude along the slide axis; hence an Udenisht Slide tsunami would be directed in the northeast - southwest axis. Tappin et al. (2001) demonstrate that also a significant amount of the energy is directed in the opposite direction of the slide propagation. Therefore the proximity of the slide to the Albanian coast is of major importance for the impact of such a tsunami on the coast. With only 150 to 250 m distance from the headwall to the shoreline, a tsunami must have hit this part of the coast strongly and immediately after the sliding process. On the opposite side of the lake a northeast-ward propagating tsunami must have impinged the Macedonian shore around a small village called Pestani (Figure 4). Houses are built very close to the lake (only few meters away) along almost all Macedonian coastal towns. This implies a high danger for coastal residents in case of a tsunami wave hitting the shoreline.

Velocity of a propagating tsunami in Lake Ohrid would be lower compared to tsunamis in open oceans because of depth dependency on the wave velocity. Nevertheless time between wave generation and impact on the Macedonian coast (in about 15 km distance) must be expected within a few minutes. This evidences another dangerous feature of landslide triggered tsunamis within lakes: very short after the slide initiation, first tsunami waves will hit the coastline. Even if the mass movement would be recognized immediately there is almost no warning time until the wave hits the coast. The direction of landslide triggered tsunamis would result in only a few affected coastal regions around the lake that further might explain the absence of historic reports of such an event in the chronicles of larger cities such as Ohrid, Struga, and Pogradec.

As the Udenisht Slide most likely was a two phase event there are also main differences in possible tsunami generation for the two individual slides. According to Haugen et al. (2005) length of a sliding body mainly influences the wavelength of the tsunami while the thickness of the body determines surface elevation (besides sliding velocity, wave speed and water depth). Applied to the Udenisht case this implies that a wave of the first slide had a longer wavelength than the second one because of the dimensions of the two different sliding bodies. Height of the slide bodies was relatively similar for both events. Velocity of the second slide is assumed to be higher because the starting position was located on steeper slopes and the longer run-out distance of this event. Ward (2001) points out that tsunamis from landslides occurring in shallow water result in more hazardous waves than if the same slide would take place in deep water. This is either due to higher wave speeds but also an effect of the smaller distance available for

radial damping (Harbitz et al., 2006). Altogether this shows that the second event of Udenisht Slide must be considered as the more dangerous one in terms of its tsunami potential even though its volume is smaller than for first slide.

In case that the Udenisht Slide had its origin onshore, a generated tsunami would have been even more dangerous. As several examples of sub-aerial landslides propagating into the water showed (Okal et al., 2002; Papadopoulus and Kortekaas, 2003; McMurtry et al., 2003) these kinds of mass wasting processes are very likely to trigger tsunamis with extremely high amplitudes. This was probably not the case for Udenisht Slide, because it is very likely that the slide originated within the lake (see above). Harbitz et al. (2006) show that sudden deceleration of the sliding mass results in larger wave amplitudes, while large run-out corresponds to reduced wave heights. The long run-out distance of Udenisht Slide suggests that the deceleration phase of the mass movement was relatively slow causing the mass movement to stop far away from its starting position.

In summary estimating a tsunami wave from the Udenisht event is a very complex task. There are numerous parameters that favor the generation of a significant wave such as the large volume of the slide, steep slopes which probably lead to high velocities for the second slide and proximity to the coastline. On the other hand, indicators like the long run-out distance (suggesting slow deceleration phase) point to small surface elevations and hence a small effect on the coastline. A wave generated from Udenisht Slide(s) was probably much smaller than simple volume estimations would suggest. While a definite answer about a tsunami wave from this slide is not possible based on the data analyzed in this thesis, only a personal evaluation can be given taking all the presented observations, calculations and comparisons into account: In my opinion at least the second slide of the Udenisht event has caused a wave of about 1 or 2 meters height.

6. Conclusion

The now available high resolution bathymetric map of Lake Ohrid allows detection of several geological structures at the lake floor including areas that were affected by sub-aquatic mass movements proofing that the flanks of Lake Ohrid are unstable. Two mass failures detected along the western slope area (WS1 and WS2) show similar features in terms of source region, slide dimensions and run-out distances and suggest rather rotational sliding. Pre-conditioning factors such as fluid migration at the base of steep slopes are found and activation along faults close to the headwall areas is assumed to have finally triggered the landslides.

The large Udenisht landslide at the south-western part of the lake was found to consist of two successive events not allowing to define whether the process was retrogressive or consists of two independent events. The first event stared at ca. 160 m water depth related to a change in slope gradient and a change in slide direction. Although no actual failure scarp can be detected there are no evidences that origin of the second slide was on land. The age of the second slide lies between 200 and 800 years BP. Both events show a strongly erosive character indicating highly energetic mass movements able to transport slope material for several kilometers into the Central Basin. Investigation of structures in the sliding area illustrates intense sediment transport along a channel in the central part of the slide associated with down-ward migration of the basal shear plane. Evidences of fluid migration have also been found at the base of Udenisht Slide acting as instability factors for slope sediments as well as missing down-slope resistance due to removed sediments for the second event. While no large historic earthquake could be related to the time of Udenisht Slide local medium sized earthquakes are assumed to have finally triggered the mass failure.

Analysis of older mass wasting deposits that are buried under numerous layers of sediments show that such events occur irregularly in Lake Ohrid and that Udenisht Slide was the largest and youngest event on the southern part of the lake. Estimation of tsunami potential of the Udenisht Slide is a rather complex approach. However by comparison with other case studies it is conceivable that the slide triggered a wave of probably 1 to 2 m. This estimation still keeps several uncertainties and more complex tsunami modeling could provide more accurate amplitude approximations and also imply inundation effects on the shoreline of the lake. However it points out that risk assessment of landslides within Lake Ohrid must also consider tsunamis as an additional threat.

Acknowledgement

At the end of this master thesis there is still room enough I want to use to thank several people without them I could not have finished this thesis.

First of all I want to thank Prof. Sebastian Krastel for giving me the opportunity to terminate my study by offering me this project and for all of his explanations, suggestions and so much of his time, especially during the last weeks of my thesis. But also for enabling very interesting cruises and a great time in his working group. Special thanks go to Katja Lindhorst with her never-ending patience and for all the thinks she taught me. For every question I had concerning Lake Ohrid or whatever was on my mind she tried to find an answer and most of the time she did. I also want to thank Willi Weinrebe for being my second supervisor and introducing me to the complex world of multibeam echo sounders. Thanks also to Mathias Meier and Andrea Anasetti for sharing office, coffee and all kinds of geophysical ideas. Additionally all the people I came across during my thesis and who helped me in many different ways, especially Maxlimer Vallée, Stephanie Koch, Marion Liebetrau, Zoran Brdarovski, Robert Weis. Special thanks go to Lisa Bohlen for the non-geophysical support and of course to my family. And as always to Sabrina Kammerer.

References

Albrecht, C. & Wilke, T., 2008. Ancient Lake Ohrid: biodiversity and evolution, *Hydrobiologia,* 615**,** 103-140.

Aliaj, S., Adams, J., Halchuk, S., Sulstarova, E., Peci, V. & Muco, B., 2004. Probabilistic seismic hazard maps for Albania.

Aliaj, S., Baldassarre, G. & Shkupi, D., 2001. Quaternary subsidence zones in Albania: some case studies, *Bulletin of Engineering Geology and the Environment,* 59**,** 313-318.

Ambraseys, N. & Jackson, J., 1990. Seismicity and associated strain of central Greece between 1890 and 1988, *Geophysical Journal International,* 101**,** 663-708.

Ambraseys, N. & Jackson, J., 1998. Faulting associated with historical and recent earthquakes in the Eastern Mediterranean region, *Geophysical Journal International,* 133**,** 390-406.

Anselmetti, F. & Eberli, G., 1993. Controls on Sonic Velocity in Carbonates, *PAGEOPH,* 141.

Assier-Rzadkieaicz, S., Heinrich, P., Sabatier, P., Savoye, B. & Bourillet, J., 2000. Numerical modelling of a landslide-generated tsunami: The 1979 Nice event, *Pure and Applied Geophysics,* 157**,** 1707-1727.

Ataie-Ashtiani, B. & Malek-Mohammadi, S., 2008. Mapping impulsive waves due to sub-aerial landslides into a dam reservoir: a case study of Shafa-Roud Dam, *Dam Engineering,* 18**,** 243.

Bondevik, S., Løvholt, F., Harbitz, C., Mangerud, J., Dawson, A. & Svendsen, J., 2005. The Storegga Slide tsunami—comparing field observations with numerical simulations, *Marine and Petroleum Geology,* 22**,** 195-208.

Bull, S., Cartwright, J. & Huuse, M., 2009. A review of kinematic indicators from mass-transport complexes using 3D seismic data, *Marine and Petroleum Geology,* 26**,** 1132-1151.

Burchfiel, B., King, R., Nakov, R., Tzankov, T., Dumurdzanov, N., Serafimovski, T., Todosov, A. & Nurce, B., 2008. Patterns of Cenozoic Extensional Tectonism in the South Balkan Extensional SystemSpringer.

Chatenoux, B. & Peduzzi, P., 2006. Impacts from the 2004 Indian Ocean Tsunami: analysing the potential protecting role of environmental features, *Natural Hazards,* 40**,** 289-304.

Coleman, J. & Prior, D., 1988. Mass Wasting on Continental Margins, *Annual Review of Earth and Planetary Sciences,* 16.

Dan, G., Sultan, N. & Savyoe, B., 2007. The 1979 Nice harbour catastrophe revisited: Trigger mechanism inferred from geotechnical measurements and numerical modelling, *Marine Geology,* 245**,** 40-64.

Dilek, Y., Shallo, M. & Furnes, H., 2005. Rift-drift, seafloor spreading, and subduction tectonics of Albanian ophiolites, *International Geology Review,* 47**,** 147-176.

Driscoll, N., Weissel, J. & Goff, J., 2000. Potential for large-scale submarine slope failure and tsunami generation along the US mid-Atlantic coast, *Geology,* 28**,** 407.

Dumurdzanov, N., Serafimovski, T. & Burchfiel, B., 2005. Cenozoic tectonics of Macedonia and its relation to the South Balkan extensional regime, *Geosphere,* 1**,** 1-22.

ELAC, N. SEA BEAM 1180 - Multibeam Sonar. Product description

Fine, I., Rabinovich, A., Thomson, R. & Kulikov, E., 2002. Numerical modeling of tsunami generation by submarine and subaerial landslides, *Earth and Environmental Sciences,* 21**,** 69.

Frey-Martinez, J., Cartwright, J. & James, D., 2006. Frontally confined versus frontally emergent submarine landslides: A 3D seismic characterisation, *Marine and Petroleum Geology,* 23**,** 585-604.

Fritz, H., Mohammed, F. & Yoo, J., 2009. Lituya Bay Landslide Impact Generated Mega-Tsunami 50 th Anniversary, *Pure and Applied Geophysics,* 166**,** 153-175.

Fryer, G., Watts, P. & Pratson, L., 2004. Source of the great tsunami of 1 April 1946: a landslide in the upper Aleutian forearc, *Marine Geology,* 203**,** 201-218.

Gardner, J., Mayer, L. & Hughs Clarke, J., 2000. Morphology and processes in Lake Tahoe (California-Nevada), *Bulletin of the Geological Society of America,* 112**,** 736-746.

Gardner, J., Prior, D. & Field, M., 1999. Humboldt Slide — a large shear-dominated retrogressive slope failure, *Marine Geology,* 154**,** 323-338.

Gee, M., Uy, H., Warren, L., Morley, C. & Lambiase, J., 2007. The Brunei slide: A giant submarine landslide on the North West Borneo Margin revealed by 3D seismic data, *Marine Geology,* 246**,** 9-23.

Geist, E., Lynett, P. & Chaytor, J., 2009. Hydrodynamic modeling of tsunamis from the Currituck landslide, *Marine Geology,* 264**,** 41-52.

Ghikas, C., Dilek, Y. & Rassios, A.E., 2010. Structure and tectonics of subophiolitic mélanges in the western Hellenides (Greece): implications for ophiolite emplacement tectonics, *International Geology Review,* 52**,** 423-453.

Greene, H., Murai, L., Watts, P., Maher, N., Fisher, M., Paull, C. & Eichhubl, P., 2006. Submarine landslides in the Santa Barbara Channel as potential tsunami sources, *Natural Hazards and Earth System Sciences,* 6**,** 63-88.

Haflidason, H., Sejrup, H., Nygård, A., Mienert, J., Bryn, P., Lien, R., Forsberg, C., Berg, K. & Masson, D., 2004. The Storegga Slide: architecture, geometry and slide development, *Marine Geology,* 213**,** 201-234.

Hampton, M., Lee, H. & Locat, J., 1996. Submarine landslides, *Reviews of Geophysics,* 34**,** 33-59.

Harbitz, C., 1992. Model simulations of tsunamis generated by the Storegga slides, *Marine Geology,* 105**,** 1-21.

Harbitz, C., Løvholt, F., Pedersen, G. & Masson, D., 2006. Mechanisms of tsunami generation by submarine landslides: a short review, *Norwegion Journal of Geology,* 86**,** 255-264.

Haugen, K., Løvholt, F. & Harbitz, C., 2004. Fundamental mechanisms for tsunami generation by submarine mass flows in idealised geometries, *Marine and Petroleum Geology,* 22**,** 209-217.

Hoffmann, N., Reicherter, K., Fernández-Steeger, T. & Grützner, C., 2010. Evolution of ancient Lake Ohrid: a tectonic perspective, *Biogeosciences Discussions,* 7**,** 4641-4664.

Hovland, M., Judd, A. & King, L., 1984. Characteristic features of pockmarks on the North Sea Floor and Scotian Shelf, *Sedimentology,* 31**,** 471-480.

Ichinose, G., Anderson, J., Satake, K., Schweickert, R. & Lahren, M., 2000. The potential hazard from tsunami and seiche waves generated by large earthquakes within Lake Tahoe, California-Nevada, *Geophysical Research Letters,* 27**,** 1203-1206.

Iglesias, J., Ercilla, G., García-Gil, S. & Judd, A., 2009. Pockforms: an evaluation of pockmark-like seabed features on the Landes Plateau, Bay of Biscay, *Geo-Marine Letters***,** 1-13.

Innomar, T., 2005. SES-2000 Parametric Sediment Echo Sounder - Users Guide.

Klaucke, I. & Cochonat, P., 1999. Analysis of past seafloor failures on the continental slope off Nice (SE France), *Geo-Marine Letters,* 19**,** 245-253.

Kvalstad, T., Andresen, L., Forsberg, C., Berg, K., Bryn, P. & Wangen, M., 2005. The Storegga slide: evaluation of triggering sources and slide mechanics, *Marine and Petroleum Geology,* 22**,** 245-256.

L'Heureux, J., Hansen, L., Longva, O., Emdal, A. & Grande, L., 2010. A multidisciplinary study of submarine landslides at the Nidelva fjord delta, Central Norway–implications for geohazards assessment, *Norw. J. Geol,* 90**,** 1–20.

Locat, J., 2001. Instabilities along ocean margins: a geomorphological and geotechnical perspective, *Marine and Petroleum Geology,* 18**,** 503-512.

Locat, J. & Lee, H., 2002. Submarine landslides: advances and challenges, *Canadian Geotechnical Journal,* 39**,** 193-212.

Løvholt, F., Harbitz, C. & Haugen, K., 2005. A parametric study of tsunamis generated by submarine slides in the Ormen Lange/Storegga area off western Norway, *Marine and Petroleum Geology,* 22**,** 219-231.

Masson, D., Harbitz, C., Wynn, R., Pedersen, G. & Lovholt, F., 2006. Submarine landslides: processes, triggers and hazard prediction, *Philosophical Transactions of the Royal Society A: Mathematical, Physical and Engineering Sciences,* 364**,** 2009-2039.

Matsumoto, T. & Tappin, D., 2003. Possible Coseismic Large-scale Landslide off the Northern Coast of Papua New Guinea in July 1998: Geophysical and Geological Results from SOS Cruises, *Pure and applied Geophysics,* 160**,** 1923-1943.

Matzinger, A., Spirkovski, Z., Patceva, S. & Wuest, A., 2006. Sensitivity of ancient Lake Ohrid to local anthropogenic impacts and global warming, *Journal of Great Lakes Research,* 32**,** 158-179.

McAdoo, B. & Watts, P., 2004. Tsunami hazard from submarine landslides on the Oregon continental slope, *Marine Geology,* 203**,** 235-245.

McMurtry, G., Watts, P., Fryer, G., Smith, J. & Imamura, F., 2004. Giant landslides, mega-tsunamis, and paleo-sea level in the Hawaiian Islands, *Marine Geology,* 203**,** 219-233.

Mienert, J., Berndt, C., Laberg, J. & Vorren, T., 2002. Slope Instability of Continental Margins, *Ocean Margin Systems***,** 179-193.

Moernaut, J., De Batist, M., Charlet, F., Heirman, K., Chapron, E., Pino, M., Brümmer, R. & Urrutia, R., 2007. Giant earthquakes in South-Central Chile revealed by Holocene mass-wasting events in Lake Puyehue, *Sedimentary Geology,* 195**,** 239-256.

Mosher, D., Moscardelli, L., Shipp, R., Chaytor, J., Baxter, C., Lee, H. & Urgeles, R., 2010. Submarine Mass Movements and Their Consequences, *Advances in Natural and Technological Hazard Research,* 28**,** 1-8.

Muço, B., Vaccari, F., Panza, G. & Kuka, N., 2002. Seismic zonation in Albania using a deterministic approach, *Tectonophysics,* 344**,** 277-288.

Mulder, T. & Syvitski, J., 1995. Turbidite currents generated at river mouths during expectional discharges to the world ocean, *J. Geol. ,* 103**,** 285-299.

Murty, T., 2003. Tsunami wave height dependence on landslide volume, *Pure and Applied Geophysics,* 160**,** 2147-2153.

Nautik, E., 1999. SEA BEAM 1185/1180/1055/1050 - Operating Manual.

Okal, E., Fryer, G., Borrero, J. & Ruscher, C., 2002. The landslide and local tsunami of 13 september 1999 on Fatu Hiva (Marquesas Islands; French Polynesia), *Bulletin de la Societe Geologique de France,* 173**,** 359.

Papadopoulos, G. & Kortekaas, S., 2003. Characteristics of landslide generated tsunamis from observational data, pp. 367Kluwer Academic Pub.

Popovska, C. & Bonacci, O., 2007. Basic data on the hydrology of Lakes Ohrid and Prespa, *Hydrological Processes,* 21**,** 658-664.

Pratson, L. & Coakley, B., 1996. A model for the headward erosion of submarine canyons induced by downslope-eroding sediment flows, *Geological Society of America Bulletin,* 108**,** 225.

Prior, D., Bornhold, B. & Johns, M., 1984. Depositional characteristics of a submarine debris flow, *The Journal of Geology***,** 707-727.

Reicherter, K., submitted. Active basins and neotectonics: morphotectonics of the Lake Ohrid Basin (FYROM and Albania), *Zeitschrift der Deutschen Gesellschaft für Geowissenschaften*

Robertson, A., 2007. Overview of tectonic settings related to the rifting and opening of Mesozoic ocean basins in the Eastern Tethys: Oman, Himalayas and Eastern Mediterranean regions, *Geological Society London Special Publications,* 282**,** 325.

Robertson, A., Clift, P., Degnan, P. & Jones, G., 1991. Palaeogeographic and palaeotectonic evolution of the Eastern Mediterranean Neotethys, *Palaeogeography, Palaeoclimatology, Palaeoecology,* 87**,** 289-343.

Robertson, A., Dixon, J., Brown, S., Collins, A., Morris, A., Pickett, E., Sharp, I. & Ustaomer, T., 1996. Alternative tectonic models for the Late Palaeozoic-Early Tertiary development of Tethys in the Eastern Mediterranean region, *Geological Society London Special Publications,* 105**,** 239.

Satake, K. & Tanioka, Y., 2003. The July 1998 Papua New Guinea earthquake: Mechanism and quantification of unusual tsunami generation, *Pure and Applied Geophysics,* 160**,** 2087-2118.

Sayago-Gil, M., Long, D., Fernández-Salas, L., Hitchen, K., López-González, N., Díaz-del-Río, V. & Durán-Muñoz, P. Geomorphology of the Talismán Slide (Western slope of Hatton Bank, NE Atlantic Ocean), *Submarine Mass Movements and Their Consequences***,** 289-300.

Schnellmann, M., Aanselmetti, F., Giardini, D. & McKenzie, J., 2005. Mass movement-induced fold-and-thrust belt structures in unconsolidated sediments in Lake Lucerne (Switzerland), *Sedimentology,* 52**,** 271-289.

SeaBeam, I., 2000. Multibeam Sonar Theory of Operation.

Stiros, S., 1998. Historical seismicity, palaeoseismicity and seismic risk in Western Macedonia, Northern Greece, *Journal of Geodynamics,* 26**,** 271-287.

Strasser, M., Stegmann, S., Bussmann, F., Anselmetti, F., Rick, B. & Kopf, A., 2007. Quantifying subaqueous slope stability during seismic shaking: Lake Lucerne as model for ocean margins, *Marine Geology,* 240**,** 77-97.

Suhadolc, P., Sandron, D., Fitzko, F. & Costa, G., 2004. Seismic ground motion estimates for the M6. 1 earthquake of July 26, 1963 at Skopje, Republic of Macedonia, *Acta Geodaetica et Geophysica Hungarica,* 39**,** 319-326.

Synolakis, C., Bardet, J., Borrero, J., Davies, H., Okal, E., Silver, E., Sweet, S. & Tappin, D., 2002. The slump origin of the 1998 Papua New Guinea tsunami, *Proceedings of the Royal Society of London. Series A: Mathematical, Physical and Engineering Sciences,* 458**,** 763.

Syvitski, J., 1989. On the deposition of sediment within glacier-influenced fjords: oceanographic controls, *Marine Geology,* 85**,** 301-329.

Tappin, D., Watts, P., McMurtry, G., Lafoy, Y. & Matsumoto, T., 2001. The Sissano, Papua New Guinea tsunami of July 1998 - offshore evidence on the source mechanism, *Marine Geology,* 175**,** 1-23.

Tinti, S., Armigliato, A., Manucci, A., Pagnoni, G., Zaniboni, F., Yalçiner, A. & Altinok, Y., 2006. The generating mechanisms of the August 17, 1999 Izmit bay (Turkey) tsunami: Regional (tectonic) and local (mass instabilities) causes, *Marine Geology,* 225**,** 311-330.

Vogel, H., Zanchetta, G., Sulpizio, R., Wagner, B. & Nowaczyk, N., 2010. A tephrostratigraphic record for the last glacial–interglacial cycle from Lake Ohrid, Albania and Macedonia., *J. Quaternary Sci.,* 25**,** 320-338.

Wagner, B., Reicherter, K., Daut, G., Wessels, M., Matzinger, A., Schwalb, A., Spirkovski, Z. & Sanxhaku, M., 2008. The potential of Lake Ohrid for long-term palaeoenvironmental reconstructions, *Palaeogeography, Palaeoclimatology, Palaeoecology,* 259**,** 341-356.

Ward, S., 2001. Landslide tsunami, *Journal of Geophysical Research,* 106**,** 201–211.

Watts, P., 1998. Wavemaker curves for tsunamis generated by underwater landslides, *Journal of Waterway, Port, Coastal, and Ocean Engineering,* 124**,** 127.

Watts, P., 2001. Some opportunities of the landslide tsunami hypothesis, *Sci. Tsunami Hazards,* 19**,** 126–149.

Watts, P., Grilli, S., Tappin, D. & Fryer, G., 2005. Tsunami generation by submarine mass failure. II: Predictive equations and case studies, *Journal of Waterway, Port, Coastal, and Ocean Engineering,* 131**,** 298.

List of Figures

Appendix

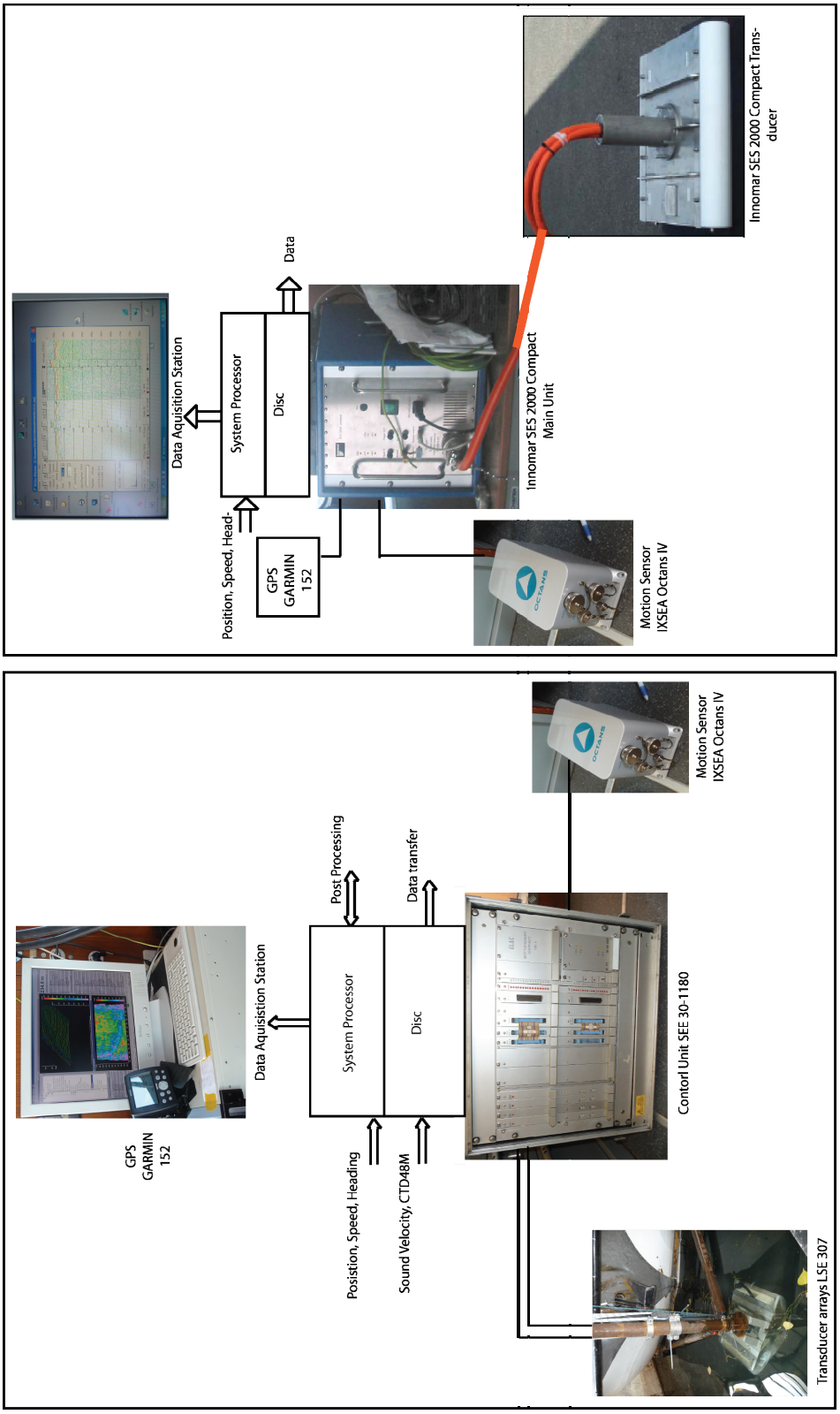

Figure A 1: Installation of sediment echo sounder (top) and multibeam system (bottom) on board of the research vessel during the BLOSSOM campaign in Lake Ohrid.

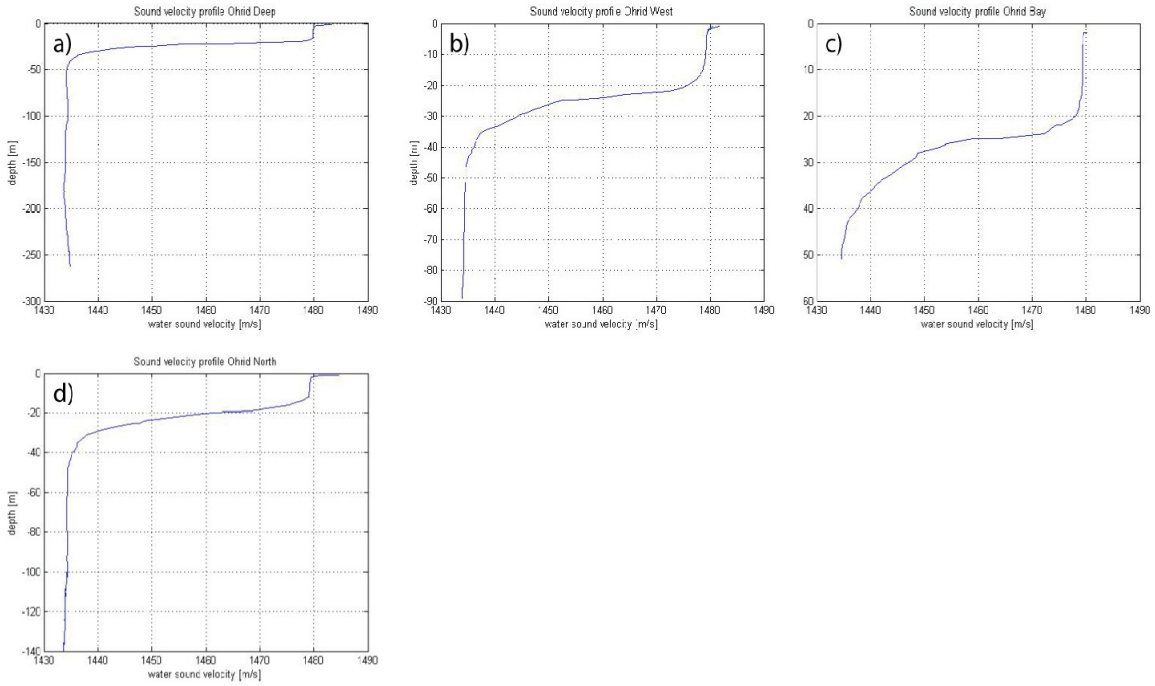

Figure A 2: Measured sound velocity profiles at four locations at Lake Ohrid (for position of CTD-measurements see Figure 16, green dots a - c)

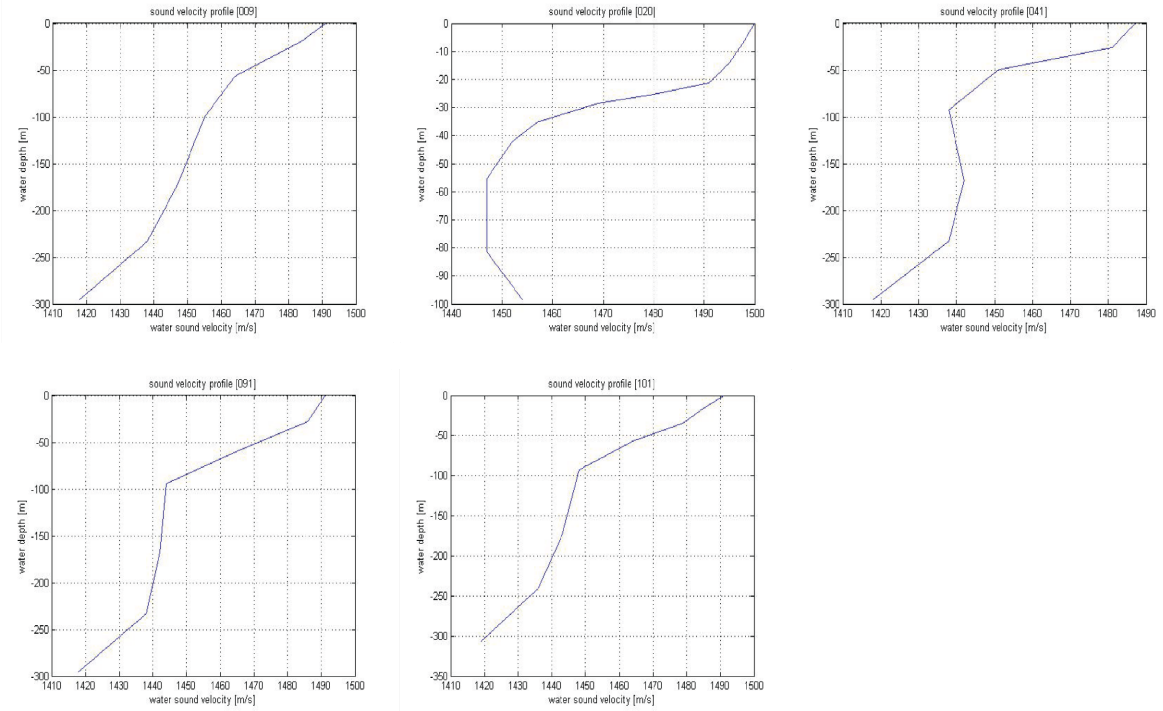

Figure A 3: Sound velocity profiles used for processing of bathymetry data; generated with mbvelocitytool. These five profiles are representative for the five defined regions in Lake Ohrid: South-East (009), North (020), Ohrid Bay (041), South-West (091) and Central Basin (101). Zones of representative sound velocity profiles are shown in Figure 19.

Documentation: Processing bathymetric data for Lake Ohrid data with MB-Systems

1) Creating datalist:
   mbm_makedatalist

2) Convert "xse" files in "mb94":
   mbm_copy -Idatalist.mb-1 –F

3) Creating new datalist with "mb94" filest instead of "xse" files (find and replace); new datalist: datalist_all.mb-1

4) Generating ancillary files (inf, fbt, fnv, par, nav) for every profile
   mbdatalist -Idatalist_all.mb-1 -N –V

5) Generating sound velocity profiles:
   mbvelocitytool
   In the ".par" files PSVPMODE: must be set to 1 and PSVPFILE must contain the sound velocity profile:
   mbset -Idatalist_all.mb-1 -PSVPMODE:1 -PSVPFILE:"profile_xxx.svp"
6) Applying filter for cleaning the swath data files:
   mbclean -Isouth_west_list.mb-1 -X7 -Q -S0.5/3/0 C0.6 –V
   mbclean -Isouth_east_list.mb-1 -X7 -Q -S0.5/3/0 C0.6 –V
   mbclean –Icentral_basin_list.mb-1 -X7 -Q -S0.5/3/0 C0.6 –V

   mbclean -Inorth_list.mb-1 –X6 -Q -S0.5/3/0 C0.6 –V
   mbclean –Iohrid_bay_list.mb-1 –X6 -Q -S0.5/3/0 C0.6 –V

7) Additional manual cleaning of swath data files:
   mbedit

8) Processing the data:
   mbprocess -Idatalist_all.mb-1

9) Generating new datalist with "p.mb94"-files instead of "mb94"-files (find and replace); new datalist: datalist_all_pro.mb-1

10) Generating grid:
    mbgrid -Idatalist_all_pro.mb-1 –E5/5 -A2 -V -N -C15/3
    mbgrid -Idatalist_all_pro.mb-1 –E10/10 -A2 -V -N -C15/3
    mbgrid -Idatalist_all_pro.mb-1 –E20/20 -A2 -V -N -C15/3
    mbgrid -Idatalist_all_pro.mb-1 –E50/50 -A2 -V -N -C15/3

Documentation: Processing backscatter data for Lake Ohrid data with MB-Systems

1) Correcting amplitude data:
   mbbackangle –Idatalist.mb-1 -F –A2 -P50 -N63/75 –V

2) Processing backscatter data:
   mbprocess –Idatalist.mb-1 –F –V

3) Creating backscatter mosaic:
   mbmosaic –Idatalist.mb-1 –A3 –C5 –F0.10 –G3 –N –Yangleprio_bs.dat –E5/5

```
profil_008.mb94 94
profil_013.mb94 94
profil_035.mb94 94
profil_036.mb94 94
profil_048.mb94 94
profil_049.mb94 94
profil_050.mb94 94
profil_080.mb94 94
```

Figure A 4: Example of a datalist used for processing with MB-Systems (here: first profiles of the datalist for Central Basin area)

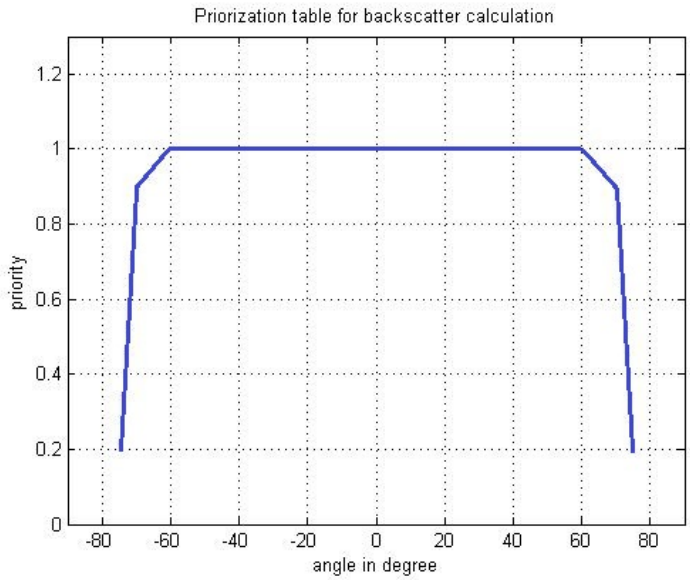

Figure A 5: Priorization table for backscatter processing. Beams in the center of the swath are amplified.

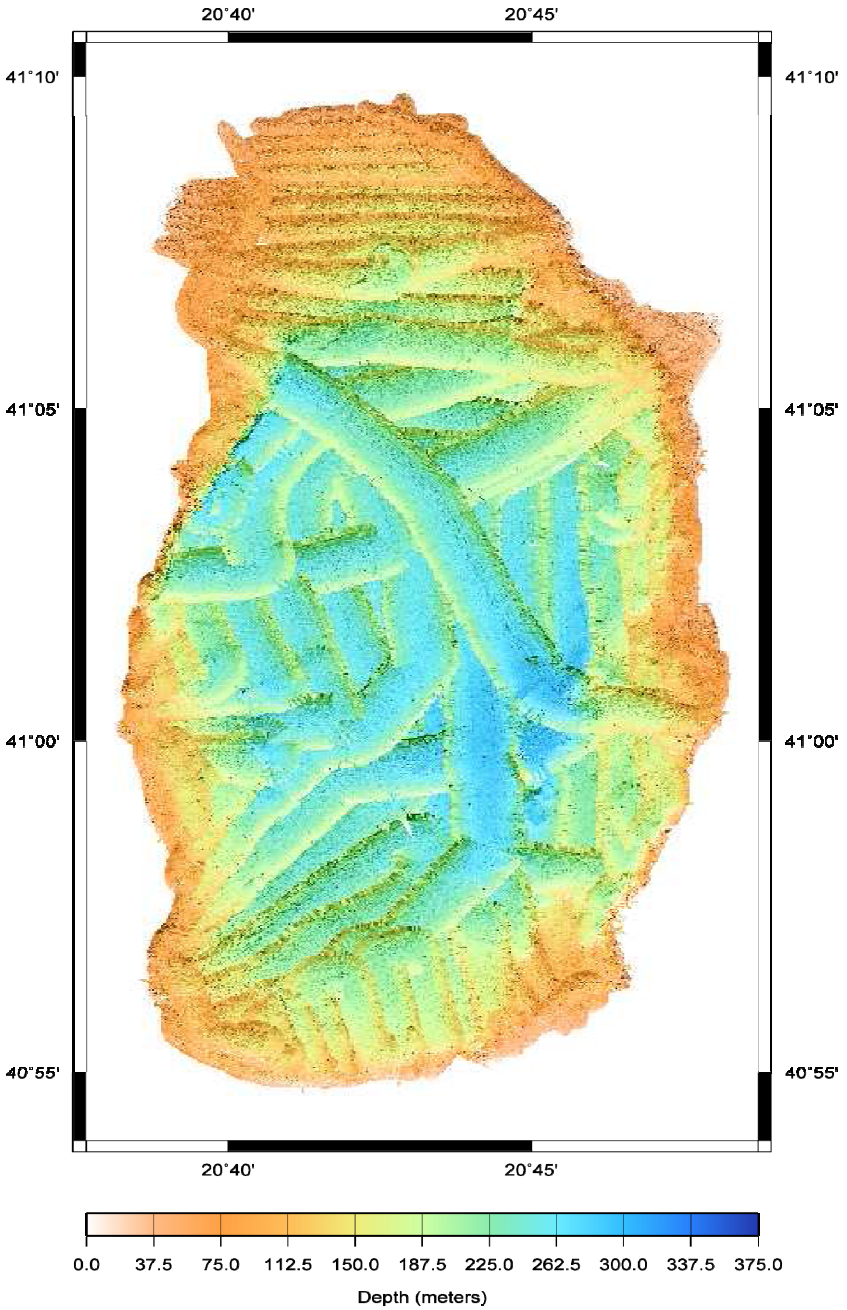

Figure A 6: Unprocessed multibeam bathymetry data of Lake Ohrid. Outer pings of swath files show discrepancies to swath data of adjacent profiles.

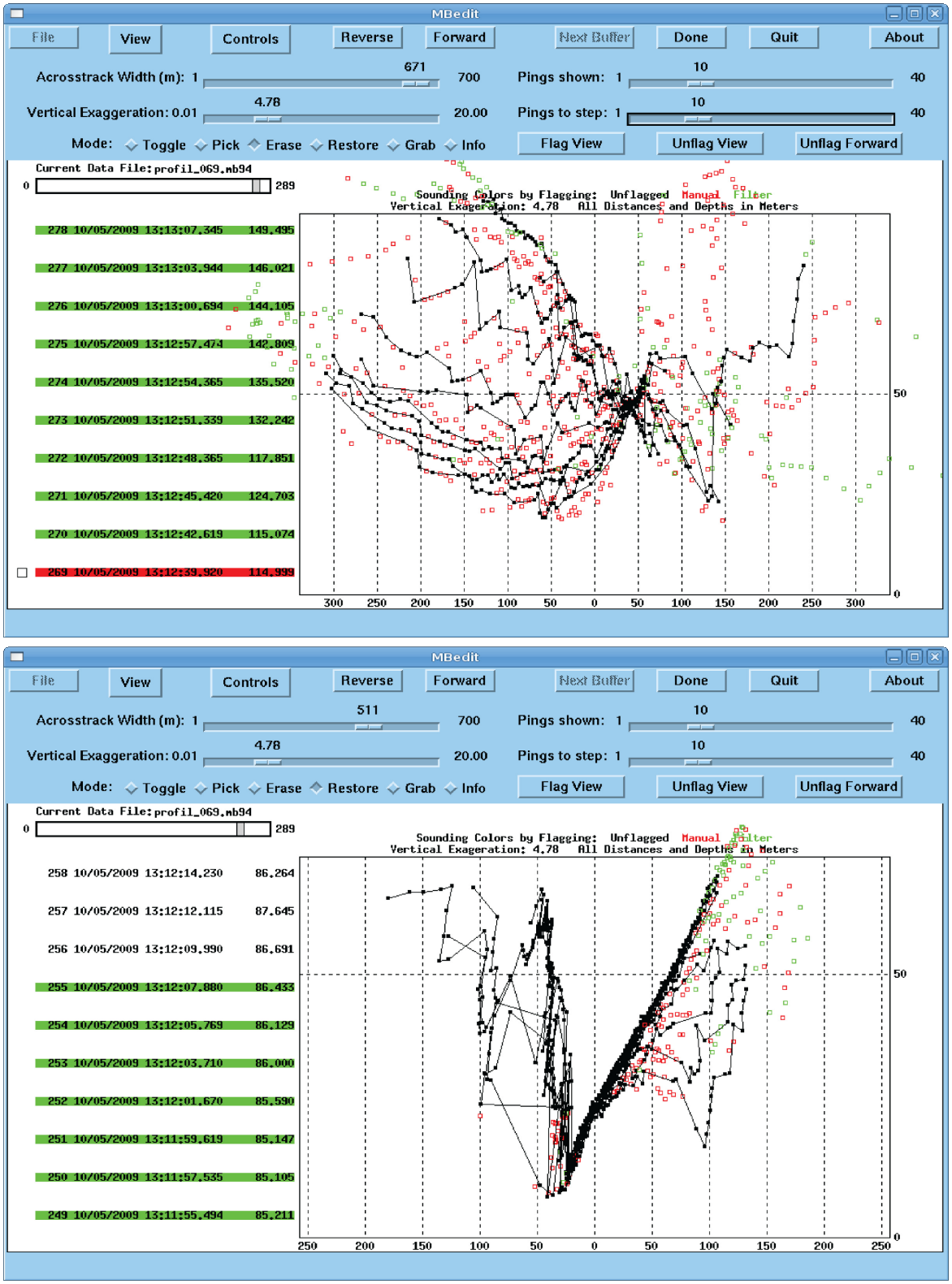

Figure A 7: Examples of recorded swath data (displayed with mbedit) showing swath data during a ship turn (top) and swath data along a steep slope (bottom). Along track view for 20 pings at the same time. Red and green dots represent manual and automatic filtered data points.

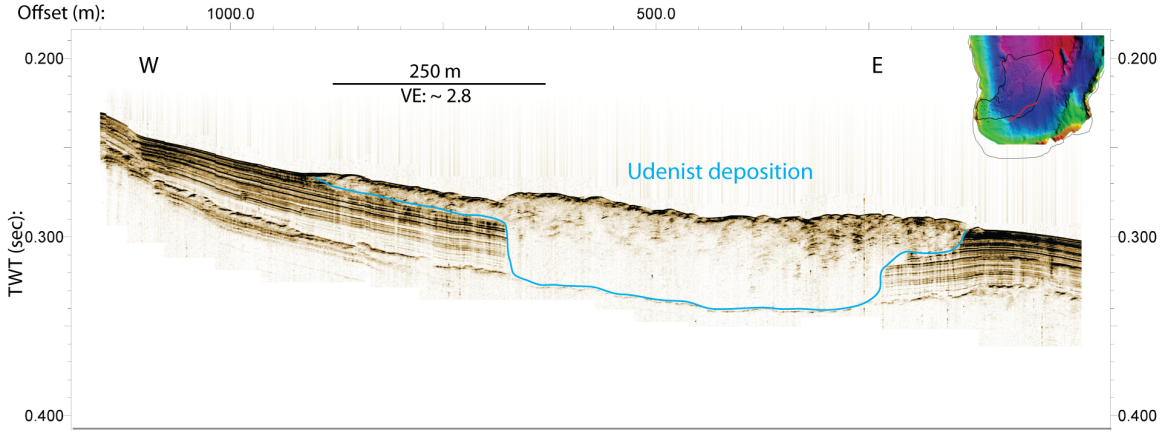

Figure A 8: Sediment echo sounder profile at the south eastern margin of Udenisht Slide. Slide deposit (blue line) is marked as transparent unit enclosed by well stratified and undisturbed sediments. Strong irregular reflector revealing base of transparent unit can be traced through the whole profile in around 0.04 sec TWT depth. This reflector indicated top of Naum slide deposit with nearly no reflections beneath. Patchy reflections in the uppermost part and two thickness steps at western and eastern margin of the slide deposit from 0.04 sec TWT to ca. 0.01 sec TWT. Position of western thickness step coincides with morphological step at the lake floor.

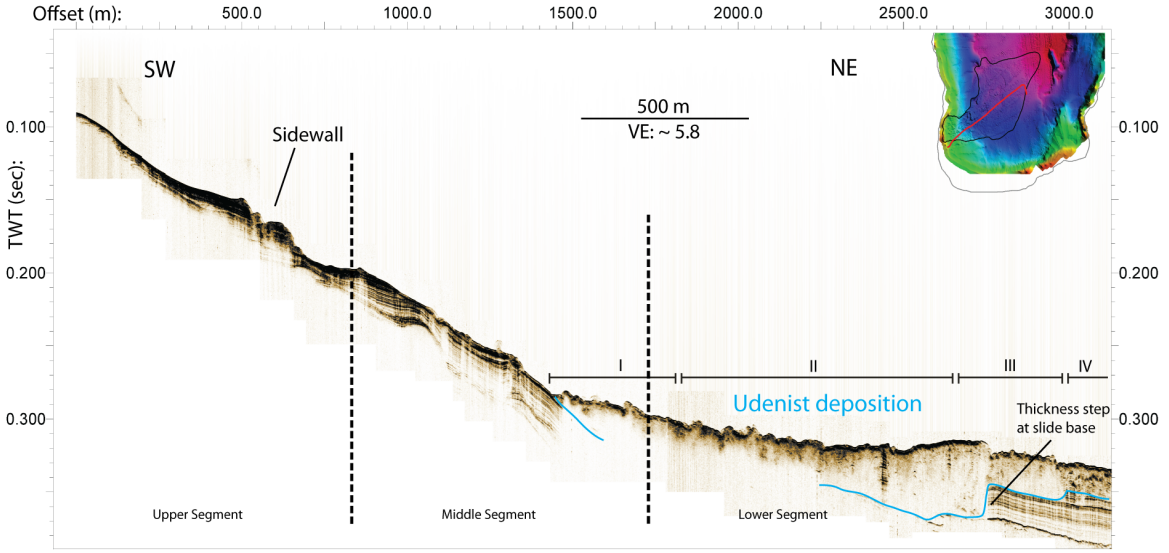

Figure A 9: Sediment echo sounder profile along Udenisht Slide. Low penetration and rough topography of the southern sidewall can be seen in the Upper segment. Middle segment is characterized by layered reflections below the lake floor and begin of deposition body of Udenisht Slide (blue line). Lake floor is marked by extremely rough topography above slide unit. Transparency of deposition is high and between Middle and Lower segment its base cannot be traced (section I-II). Obvious thickness step in section III with undisturbed sediments beneath comes together with morphological step at the lake floor. Strong irregular reflector with transparent unit below undisturbed sediments is imaged on the NE edge of the profile. More internal reflections within the slide deposit are imaged in direction to the toe of the slide (III – IV).

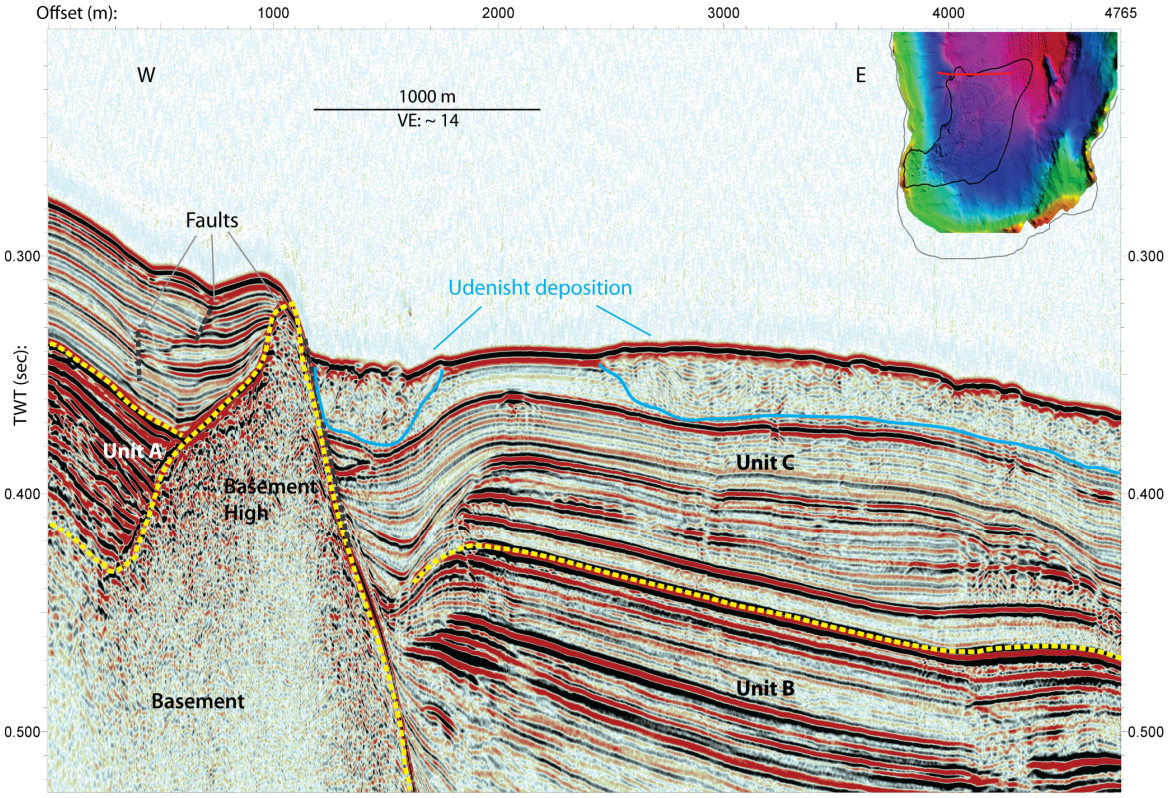

Figure A 10: Multichannel profile showing northern part of Udenisht deposition. A striking basement high is located at the western margin of the profile reaching the lake floor. Eastward dipping sediments are located west of the basement high with smaller faults displacing the sediments above Unit A. A large fault structure can be seen east of basement high. Deformed reflectors (Units B and C) east of basement high are followed by alternation of higher and lower, relatively undisturbed amplitude layers farther east. At the eastern margin a slightly eastern dip of reflectors is visible. Two deposition structures of Udenisht Slide are located within the uppermost layers of Unit C showing low reflectivity and deformed internal reflections. Small western element of deposition adjoins to basement high and shows rougher topography. Eastern and western elements are separated by undisturbed reflectors of Unit C.

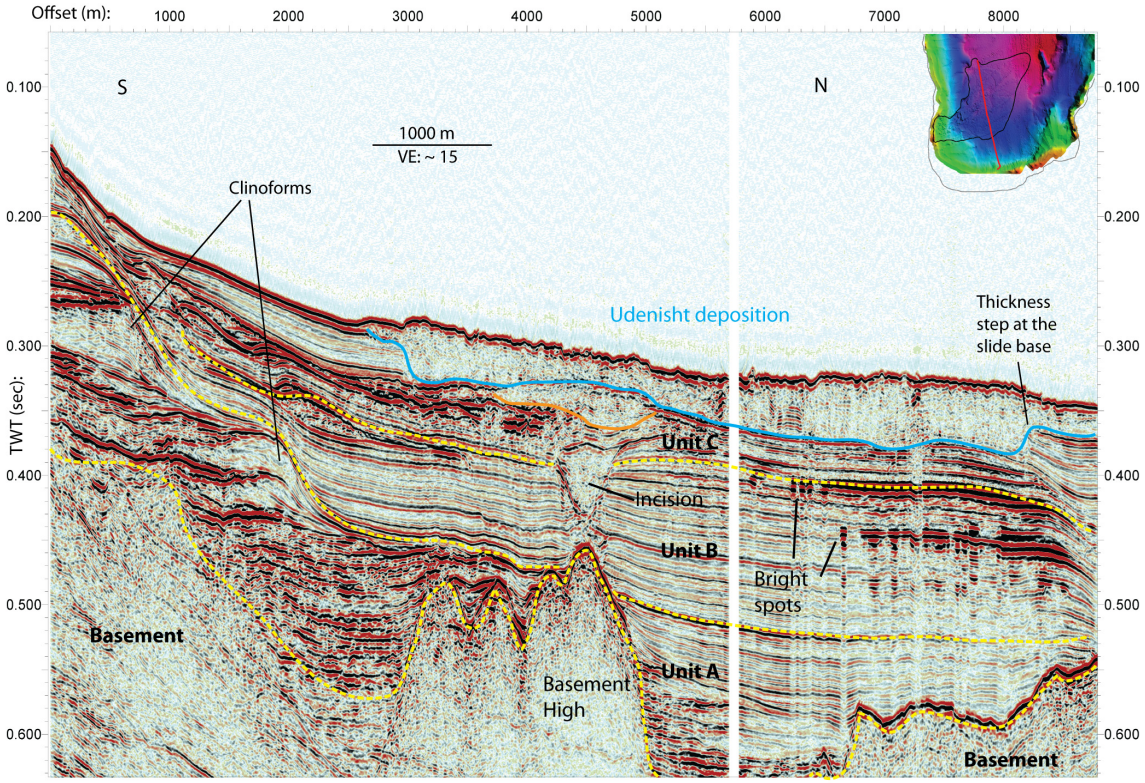

Figure A 11: Multichannel seismic profile from southern margin of Lake Ohrid northwards. Seismic Units A-C can be seen on top of basement rocks. Basement highs are located in the central part. South of basement high Unit A showing clinoforms at transition to undisturbed sediment layers of Unit B. West of basement high sediment layers of Unit A show lower amplitudes and are less deformed. Bright spots and high amplitude layers are located between Unit B and C in the northern part of the profile. A cone like incision of transparent infill is situated above the basement high, pervading Unit B. Small part of the Naum deposit is illustrated by the orange line, above the cone like incision. Udenisht Slide deposit shown as transparent body with few internal reflections is situated in Unit C. Sudden thickness decrease in slide body seen at the northern margin of the profile.

Pre-slide slope reconstruction:

1) Extracting of 17 profiles along the slide (Figure A12) with same depth values for northern and southern sidewall of each profile. Each profile contains latitude, longitude and depth value.
2) Importing these profiles in matlab script (Figure A13) and changing depth values lower than depth at the sidewall to the respective sidewall of each profile
3) Saving the recalculated profiles.
4) Merging all single profile to one large file.
5) Importing the file into Global Mapper as "Elevation Grid from 3D Point Data"

-> Artifacts at the margins of the generated grid exist

6) Creating shape file wit slope extension
7) Blending of generated grid with the shape file: Export grid as xyz-file -> Import xyz-file -> mark points of the grid within the shape file ("Advanced Selection Options" -> "Select all Points" -> Create new feature of the selected points
8) Change new feature to: "Create Elevation Grid from 3D Data"

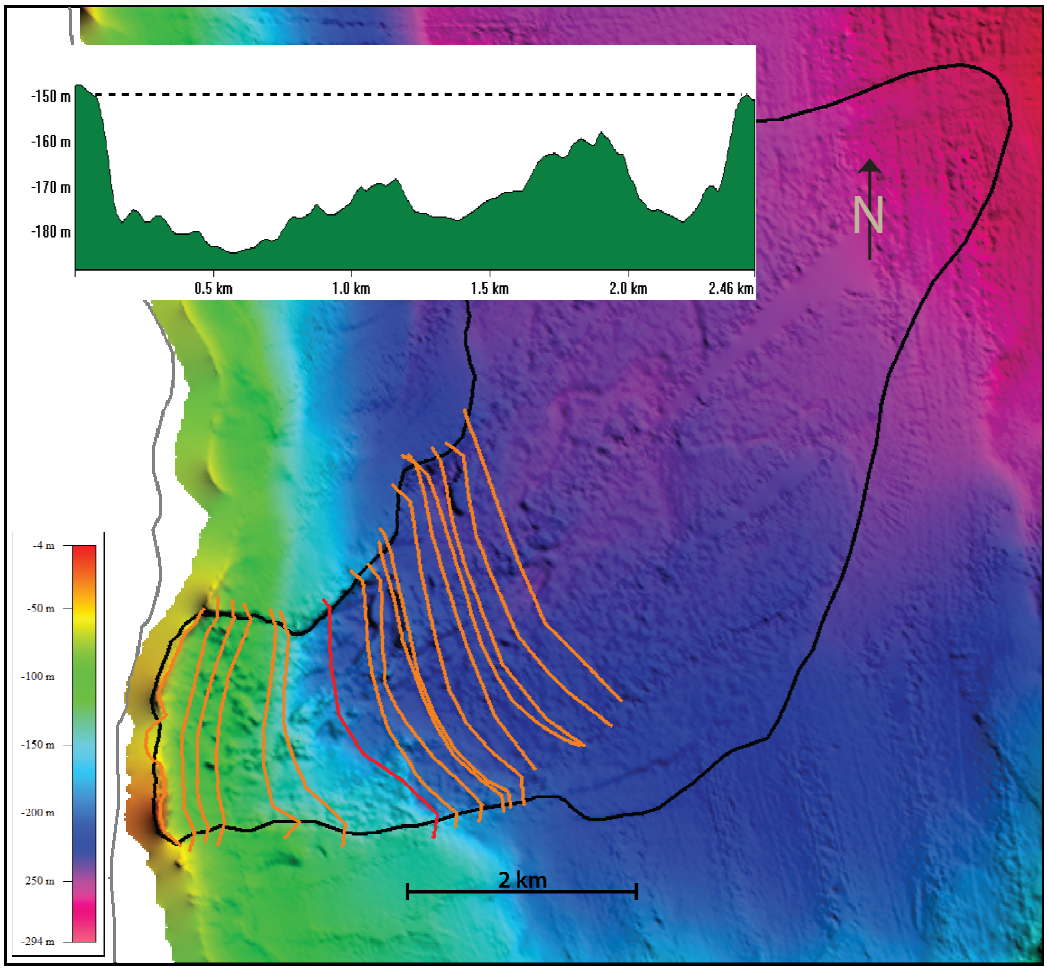

Figure A 12: Profiles for reconstructing the former slope over the Udenisht Slide. Profile at the top shows an example of the 150 m - depth profile (indicated by red line). Every depth value of this particular profile was set to 150 m (dashed black line). Accordingly done for all 17 profiles (orange lines).

```
%% Recalculating former slope %%

close all
clear all
clc

%% Every depth value of the profile that is below the sidewall depth will
%% be changed to the sidewall depth. Sidewall depth is written in the
%% profile name (f.e.: p120.pfl)


files = dir('*.pfl');                    %Creating list with all profiles in the current folder
%%

for i=1:length(files)                    %load all profiles in matlab
   b=load('-ascii', files(i).name)       %b is the actual profile
      a=files(i).name;
   depth=-sscanf(a,'p%g.pfl');           %'depth' is the depth of the sidewall

   c=b;
   for j=1:length(c)                     %setting every depth value below sidewall depth at
sidewall depth
      if c(j,4)<depth
         c(j,4)=depth;
      end
   end

   c2=c(:,2);                            % 1st row is sampling intervall, will not be needed and is
not saved
   c3=c(:,3);
   c4=c(:,4);

   d=[c2 c3 c4]

   depth2=-depth;

   save(['r', sprintf('%d',depth2), '.txt'],'d','-ascii')

end
```

Figure A 13: Matlab programm for reconstructing the former slope. Profiles have been extracted with Global Mapper and saved as "ascii"-files containing: sample interval, latitude, longitude and depth. Depth values have been modified by this program with respect to the value of the respective sidewall depth.

Erklärung

Hiermit erkläre ich, dass ich die vorliegende Arbeit selbständig und ohne fremde Hilfe angefertigt und keine anderen als die angegebenen Quellen und Hilfsmittel verwendet habe.
Die eingereichte schriftliche Fassung der Arbeit entspricht der auf dem elektronischen Speichermedium.
Weiterhin versichere ich, dass diese Arbeit noch nicht als Abschlussarbeit an anderer Stelle vorgelegen hat.

Kiel, den _____

_____

Matthias Grün